VOL. 8 NO. 4 OCTOBER 1964
PUBLISHED MONTHLY

Journal of

ELECTROANALYTICAL CHEMISTRY

International Journal Dealing with all Aspects of Electroanalytical Chemistry, Including Fundamental Electrochemistry

E L S E V I E R

GENERAL INFORMATION

See also Suggestions and Instructions to Authors which will be sent free, on request to the Publishers.

Types of contributions

(a) Original research work not previously published in other periodicals.
(b) Reviews on recent developments in various fields.
(c) Short communications.
(d) Bibliographical notes and book reviews.

Languages

Papers will be published in English, French or German.

Submission of papers

Papers should be sent to one of the following Editors:

Professor J. O'M. Bockris, John Harrison Laboratory of Chemistry, University of Pennsylvania, Philadelphia 4, Pa., U.S.A.
Dr. R. Parsons, Department of Chemistry, The University, Bristol 8, England.
Professor C. N. Reilley, Department of Chemistry, University of North Carolina, Chapel Hill, N.C., U.S.A.

Authors should preferably submit two copies in double-spaced typing on pages of uniform size. Legends for figures should be typed on a separate page. The figures should be in a form suitable for reproduction, drawn in Indian ink on drawing paper or tracing paper, with lettering etc. in thin pencil. The sheets of drawing or tracing paper should preferably be of the same dimensions as those on which the article is typed. Photographs should be submitted as clear black and white prints on glossy paper.
All references should be given at the end of the paper. They should be numbered and the numbers should appear in the text at the appropriate places.
A summary of 50 to 200 words should be included.

Reprints

Twenty-five reprints will be supplied free of charge. Additional reprints can be ordered at quoted prices. They must be ordered on order forms which are sent together with the proofs.

Publication

The *Journal of Electroanalytical Chemistry* appears monthly and has six issues per volume and two volumes per year, each of approx. 500 pages.

Subscription price (post free): £ 10.15.0 or $ 30.00 or Dfl. 108.00 per year; £ 5.7.6 or $ 15.00 or Dfl. 54.00 per volume.
Additional cost for copies by air mail available on request.
For advertising rates apply to the publishers.

Subscriptions

Subscriptions should be sent to:

ELSEVIER PUBLISHING COMPANY, P.O. Box 211, Amsterdam, The Netherlands.

SUMMARIES OF PAPERS PUBLISHED IN JOURNAL OF ELECTROANALYTICAL CHEMISTRY

Vol. 8, No. 4, October 1964

THE POLAROGRAPHY OF THE NICKEL(II)–ETHYLENEDIAMINE SYSTEM

II. EFFECTS OF VARIATION OF ETHYLENEDIAMINE CONCENTRATION

The effect of variation of ethylenediamine concentration from 0–2.1 × 10^{-2} *M* on the polarography of 2.4 × 10^{-3} *M* Ni^{2+} solutions is studied. Two new waves are observed over this concentration range; a pre-wave arising before the $Ni(H_2O)_6^{2+}$ wave for low concentrations of ethylenediamine, and a wave occurring at a slightly more negative potential than the $Ni(H_2O)_6^{2+}$ wave for intermediate ethylenediamine concentrations. At high concentration of ethylenediamine, the Ni^{2+} wave is not observed. The nature of the species and reactions corresponding to these waves is described. The visible and ultra-violet spectra of the system are also reported for the same ratios of Ni^{2+}: ethylenediamine concentrations and are compared with the spectra obtained for the Ni(II)–*o*-phenylenediamine system which also exhibits a pre-wave.

H. B. MARK, JR.,

J. Electroanal. Chem., 8 (1964) 253–261.

POLAROGRAPHIC STUDY OF METAL COMPLEXES

VII. TETRACYANO-MONO(ETHYLENEDIAMINE) COBALTATE(III) COMPLEX

Tetracyano-mono(ethylenediamine)cobaltate(III) complex, $K[Co^{III}(CN)_4\ en] \cdot H_2O$ (a new compound) was found to be reduced to the metal through the cobaltate(I) complex at the dropping mercury electrode in the presence of ethylenediamine.

In the absence of excess ethylenediamine, the irreversible wave apparently of one step, corresponding to three electron reduction, was obtained in 0.5 *M* sodium sulphate solution. The oscillopolarogram, however, indicated that the reaction proceeds in two stages. This phenomenon was considered to be due to the aquation of the complex in solution.

The resulting cobaltate(I) complex was presumed to have the same hexacoordinate formula, $[Co^{I}(CN)_4\ en]^{3-}$, as that of the original cobaltate(III) complex.

Further reduction of the cobaltate(I) complex to the metal was interpreted as being due to the structure of the *cis*-form, compared with that of the $[Co^{III}(CN)_4(SO_3)_2]^{5-}$ ion.

This is the first time that the reduction of a cobalt(III) complex by the path Co(III) → Co(I) → Co(O) has been reported.

N. MAKI AND K. OKAWA,

J. Electroanal. Chem., 8 (1964) 262–267.

AN ALL-ELECTRONIC SYSTEM FOR THE AUTOMATIC MEASUREMENT OF SLOPES OF REACTION-RATE CURVES

A new method is described for the automatic measurement of reaction rates. Slopes of response curves are matched with output slopes from an electronic integrator. When the net output is zero, the input to the integrator is proportional to the slope of the response curve and is read directly on a meter near zero reaction time. All the necessary circuitry is wired into a blank plug-on chassis for commercially available equipment.

The method is evaluated for the determination of cystine in a reaction where the slope of the response curve is proportional to the cystine concentration. Cystine is determined over the range of 1.0–25 p.p.m. with a relative standard deviation of less than 1%. Automatic direct readout of p.p.m. cystine is obtained within 15 sec after mixing sample and reagents.

H. L. PARDUE AND W. E. DAHL,
J. Electroanal. Chem., 8 (1964) 268–276.

THE REPRESENTATION OF ELECTROLYSIS AT CONSTANT CURRENT IN THE CASE OF PLANE FINITE DIFFUSION USING AN ANALOGUE COMPUTER

An electronic analogue of electrolysis at constant current in the case of plane finite diffusion is presented. This makes it possible to avoid the complications in the use of the analytical solution of the diffusion equation in practice.

The realization of the model with a universal electronic analogue computer and the procedure are indicated. The possibilities of the model are discussed and it is shown that the alteration of the concentration can be followed not only in the boundary layer, but also in the inside of the diffusion layer; the distribution of the concentration as a function of the distance is also known at every moment. It is shown that the minimum error of the model is conditioned by the nominal error of the analogue computer. A numerical example is given from which it is evident, that even when using only four operational amplifiers, the error does not exceed 8% and that this value, dependent upon the numerical values, drops to 3%. From this it is obvious, that with the aid of a minimal switching arrangement, useful information can be obtained quickly.

The suggested analogue can be constructed and employed easily. Only elementary knowledge of analogue calculation is needed and can be performed with a small analogue computer containing only linear elements.

R. V. BUCUR, I. COVACI AND C. MIRON,
J. Electroanal. Chem., 8 (1964) 277–285.

POLAROGRAPHY OF BISMUTH(III)–GLUCONATE COMPLEXES

The polarographic behavior of the bismuth(III)–gluconate complex in alkaline solution has been studied. For a solution containing 0.1 *F* sodium gluconate and 1 *F* NaOH, a well-defined irreversible reduction wave is obtained with a half-wave potential of −0.80 V *vs.* S.C.E. and a diffusion current constant, I_{max}, of 4.26 ± 0.04. The diffusion current is proportional to bismuth(III) concentration for metal ion concentrations from 10^{-5} to 10^{-2} *F*. The data indicate that the complex contains one gluconate group and one and one-half hydroxide ions per metal ion. Polarographic determinations of the solubility of bismuth(III) in KOH solutions has permitted the formation constant for the reaction $Bi(OH)_3$ (s) + $OH^- \rightarrow Bi(OH)_4^-$ to be evaluated, $K = 5.1 \times 10^{-5}$.

J. R. BRANNAN AND D. T. SAWYER,
J. Electroanal. Chem., 8 (1964) 286–290.

ON THE PROBLEM OF THE IDEAL DROPPING MERCURY ELECTRODE

Current–time curves were recorded with a short period pen recorder using extremely thin-walled dropping mercury capillaries in a 10^{-3} *N* Tl^+-solution. Even by inclining the capillary it was not possible to eliminate completely the depletion effect as with the 45°–SMOLER capillary, although the shielding and resistance to streaming of the capillary wall (thickness 0.003 to 0.01 mm) are negligible. Since the time *t'* which elapses before the current on the second drop coincides with that on the first still amounts to 0.2 sec for the thinnest-walled capillaries, it seems impossible in principle to realise an ideal vertical dropping mercury capillary in "unstirred" medium under normal conditions. Contrary to theoretical expectations the oxygen maximum continues to be observed.

The causes of these effects and discrepancies are discussed.

J. FLEMMING AND H. BERG,
J. Electroanal. Chem., 8 (1964) 291–301.

INVESTIGATION OF THE ANODIC OXIDATION OF AZIDE ION ON PLATINUM ELECTRODES

A detailed study of the mechanism of the anodic oxidation of the azide ion was carried out using cyclic voltammetry, chronopotentiometry, coulometry, and macro-scale electrolysis. The results of this work show that the oxidation of the azide ion on platinum electrodes in neutral and basic aqueous media proceeds according to the mechanism:

$$N_3^- \overset{\text{rapid}}{\rightleftharpoons} N_3\cdot + e$$
$$N_3\cdot \xrightarrow{\text{rapid}} N_2$$

In acidic solutions, HN_3 is also oxidized, but at a slightly more anodic potential.

This reaction has been shown to be diffusion-controlled, and may be used as the basis of a cyclic voltammetric method for the determination of azide, with a limit of detection of $2 \cdot 10^{-4}$ *M* under typical conditions.

Other anions which are also oxidized at the platinum electrode, and thus interfere in the method are: NO_2^-, Br^-, I^-, S^{2-}, CN^-, ClO^-, SO_3^{2-} and SCN^-.

G. A. WARD AND C. M. WRIGHT,
J. Electroanal. Chem., 8 (1964) 302–309.

VERIFICATION OF THE COULOMETRIC METHOD OF ANALYSIS OF HYDROGEN IN IRON

The coulometric method of analysis for hydrogen sorbed in iron was checked against the volume of hydrogen evolved from the iron on standing. The two methods were in agreement.

T. C. FRANKLIN AND N. F. FRANKLIN,
J. Electroanal. Chem., 8 (1964) 310–311.

POTENTIOMETRIC ACID–BASE TITRATIONS IN MOLTEN SALTS
THE ACID CHARACTER OF GROUP V OXIDES AS INFERRED FROM THEIR REACTION WITH MOLTEN KNO_3

The acid characters of P_2O_5, As_2O_5, and V_2O_5 were compared on the basis of their reaction with fused KNO_3 at 350°. The attack on the nitrate was found to decrease in the series $P_2O_5 > As_2O_5 > V_2O_5$. The products of these reactions were determined by conducting *in situ* potentiometric acid–base titrations using an oxygen electrode as indicator electrode and Na_2O_2 as titrant. In principle, the three pentoxides reacted with the nitrate melt in a similar fashion to yield the corresponding meta-salts. Meta-vanadate is, however, a strong Lux acid which directly attacks the base electrolyte to yield pyro-vanadate. Similarly, the controlled neutralization of meta-phosphate and meta-arsenate with Na_2O_2 gives rise to the corresponding pyro-salts. All pyro-compounds react with Na_2O_2 to yield the ortho-salts.

The neutralization of KH_2AsO_4 in molten potassium nitrate occurs in two successive steps due to the formation of the di- and tri-sodium salts.

Acidity (basicity) numbers and equilibrium constants of the different oxy-anions have been determined. On the basis of these figures, the different oxy-anions are arranged in the descending order of their strength as:

$$VO_3^- > PO_3^- > AsO_3^-$$
$$V_2O_7^{4-} > P_2O_7^{4-} > As_2O_7^{4-}$$
$$H_2PO_4^- > H_2AsO_4^-$$
$$HPO_4^{2-} > HAsO_4^{2-}$$

A. M. SHAMS EL DIN, A. A. EL HOSARY AND A. A. A. GERGES,
J. Electroanal. Chem., 8 (1964) 312–323.

THE POLAROGRAPHY OF THE NICKEL(II)–ETHYLENEDIAMINE SYSTEM*

II. EFFECTS OF VARIATION OF ETHYLENEDIAMINE CONCENTRATION

HARRY B. MARK, JR.

Department of Chemistry, The University of Michigan, Ann Arbor, Michigan (U.S.A.)

(Received April 13th, 1964)

INTRODUCTION

A previously reported study[1] showed that the polarographic reduction of $Ni(H_2O)_6^{2+}$, in the presence of small amounts of ethylenediamine, exhibits a small pre-wave before the main metal ion wave. The general characteristics of this pre-wave were similar to those reported for the reduction of Ni^{2+} in the presence of certain aromatic organic compounds containing basic nitrogen such as pyridine[1,2] and *o*-phenylenediamine[1,3,4] in aqueous solution, and in the presence of chloride ion in acetonitrile[5]; the ethylenediamine pre-wave arises, however, at a somewhat more negative potential. It is believed that these pre-waves are probably the result of the reduction of mixed Ni^{2+} complexes formed with these added species and the differences in the pre-wave potentials are considered to be the result of differences in the stability constant of the complexes[1].

It has also been reported that on increasing the concentration of a weak complexing agent such as pyridine[6,7], chloride[5,7], and *o*-phenylenediamine[4] so that it is in excess with respect to the Ni^{2+} ion concentration, the entire Ni^{2+} reduction wave shifts to the more positive reduction potential of the pre-wave. This would not be expected to occur, however, with excess of a strong complexing agent, such as ethylenediamine. Usually, the formation of a stable complex is expected to shift the reduction potentials of the central metal ion to more negative potentials[8]. For example, no wave is observed for the reduction of Ni^{2+} in the presence of an excess of tartrate ion[7] which forms complexes with Ni^{2+} of only slightly higher stability than ethylenediamine[5]. Thus, it was of interest to study the characteristics of the polarographic reduction of Ni^{2+} as a function of ethylenediamine concentration to determine if the reduction potential undergoes a second shift (in this case to more negative potentials) as the concentration of ethylenediamine is increased.

It was of interest also to attempt to characterize the nature of the electro-active species in the reduction reaction taking place at the more positive potentials corresponding to the pre-wave. DANDOY AND GIERST[9] showed that, in a non-complexing media, $Ni(H_2O)_6^{2+}$ itself was electro-inactive and the mechanism involved a slow

* Presented at *The 146th Meeting of the American Chemical Society, Analytical Chemistry Division*, Chicago, Illinois, September 1964.

dehydration reaction to produce the electro-active species, $Ni(H_2O)_x^{2+}$:

$$\begin{array}{c} Ni(H_2O)_6^{2+} \xrightarrow{\text{slow}} Ni(H_2O)_x^{2+} + (6-x)H_2O \\ \text{fast} \downarrow 2e \\ Ni^\circ + xH_2O \end{array} \qquad (1)$$

NELSON AND IWAMOTO[5], in their study of the effect of chloride ion on the Ni^{2+} reduction in acetonitrile, concluded also that the rate-determining step in the electrode mechanism was a dehydration reaction to form the electro-active species; this reaction was accelerated by the presence of Cl^-. They noted that CONNICK[10] had demonstrated that the introduction of a foreign ligand in the primary solvation sphere of certain metal ions dramatically increased the lability of the remaining water molecules of the hydration sphere. They suggested, therefore, that the effect of Cl^- in shifting the reduction potential to more positive values was simply the result of the increase in the rate of the dehydration reaction by formation of a mixed complex to give the electro-active species:

$$\begin{array}{c} Ni(H_2O)_yCl_{6-y} \xrightarrow{\text{fast}} Ni(H_2O)_x \cdots Cl_{6-y} + (y-x)H_2O \\ \text{fast} \downarrow 2e \\ Ni^\circ + xH_2O + (6-y)Cl^- \end{array} \qquad (2)$$

(They did not consider whether the Cl^- ions remained in the first co-ordination sphere of the electro-active species).

A recent study of the Ni(II)–*o*-phenylenediamine system[4] suggested another possible type of electro-active species in complexing media. The ultra-violet and visible spectra of the Ni(II)–*o*-phenylenediamine system indicated that a small amount of a tetrahedral Ni^{2+} complex was forming in the bulk of the solution. This data, coupled with the fact that $NiCl_4^{2-}$ (thought by some investigators to be the more easily reduced species in aqueous chloride media[11,12]) is also a tetrahedral complex[13,14], indicates that the pre-waves may correspond to the reduction of a tetrahedral complex. It was suggested that the orbital configuration of the tetrahydral complex might be more closely analogous to that of the activated reduction intermediate than the orbital configuration of the octahedral $Ni(H_2O)_6^{2+}$ complex; this would result in the lowering of the activation energy of the reaction. The following mechanism could be considered:

$$\begin{array}{c} Ni(H_2O)_6^{2+}\text{ (octahedral)} + yL \xrightarrow{\text{fast}} Ni(H_2O)_xL_y\text{ (tetrahedral)} + (6-x)H_2O \\ \text{fast} \downarrow 2e \\ Ni^\circ + xH_2O + yL \end{array} \qquad (3)$$

where L is the added ligand. If a tetrahedral form of Ni(II) is the electroactive species in complexing media, this might also be true of the reaction in non-complexing media (eqn. (1)). The species $Ni(H_2O)_x^{2+}$ proposed by DANDOY AND GIERST[9] might also be a tetrahedral complex.

It was impossible previously to distinguish between the two proposed mechanisms (represented by eqns. (2) and (3)) in the studies of Ni^{2+} in the presence of the weak complexing agents, Cl^- [5], pyridine[1], and *o*-phenylenediamine[4]. The stability constants of the species in aqueous media are sufficiently small to ensure that the mixed

complex is present in only small concentration. Furthermore, these mixed complexes appear to be very labile[1,4] so that it is impossible to say with any certainty that the tetrahedral complex is the electroactive species even if it does exist in large amounts in the bulk of the solution. For the Ni(II)-ethylenediamine system, however, there is the possibility of distinguishing between the two reaction mechanisms, as these complexes are quite stable[15] and relatively inert to the displacement of the ethylenediamine. As the species corresponding to the pre-wave in this system is probably the same as that existing in the bulk of the solution (probably a 1:1 Ni(II):ethylenediamine complex under conditions where $[Ni^{2+}] \gg [en]$), ultra-violet and visible spectral studies would show if this complex exhibits tetrahedral character. The results of the electrochemical and spectrophotometric study of this system are reported in this paper.

EXPERIMENTAL

The dropping mercury electrode (D.M.E.) used in these experiments had a drop time of 3.10 sec at a height of 62.8 cm of mercury in 0.1 *M* KCl with no applied potential. Under these conditions, the outflow of mercury was 2.25 mg/sec. A saturated calomel electrode (S.C.E.) was used as the reference electrode, and its electrical contact with the sample solution in the polarograph cell was made through an agar-agar KCl bridge.

The polarograms were obtained with a Leeds and Northrup Type E Electrochemograph with no damping. The ultra-violet and visible spectral data were obtained with a Beckmann Model DB recording spectrophotometer using matched 1-cm silica cells.

The ethylenediamine was purified by recrystallization from concentrated hydrochloric acid. All other solutions were prepared with reagent-grade chemicals and deionized water.

All polarograms reported in this paper are drawn as the maximum current attained during drop life. All solutions were de-aerated with nitrogen gas purified according to standard practice[16]. The Ca^{2+} ion was added to the Ni^{2+} solutions as a maximum suppresor[1,17,18] for the $Ni(H_2O)_6^{2+}$ wave. Its presence did not affect the characteristics of the pre-wave but did increase its definition by decreasing the rate of rise of the foot of the background wave. The polarograph cell was thermostated and all experiments were run at 25° ± 0.1.

RESULTS AND DISCUSSION

The effect of ethylenediamine concentration, over the range 0–2.1×10^{-2} *M*, on the polarograms of 2.4×10^{-3} *M* $Ni(Ac)_2$, 4.8×10^{-3} *M* $Ca(Ac)_2$, and 0.10 *M* KAc solutions are shown in Figs. 1 and 2. The pH of the solutions was 6.8 ± 0.1. Figure 1 shows that as the concentration of ethylenediamine is increased to $\sim 8.6 \times 10^{-4}$ *M*, a pre-wave, the current of which increases with ethylenediamine concentration in a non-linear manner, is observed to arise before the main $Ni(H_2O)_6^{2+}$ background wave. The characteristics of this pre-wave, such as wave shape and the fact that its "limiting" current is not proportional to concentration of ethylenediamine, are very similar to those observed for the pre-waves obtained for Ni(II) reduction in aqueous solution in the presence of pyridine[1,2] and *o*-phenylenediamine[3,4], and in the presence of Cl^- in acetonitrile media[5]. The magnitude of the current, i_p, of the pre-wave at −0.90*V* *vs.* S.C.E. (the current was measured at this potential just prior to the onset

of the $Ni(H_2O)_6^{2+}$ reduction to eliminate the necessity for any correction resulting from the competing reductions of both the complex and $Ni(H_2O)_6^{2+}$ which occurs at more negative potentials[1]) appears to be catalytic in nature with respect to ethylenediamine concentration for [en] less than about $4 \cdot 10^{-4}$ M. For example, the value of i_p obtained for a 1.7×10^{-4} M ethylenediamine concentration in a 2.4×10^{-3} M Ni^{2+} solution was 2.5 μA. The expected diffusion-controlled current would be about

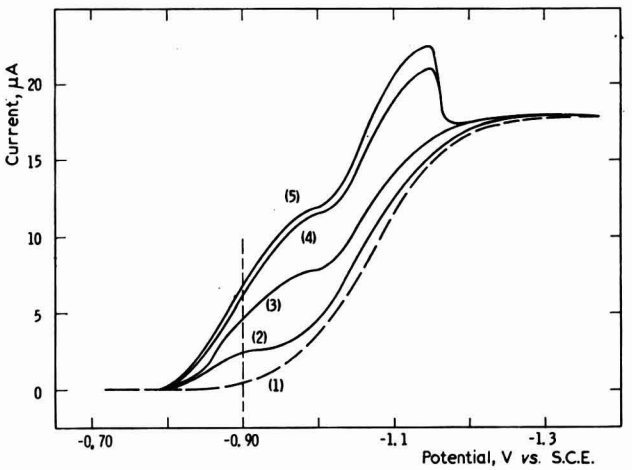

Fig. 1. Effect of ethylenediamine concn. on the polarograms of Ni(II), ([en]:[Ni^{2+}] < 0.5). [Ni^{2+}], 2.4×10^{-3} M; [Ca^{2+}], 4.8×10^{-3} M; [KAc], 0.10 M; pH, 6.8. [en]: curve 1, 0 M; curve 2, 1.7×10^{-4} M; curve 3, 3.4×10^{-4} M; curve 4, 5.1×10^{-4} M; curve 5, 8.5×10^{-4} M.

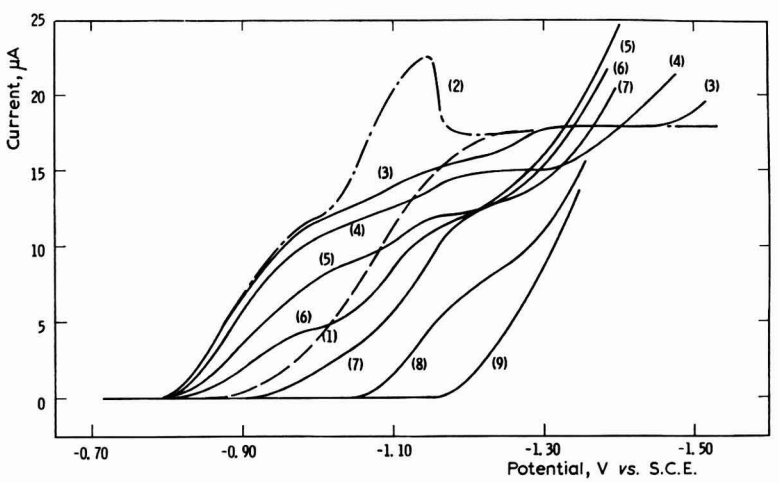

Fig. 2. Effect of ethylenediamine concn. on the polarograms of Ni(II), ([en]:[Ni^{+}] > 0.5). [Ni^{2+}], 2.4×10^{-3} M; [Ca^{2+}], 4.8×10^{-3} M; [KAc], 0.10 M; pH, 6.8. [en]: curve 1, 0 M; curve 2, 8.5×10^{-4} M; curve 3, 1.7×10^{-3} M; curve 4, 2.1×10^{-3} M; curve 5, 3.4×10^{-3} M; curve 6, 4.3×10^{-3} M; curve 7, 5.6×10^{-3} M; curve 8, 8.6×10^{-3} M; curve 9, 2.1×10^{-2} M; curves 1 and 2 are the same as in Fig. 1.

1.2 μA (this is assumed to be the same as the diffusion-controlled limiting current of a $Ni(H_2O)_6^{2+}$ solution of the same concentration). The magnitude of catalytic enhancement of the pre-wave current is approximately the same as that reported in a previous study[1]. The catalytic reaction mechanism is presumably the same as that suggested for the Ni(II)–pyridine[1] and -*o*-phenylenediamine pre-waves[4] where the electroactive species is a mixed complex of unknown composition.

$$Ni(en)_1(H_2O)_x^{2+} \overset{2e}{\rightarrow} Ni^\circ + en + x\,H_2O \qquad (4)$$

$$Ni(H_2O)_6^{2+} + en \rightarrow Ni(en)_1(H_2O)_x^{2+} + (6 - x)H_2O \qquad (5)$$

As the concentration of ethylenediamine is increased from $4 \cdot 10^{-4}$ to about $9 \cdot 10^{-4}$ *M*, the rate of change of i_p with [en] decreases sharply, and at [en] = $9 \cdot 10^{-4}$ *M*, i_p is approximately equal to the value of the diffusion-controlled current for the reduction of a 1:1 Ni(II):ethylenediamine complex. Also, a polarographic maxima is observed in this concentration range.

As the concentration of ethylenediamine is increased beyond $9 \cdot 10^{-4}$ *M*, a sharp change occurs in the characteristics of the polarograms, as shown by the curves of Fig. 2. The polarographic maximum disappears and the magnitude of the pre-wave begins to decrease. Also, a new wave starts to appear which has a half-wave potential of about −1.15 V *vs.* S.C.E. and does not appear to correspond to the reduction of $Ni(H_2O)_6^{2+}$ (which has a half-wave potential of about −1.06 V *vs.* S.C.E. under these conditions). The magnitude of this second wave increases as the ethylenediamine concentration increases to about $6 \cdot 10^{-3}$ *M*. In this same concentration range the magnitude of the pre-wave decreases essentially to zero. With further increase of ethylenediamine concentration above $6 \cdot 10^{-3}$ *M*, the magnitude of the second wave begins to decrease and is essentially zero at [en] = 2.1×10^{-2} *M*. At this point, curve (9) of Fig. 2, only a background wave is observed. Ni(II) has been converted to a complex, presumably $Ni(en)_3^{2+}$, which because of its large stability constant is reduced at potentials more negative than that of the reduction of the medium itself.

Thus, polarography indicates that there are at least four species of Ni(II) formed in this system below an ethylenediamine concentration of $2 \cdot 10^{-2}$ *M*: species (I) corresponding to the Ni(II) wave in the absence of ethylenediamine; species (II) corresponding to the pre-wave (see Fig. 1); species (III) corresponding to the wave at −1.15 V *vs.* S.C.E. (see Fig. 2); species (IV) corresponding to the "non-reducible" form of Ni(II).

In order to determine the nature of the species present in the bulk of the solution at different concentrations of ethylenediamine, the visible and ultra-violet spectra of 0.044 *M* $Ni(Ac)_2$, 0.088 *M* $Ca(Ac)_2$, and 0.10 *M* KAc (pH = 6.8) solutions containing 0–0.16 *M* ethylenediamine were determined. The resulting spectra are shown in Fig. 3. When the ratio of [en]:$[Ni^{2+}]$ is less than 1:1, the spectra (curves 1–3) show a peak growing at about 640 mμ and a slight shift of the peak in the 400 mμ range to shorter wave lengths without any appreciable change in its molar absorptivity. This change in the spectra probably corresponds to the formation of a 1:1 Ni(II):ethylenediamine complex. When the ratio of [en]:$[Ni^{2+}]$ is greater than 1:1 but less than 2:2 (curves 4 and 5) both peaks of the spectrum have shifted to shorter wave lengths and both show increases in the molar absorptivity, which indicates that a 1:2 Ni(II):ethylenediamine complex is probably forming, as would be expected from the magnitude of the

stability constant of the 1:2 complex[15]. The increase of ethylenediamine concentration to 0.16 M (in excess of a 3:1 [en]:[Ni^{2+}] ratio) results in a spectrum (curve 6) which is identical to those reported by ROBERTS AND FIELD[18] and JØRGENSEN[19] for the $Ni(en)_3^{2+}$ complex, which again would be expected from the magnitude of the $Ni(en)_3^{2+}$ stability constant[15].

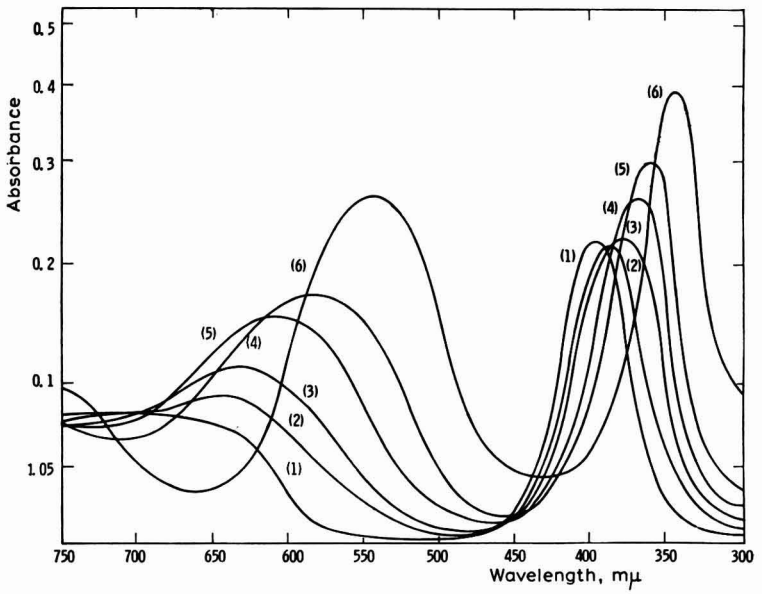

Fig. 3. Ultra-violet and visible absorption spectra of 0.044 M $Ni(Ac)_2$ and 0.088 M $Ca(Ac)_2$ in 0.10 M KAc in the presence of ethylenediamine. pH, 6.8 ± 0.1. [en]: curve 1, 0 M; curve 2, 0.01 M; curve 3, 0.02 M; curve 4, 0.04 M; curve 5, 0.06 M; curve 6, 0.16 M.

CONCLUSIONS

Calculations based on the successive stability constants of the Ni(II)–ethylenediamine complexes, $pK_1 = 7.6$, $pK_2 = 6.5$, $pK_3 \simeq 4.6$[15] show that a 1:1 nickel:ethylenediamine complex is, as expected, is the predominant species in the solution for concentration ratios of [en]:[Ni^{2+}] less than 1. Similarly the 1:2 complex predominates in the concentration region where [en]:[Ni^{2+}] is greater than 1 but less than 2, and the 1:3 complex is the predominant species when the concentration ratio exceeds about 2.5:1. The spectral data given, support these calculations. Thus, the concentration ratio region where the catalytic pre-wave is observed ([en]:[Ni^{2+}]$<$1) also corresponds qualitatively with the same concentration region where the $Ni(en)_1^{2+}$ form of Ni^{2+} predominates. As the pK_1 of this complex is large, it can be calculated that essentially all the ethylenediamine is complexed to Ni^{2+}, and it is reasonable to assume, as stated before, that the electroactive species corresponding to the pre-wave is a $Ni(en)_1(H_2O)_x$ mixed complex. As this species is reduced at the D.M.E., the ethylenediamine released by the reaction (eqn. (4)) is available to react with $Ni(H_2O)_6^{2+}$ in the vicinity of the electrode to reform the electroactive species according to eqn.

(5) (as shown by previous study of the ethylenediamine catalytic hydrogen wave[20], some of the ethylenediamine freed by the reduction of the complex is probably actually adsorbed on the mercury surface). As this concentration of $Ni(H_2O)_6^{2+}$ in the bulk of the solution is decreased with respect to $Ni(en)_1(H_2O)_x^{2+}$ (as the ratio of [en]:[Ni^{2+}] increased above 0.5, see curves 3–6 of Fig. 2), the accumulated ethylenediamine at or near the electrode surface will begin to react with the $Ni(en)_1(H_2O)_x^{2+}$ to form a 1:2 Ni(II):ethylenediamine complex which would be expected to be reduced at more negative potentials than the 1:1 complex. Therefore, the wave which begins to appear at −1.15 V *vs.* S.C.E. when the [en]:[N_1^{2+}] ratio becomes larger than ~0.5, probably corresponds to the reduction of a $Ni(en)_2(H_2O)_{x-2}^{2+}$ species.

A similar process is repeated as the concentration of $Ni(en)_2(H_2O)_{x-2}^{2+}$ begins to exceed the concentration of $Ni(en)_1(H_2O)_x^{2+}$. The freed ethylenediamine at the electrode surface begins to react with $(Ni(en)_2(H_2O)_{x-2}$ to form the $Ni(en)_3^{2+}$ complex which is reducible only at potentials more negative than the background reduction. Hence, the magnitude of the wave at −1.15 V *vs.* S.C.E. begins to decrease as the ratio of [en] : [Ni^{2+}] increases above 2.5 (see curve 8 of Fig. 2). When the ethylenediamine concentration is increased to a ten-fold excess (see curve 9), the Ni^{2+} in the bulk of the solution is essentially completely in the $Ni(en)_3^{2+}$ form which does not exhibit a wave.

The fact that a slight wave corresponding to the $Ni(en)_1(H_2O)_x^{2+}$ reduction is observed even when the ratio [en]:[Ni^{2+}] is 2–2.5 (see curves 6 and 7) can be explained by considering that the equilibrium

$$Ni(en)_2(H_2O)_{x-2}^{2+} + 2H_2O \underset{k_b}{\overset{k_f}{\rightleftarrows}} Ni(en)_1(H_2O)_x^{2+} + en \qquad (6)$$

(although shifted to the left) is established in the solution. As the potential reaches the reduction potential of the 1:1 complex and the equilibrium concentration of the 1:1 complex is reduced, depleting its concentration at the electrode surface, the rate of the dissociation reaction of the 1:2 complex, k_f, is probably sufficiently large to shift the equilibrium to the right, thus providing additional 1:1 complex in the diffusion layer at the electrode. The wave is therefore much larger than would be anticipated from a calculation of the equilibrium concentration of the electroactive species in the system under the above concentration conditions. Such behavior, is typical of a reaction where a rapid equilibrium is established in the bulk of the solution between an electroactive and non-electroactive species[21].

It is interesting to note that the spectra of the Ni^{2+} solutions obtained when the ratio [en]:[Ni^{2+}] is 1 or less (curves 1–4 of Fig. 3) are almost identical with those reported previously for the same concentration ratios for the Ni(II)–*o*-phenylenediamine system. Thus, the orbital configuration of the central Ni(II) ion of the complexes in the bulk of the solution is essentially the same for both systems. This substantiates the theory that the resulting change in the orbital configuration of the central atom on complexation is responsible for the decrease in the activation overpotential[4,22]. However, this does not exclude the possibility that the overpotential change results from the increased lability of the remaining water molecules in the complex[5]. It does tend to rule out, however, the speculation that the spectral change in the *o*-phenylenediamine case was the result of the formation of a small

fraction of a tetrahedral Ni(II) complex which had a large molar absorptivity coefficient[4]. Because the ethylenediamine added to excess Ni^{2+} solutions can be considered to be about 100% associated (no data on the stability constants of Ni–*o*-phenylenediamine complex could be found in the literature so no calculation was possible in that case) as a 1:1 complex under these conditions[1,20], the spectral changes in the Ni(II)–ethylenediamine system cannot be the result of formation of a tetrahedral complex. The molar absorptivity for the observed complex in the 640 mμ region is only slightly greater than that of $Ni(H_2O)_6^{2+}$ and much smaller than that expected for a tetrahedral complex ($\sim$100 times that of the $Ni(H_2O)_6^{2+}$ complex[14]). Further investigation of the spectra of mixed ligand–Ni(II) complexes is now in progress to determine if there is any correlation in all cases between the spectra and the decrease in the activation overpotential.

ACKNOWLEDGEMENT

Acknowledgement is made to the donors of the Petroleum Research Fund, administered by the American Chemical Society, for partial support of this research.

SUMMARY

The effect of variation of ethylenediamine concentration from 0–2.1 $\times$ 10^{-2} M on the polarography of 2.4 $\times$ 10^{-3} M Ni^{2+} solutions is studied. Two new waves are observed over this concentration range; a pre-wave arising before the $Ni(H_2O)_6^{2+}$ wave for low concentrations of ethylenediamine, and a wave occurring at a slightly more negative potential than the $Ni(H_2O)_6^{2+}$ wave for intermediate ethylenediamine concentrations. At high concentration of ethylenediamine, the Ni^{2+} wave is not observed. The nature of the species and reactions corresponding to these waves is described. The visible and ultra-violet spectra of the system are also reported for the same ratios of Ni^{2+}: ethylenediamine concentrations and are compared with the spectra obtained for the Ni(II)–*o*-phenylenediamine system which also exhibits a pre-wave.

REFERENCES

1 H. B. MARK, JR. AND C. N. REILLEY, *Anal. Chem.*, 35 (1963) 195.
2 H. B. MARK, JR. AND C. N. REILLEY, *J. Electroanal. Chem.*, 4 (1962) 189.
3 H. B. MARK, JR., *Anal. Chem.*, 36 (1964) 940.
4 H. B. MARK, JR., *J. Electroanal. Chem.*, 7 (1964) 276.
5 I. V. NELSON AND R. T. IWAMOTO, *J. Electroanal. Chem.*, 6 (1963) 234.
6 J. J. LINGANE AND H. KERLINGER, *Ind. Eng. Chem., Anal. Ed.*, 13 (1941) 77.
7 I. M. KOLTHOFF AND J. J. LINGANE, *Polarography*, Vol. 2, Interscience Publishers Inc., New York, 2nd ed., 1962, pp. 486–488.
8 I. M. KOLTHOFF AND J. J. LINGANE, *Polarography*, Vol. 1, Interscience Publishers Inc., New York, 2nd ed., 1952, chap. XII.
9 J. DANDOY AND L. GIERST, *J. Electroanal. Chem.*, 2 (1961) 116.
10 R. E. CONNICK, T. J. SWIFT AND E. E. GENSER, paper presented at *The 142nd Meeting of the American Chemical Society, Inorganic Division*, Atlantic City, N. J., September 1962, Abstracts p. N22.
11 A. A. VLČEK, *Z. Elektrochem.*, 61 (1957) 1014.
12 U. TANAKA, R. TAMAMUSHI AND M. KODAMA, *Bull. Chem. Soc., Japan*, 33 (1960) 14.
13 D. M. GRUEN AND R. L. MCBETH, *J. Phys. Chem.*, 63 (1959) 393.
14 W. MANCH AND W. C. FERNELIUS, *J. Chem. Educ.*, 38 (1962) 192.
15 J. BJERRUM, G. SCHWARZENBACH AND L. G. SILLÉN, *Stability Constants*, Part I, *Organic Ligands*, Chem. Soc., London, 1956.

16 L. MEITES, *Polarographic Techniques*, Interscience Publishers Inc., New York, 1955, pp. 32–34.
17 N. V. EMELIANOVA AND J. HEYROVSKÝ, *Trans. Faraday Soc.*, 24 (1928) 257.
18 G. L. ROBERTS AND F. H. FIELD, *J. Am. Chem. Soc.*, (1950) 4233.
19 C. K. JØRGENSEN, *Acta Chem. Scand.*, 8 (1954) 1495.
20 H. B. MARK, JR. AND H. G. SCHWARTZ, JR., *J. Electroanal. Chem.*, 6 (1963) 443.
21 I. M. KOLTHOFF AND J. J. LINGANE, *Polarography*, Vol. 1, Interscience Publishers Inc., New York, 2nd ed., 1952, chap. XV.
22 F. C. ANSON, *J. Electrochem. Soc.*, 110 (1963) 436.

POLAROGRAPHIC STUDY OF METAL COMPLEXES

VII[a]. TETRACYANO-MONO(ETHYLENEDIAMINE)COBALTATE(III) COMPLEX[b]

NOBUFUMI MAKI AND KUWAKO OKAWA[c]

Radiation Centre of Osaka Prefecture, Shinke-cho, Sakai, Osaka (Japan)

(Received April 8th, 1964)

Several kinds of cyano-cobalt(I) complexes have been described previously. HUME AND KOLTHOFF[2] were the first to report that the cobalt(II) or cobalt(III) ion in cyanide medium $[Co^{II}(CN)_5OH_2]^{3-}$ and $[Co^{III}(CN)_5OH_2]^{2-}$, was reduced irreversibly to a cobalt(I) state at the dropping mercury electrode (D.M.E.). Following this most of the pentacyanocobaltate(III) complexes of the $[Co^{III}(CN)_5X]$-type were found to be irreversibly reduced in one or two steps to the cobaltate(I) complexes in aqueous solution at the D.M.E., where the unidentate ligand, X denotes the ion, Cl^-, Br^-, I^-, SCN^-, NO_2^-, $S_2O_3^{2-}$, N_3^-, SO_3^{2-} or the molecule, H_2O, NH_3[2,3].

GRIFFITH AND WILKINSON[4] suggested, as a result of nuclear magnetic resonance measurements, that the cyano-cobalt(I) complex may have the formula, $[H\,Co^{I}(CN)_5]^{3-}$ or $[Co^{I}H(CN)_4]^{2-}$, in solution. Attempts to isolate these cyano-cobaltate(I) complexes have not yet been successful[5]. For example, when ethanol was added to isolate them from solution, Adamson's salt, $K_6[Co_2^{II}(CN)_{10}]$, precipitated and hydrogen was evolved[6].

On the other hand, WATT AND THOMPSON[7] have succeeded in isolating the complex $K_3[Co^{I}(CN)_4]$, as a pale yellow solid by reduction of the hexacyanocobaltate(III) complex, $K_3[Co(CN_6]$, in liquid ammonia with metallic potassium. The complex is very unstable; at room temperature the color of the complex changes to reddish-brown. In the presence of a trace of air, the complex decomposes rapidly leaving a black solid.

Previously, the tetracyano-complex, $Na_5[Co^{III}(CN)_4(SO_3)_2]$, had also been found to reduce directly to a cobaltate(I) complex in 0.5 *M* sodium sulphite solution at the D.M.E.[1].

The present communication deals with the polarography of the tetracyano-cobaltate(III) complex of the *cis*-type, $K[Co^{III}(CN)_4\,en] \cdot H_2O$ or $Na[Co^{III}(CN)_4en] \cdot 3.5\,H_2O$.

EXPERIMENTAL

Sodium tetracyano-mono(ethylenediamine)cobaltate(III) was prepared by the follow-

[a] For previous paper of this series, see ref. 1.

[b] Presented at *The 10th Symposium on Polarography*, held in Nagoya University, Nagoya, Japan, November 5–7, 1963.

[c] Address: Department of Chemistry, Osaka University, Kita-ku, Osaka, Japan.

ing series of reactions[8,9].

$$cis\text{-}NH_4[Co(NH_3)_4(OSO_2)_2] \cdot 3\ H_2O \xrightarrow{en} cis\text{-}NH_4[Co(NH_3)_2en(OSO_2)_2] \cdot 2\ H_2O$$

$$\xrightarrow{\text{dry HCl gas}} trans\text{-}[Co(NH_3)_2en\ Cl_2]\ Cl \cdot H_2O \text{(in 50\% methanol)}$$

$$\xrightarrow{Na_2S_2O_3 \cdot 5H_2O} [Co(NH_3)_2en(S_2O_3)_2]^- \text{ (not isolated from the soln.)}$$

$$\xrightarrow{4\ NaCN} Na[Co(CN)_4en] \cdot 3.5\ H_2O \text{ (pale yellow).}$$

Dry hydrogen chloride gas was passed through the 50% methanolic solution in which the complex compound, $NH_4[Co(NH_3)_2en(OSO_2)_2 \cdot 2\ H_2O$[10] was suspended and the solution was then allowed to stand for 12 h. Lusterous green crystals of the praseo-salt, $[Co(NH_3)_2en\ Cl_2]Cl \cdot H_2O$, which were slowly deposited, were filtered and washed with 80% hydrochloric acid and then with 95% ethanol. By concentrating the mother liquor on a water bath (the temperature of the solution must not exceed 55°), more of the praseo-salt was obtained. The total yield was about 65 ~ 70%. For preparation on large scale, the 50% methanolic solution is finally allowed to come to boiling point. The concentration of methanol must then be kept up to some extent and the addition of an appropriate amount of methanol is the key-point for obtaining the praseo-salt in better yield in this preparation.

10 g of the praseo-salt, $[Co(NH_3)_2\ en\ Cl_2]Cl \cdot H_2O$, was dissolved in 200 ml of water and a solution of 18.5 g sodium thiosulphate, $Na_2S_2O_3 \cdot 5\ H_2O$ in 200 ml of water, was added. The mixture was warmed gently for a few minutes on the water bath (60°); the colour of the solution should then be brownish-violet. A solution of 7.3 g of sodium cyanide dissolved in 100 ml of water was added to this solution drop by drop. The colour of the solution changed gradually from red to orange-yellow. The solution was heated again gently for a time on the water bath (45°), cooled and filtered. The filtrate was concentrated on the water bath to a volume of 200 ml; then a solution of 9.1 g barium chloride, $BaCl_2 \cdot 2\ H_2O$, dissolved in 100 ml of hot water was added drop by drop. After cooling, the precipitates of $BaS_2O_3 \cdot H_2O$, was filtered off. On concentrating the filtrate, yellow crystals, $Na[Co(CN)_4en] \cdot 3.5\ H_2O$, were obtained. The crude product was dissolved in cold water and reprecipitated with 95% ethanol. After this purification procedure had been repeated four times, the aqueous solution containing the complex was concentrated in a vacuum desiccator containing concentrated sulphuric acid. Pale yellow needle crystals were obtained.

Calcd. for $Na[Co(CN)_4en]$: Co, 23.95; C, 29.28; N, 34.15; H, 3.28; Na, 9.34%.
Found: Co, 23.55; C, 28.74; N, 34.59; H, 3.23; Na, 9.98%.

Yellow needle-crystals of potassium cobaltate(III) were obtained in a similar manner by using potassium cyanide and potassium thiosulphate in place of the sodium salts. The water of crystallization was lost completely after 24 h in a vacuum desiccator containing concentrated sulphuric acid. Both complexes are very soluble in water, less soluble in methanol and almost insoluble in ethanol.

Calcd. for $K[Co(CN)_4en]$: Co, 22.48; C, 27.48; N, 32.05; H, 3.08; K, 14.91%.
Found: Co, 22.03; C, 26.86; N, 32.39; H, 3.22; K, 15.11%.

Apparatus

A Yanagimoto Polarograph model PA 102 was used to record d.c. polarograms. For determining the half-wave potential and other precise data, a Shimadzu Potentiometer model K-2 was used for the applied potential; this potentiometer is able to measure accurately, potentials as small as 10^{-6} V. Current–potential curves were determined manually. The oscillopolarogram of $dE/dt \sim E$(potential) curves were obtained by Polaroscope model P576 (Heyrovský-Forejt type).

All the polarographic measurements were carried out with an H-type cell. The cell solution was connected to the saturated calomel electrode (S.C.E.) through a glass filter (G4) and was kept at a temperature of 25 $\pm$0.1° by a water thermostat. The internal resistance between the cathode (D.M.E.) and the mercury pool anode was kept within 550 Ω. The rate of flow of mercury (m) and drop-time (t) of the capillary were measured in an aqueous solution of 0.5 M sodium sulphate at an open circuit with a mercury head of 68 cm.

RESULTS AND DISCUSSION

The ion, $[Co^{III}(CN)_4en]^-$, gave rise to well-defined waves of two steps in 0.5 M sodium sulphate solution containing 2 M ethylenediamine at the D.M.E. The ratio of the height of the first wave to that of the second was roughly 2:1. The first wave, corresponding to an acceptance of two electrons, represents the reduction of cobalt (III) to cobalt(I), and the second, corresponding to a gain of one electron, represents the reduction to the metal. The limiting current of both the waves is proportional to

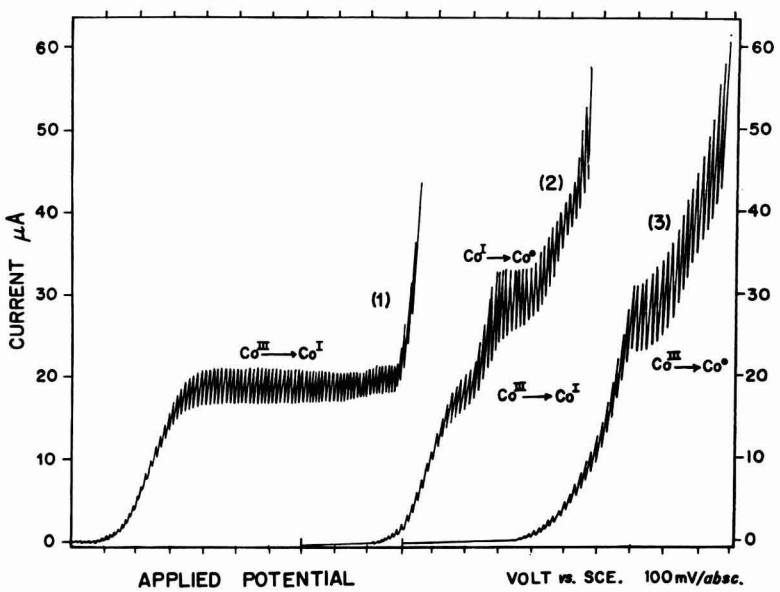

Fig. 1. D.c. polarograms of cyano-cobaltate(III) complexes obtained at a concn. of $5 \cdot 10^{-3}M$ /l (25°). (1) $K[Co^{III}(CN)_2dg_2] \cdot 3/2\ H_2O$, in 0.5 M Na_2SO_4 aq. soln., recorded from −0.90 V *vs.* S.C.E.; (2), $Na[Co^{III}(CN)_4en] \cdot 3.5\ H_2O$, in 0.5 M Na_2SO_4 + 2 M en + 0.0078% Triton X 100, recorded from −1.00 V *vs.* S.C.E.; (3), $Na[Co^{III}(CN)_4en] \cdot 3.5\ H_2O$, in 0.5 M Na_2SO_4 aq. soln., recorded from −0.50 V *vs.* S.C.E.

the concentration of the complex in the range 10^{-2}–10^{-4} M and is diffusion-controlled.

In Fig. 1 are shown the d.c. polarograms for this complex in the presence and absence of ethylenediamine; they are compared with the two electron reduction wave of dicyano-bis(dimethylglyoximato)-cobaltate(III) complex, $K[Co^{III}(CN)_2dg_2] \cdot 3/2\ H_2O$. Each wave height is seen to be proportional to the electron numbers of the reduction process.

The solution without ethylenediamine gave only one wave, corresponding to a three-electron reduction. According to the oscillopolarogram (Fig. 2), however, the apparently direct reduction to the metal can be seen to take place in two stages from the two cut-ins on the cathodic branch.

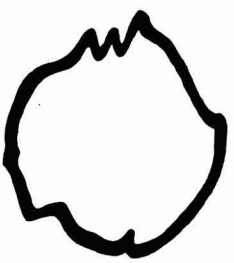

Fig. 2. The oscillopolarogram ($dE/dt \sim E$ curve) of the complex, $K[Co(CN)_4en] \cdot H_2O$, obtained at a concn. of $5 \cdot 10^{-3}$ M/l in 0.5 M Na_2SO_4 aq. soln. (25°).

These results imply that the cobaltate(II) or cobaltate(I) ion is fairly unstable in aqueous solution due to aquation of the complex.

The overall processes of the electrode reaction given below are considered to be the most plausible:

$$[Co^{III}(CN)_4(en)]^- \xrightarrow{e} [Co^{II}(CN)_4(en)]^{2-} \underset{(A)}{\xrightarrow{e}} [Co^{I}(CN)_4(en)]^{3-}$$
$$\downarrow (B) \qquad\qquad \downarrow \leftarrow e$$
$$[Co^{II}(CN)_4(OH_2)_2]^{2-} \text{ etc.} \xrightarrow{2\,e} Co(\text{metal})$$
(aquated species)

The reaction takes place in the two ways. Under experimental conditions where the aquation of the cobalt(II) ion is prevented, the reaction proceeds mainly along path(A) rather than along path(B). Otherwise, the aquated cobalt(II) ions would be all reduced directly to the metal and not through the cobalt(I) state[11].

Thus, the tetracyano-mono(ethylenediamine)cobaltate(I) complex is reduced to the metal, a result which is different from that for the disulphono-tetracyanocobaltate(I) complex. This is considered to be caused by the unstable structure of *cis*-form, since the electronic structure of cobalt(I) complexes is quite similar to that of nickel(II) complexes. The resulting cobaltate(I) complex was presumed to have the hexaco-ordinate formula, $[Co^{I}(CN)_4(en)]^{3-}$, in solution because the cobalt(I) state could be found only in the presence of excess ethylenediamine and the tetraco-ordinate complex, $K_2[Co^{I}(CN)_4]$, is known to be very unstable[7].

Generally, in the cyano-cobalt(I) complexes, the π-bonding character of the bond, $Co{=}C{=}N^-$, may be considered to play an important role for stabilizing the lower oxidation state of cobalt(I) or cobalt(O) complex in their co-ordination sphere.

First the cyano-ligand, $C{\equiv}N^-$ co-ordinates to the cobalt metal through the carbon atom and forms a σ-bond. Thus, the electron-density in p_π orbitals of the carbon atom decreases and the electron-clouds of the cobalt atom move in a reverse direction towards the p_π orbitals of the carbon atom to compensate for the decrease in the electron-density of carbon atom, *i.e.*, "back co-ordination" takes place.

The electron-transfer mechanism of the electrode reaction may be written by the atomic orbital method[12] as follows:

$$d^2d^2d^2[D^2SP^3] \xrightarrow{e} d^2d^2d^2[D^2SP^3]d^1 \longrightarrow d^2d^2d^2d^1[DSP^2\ PD] \longrightarrow d^2d^2d^2d^2[DSP^2\ PD]$$

On the other hand it can be written by the ligand-field theory[13] as follows (Fig. 3):

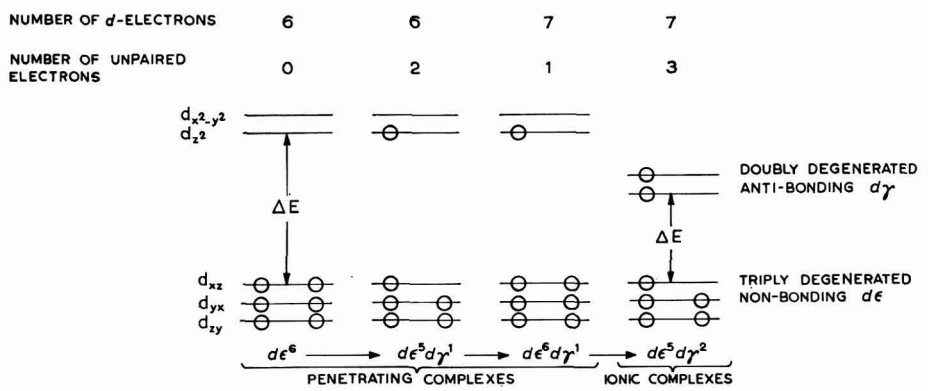

Fig. 3. Electron-transfer mechanism of the electrode reaction, for the hexaco-ordinate octahedral complex(Oh).

$$\text{Co(III)}\ (d\varepsilon^6;{}^1A_{1g}) \longrightarrow \text{Co(III)}\ (d\varepsilon^5d\gamma^1;{}^1T_{1g},{}^1T_{2g},{}^3T_{1g},{}^3T_{2g}) \xrightarrow{e}$$

$$\text{Co(II)}\ (d\varepsilon^6d\gamma^1;{}^2E_g) \longrightarrow \text{Co(II)}\ (d\varepsilon^5d\gamma^2;{}^4T_{1g})$$

TABLE 1

HALF-WAVE POTENTIALS OF THE CYANO-COBALT(III) COMPLEXES (25°)

Compound	$E_{\frac{1}{2}}$ *of 1st wave* Co(III)→Co(I)	$E_{\frac{1}{2}}$ *of 2nd wave* Co(I)→Co(O)	*Supporting electrolyte*
$Na[Co(CN)_4en] \cdot 3.5\ H_2O$	−1.36[4]	−1.51	0.5 *M* Na_2SO_4 + 2 *M* en 0.0078% Triton X 100[a]
$Na_5[Co(CN)_4(SO_3)_2]$	−1.36	No reduction	0.5 *M* Na_2SO_3
$K_4[Co(CN)_5SO_3] \cdot 2\ H_2O$	−1.53[5]	No reduction	1 *M* KCl

[a] Triton X 100 = Alkyl-aryl-polyether alcohol (Rohm & Haas Inc.).
Voltage unit: V *vs.* S.C.E.; concn. of the complex: $5 \cdot 10^{-3}M$.

The subsequent process is probably analogous to this mechanism.

The reduction type, Co(III)→Co(I)→Co(O) is, so far as we know, the first of its kind to be recorded for the cobalt(III) complexes.

ACKNOWLEDGEMENT

We wish to thank Dr. JUNNOSUKE FUJITA for his support and encouragement throughout this work.

SUMMARY

Tetracyano-mono(ethylenediamine)cobaltate(III) complex, $K[Co^{III}(CN)_4\,en] \cdot H_2O$ (a new compound) was found to be reduced to the metal through the cobaltate(I) complex at the dropping mercury electrode in the presence of ethylenediamine.

In the absence of excess ethylenediamine, the irreversible wave apparently of one step, corresponding to three electron reduction, was obtained in 0.5 *M* sodium sulphate solution. The oscillopolarogram, however, indicated that the reaction proceeds in two stages. This phenomenon was considered to be due to the aquation of the complex in solution.

The resulting cobaltate(I) complex was presumed to have the same hexacoordinate formula, $[Co^{I}(CN)_4\,en]^{3-}$, as that of the original cobaltate(III) complex.

Further reduction of the cobaltate(I) complex to the metal was interpreted as being due to the structure of the *cis*-form, compared with that of the $[Co^{III}(CN)_4(SO_3)_2]^{5-}$ ion.

This is the first time that the reduction of a cobalt(III) complex by the path Co(III)→Co(I)→Co(O) has been reported.

REFERENCES

1 N. MAKI AND R. TSUCHIDA, *Bull. Chem. Soc. Japan*, 34 (1961) 891.
2 D. N. HUME AND I. M. KOLTHOFF, *J. Am. Chem. Soc.*, 71 (1949) 867.
3 N. MAKI, J. FUJITA AND R. TSUCHIDA, *Nature*, 183 (1959) 458.
4 W. P. GRIFFITH AND G. WILKINSON, *J. Chem. Soc.*, (1959) 2757.
5 N. MAKI, *Nature*, 195 (1960) 682.
6 W. P. GRIFFITH AND G. WILKINSON, *J. Inorg. & Nucl. Chem.*, 7 (1958) 295.
7 G. W. WATT AND R. J. THOMPSON, *J. Inorg. & Nucl. Chem.*, 9 (1959) 311.
8 K. OKAWA AND J. FUJITA, unpublished.
9 A. WERNER AND H. GRÜGER, *Z. Anorg. Allgem. Chem.*, 16 (1898) 398.
10 J. C. BAILAR, JR. AND D. F. PEPPARD, *J. Am. Chem. Soc.*, 62 (1940) 105.
11 N. MAKI AND H. ITATANI, *Bull. Chem. Soc. Japan*, 36 (1963) 757; bis(2,2'-dipyridyl)cobalt-(III) complexes were also found to show a quite similar electrode process.
12 A. A. VLČEK, *Collection Czech. Chem. Commun.*, 20 (1955) 894.
13 A. A. VLČEK, *Discussions Faraday Soc.*, 26 (1958) 164.

AN ALL-ELECTRONIC SYSTEM FOR THE AUTOMATIC MEASUREMENT OF SLOPES OF REACTION-RATE CURVES

HARRY L. PARDUE AND WILLIAM E. DAHL

Department of Chemistry, Purdue University, Lafayette, Indiana (U.S.A.)

(Received June 18th, 1964)

INTRODUCTION

In a recent paper a method was described for the automatic measurement of reaction rates[2]. The rate measurement is accomplished by matching the slope of the response curve with the output from an electronic integrator (referred to below as the balancing integrator). At balance, the input to the integrator is proportional to the slope of the response curve and under controlled conditions is proportional to the concentration of the rate-determining species.

In the original work a potentiometric recorder was modified to compare the signals from the chemical system and integrator and to adjust the integrator input until the signals are changing at the same rate. In the present work the mechanically linked system is replaced by a completely electronic system which performs the same function. A second electronic integrator detects the difference in outputs from the chemical system and balancing integrator. The output from this second integrator is fed to the input of the balancing integrator in a manner such that a stable condition exists only when the output from the balancing integrator is changing at the same rate as the signal from the chemical system. The output from the second integrator is then proportional to the slope of the response curve.

The new system has been evaluated for the determination of cystine based upon its catalysis of the iodine-azide reaction[3]. It retains the advantages of high precision and accuracy demonstrated by the original method. Its principal advantages are simpler operational features and a potential increase in response speed. Also, the entire measurement circuit is constructed as a plug-on module for commercially available equipment and is therefore more compact.

The method, as described, provides digital readout directly in parts per million cystine in the concentration range from 1–25 p.p.m. Measurements are completed within 15 sec after mixing reagents and samples, yielding results with relative standard deviations less than 1%.

PRINCIPLES OF THE METHOD

Conditions for the potentiometric determination of cystine based on its catalysis of the reduction of iodine by azide have been established[3]. Under these conditions the

time-dependent portion of the cell potential E_t, is related to cystine concentration C, as shown in eqn. 1,

$$\frac{dE_t}{dt} = -kk^1 C \tag{1}$$

where k is a temperature-dependent constant from the Nernst equation and k^1 is a rate constant depending on solution conditions. Equation 1 predicts linear response with a slope proportional to cystine concentration. It has also been shown[2] that when the slope of this cell response curve is matched by an electronic integrator with an input signal e_t, an input resistor R, and a feedback capacitor C_f, the cystine concentration is related to the input signal by eqn. 2.

$$C = \left(\frac{1}{RC_f}\right)\left(\frac{1}{kk^1}\right)e_t \tag{2}$$

This expression demonstrates the proportionality between cystine concentration and integrator input.

EXPERIMENTAL

Instrumentation

The concentration cell used is that described in detail earlier[3]. Important features of the cell are rapid and precise potential response, rapid mixing of reagents and samples in the sample compartment and temperature stability to within $\pm$ 0.05°.

A simplified schematic diagram of the measurement circuit is shown in Fig. 1. The output from integrator 1 is passed through a voltage divider. A fraction of this output is compared with the cell voltage at the input of integrator 2. Any voltage difference between the divided output from integrator 1 and the cell is integrated by integrator 2. This integrated signal is fed through an inverter to the input of integrator 1.

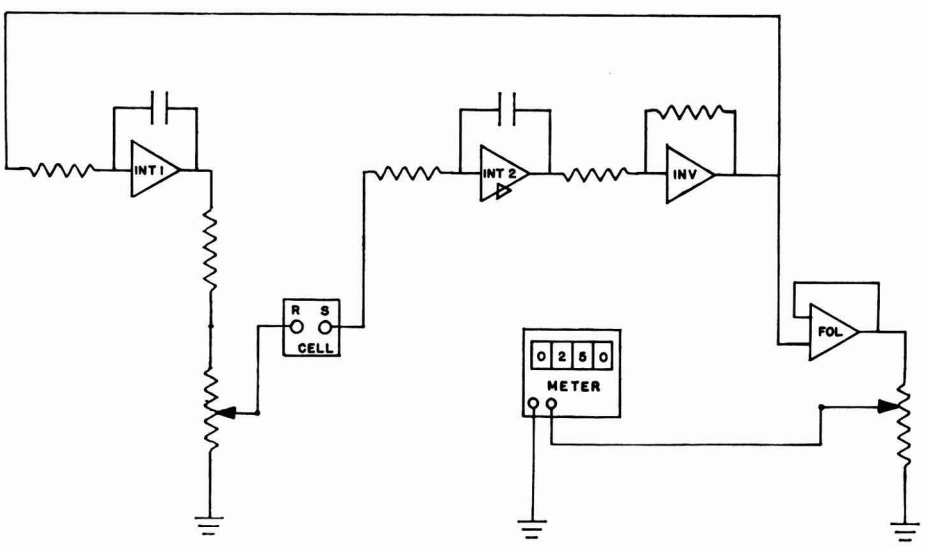

Fig. 1. Simplified schematic diagram for slope-measuring control circuit.

The inverted signal at the input of integrator 1 causes its output to change to eliminate the difference signal which produced the change. The output from the second integrator becomes constant only when the output from integrator 1 matches the cell voltage. It remains constant only when the outputs from the cell and integrator 1 are changing at the same rate. The inverted output from integrator 2 is passed through a follower amplifier and measured by a digital voltmeter (Digatek, United Systems Corp., Dayton, Ohio). The potentiometer at the follower output permits calibration of the voltmeter read-out in concentration units.

Operating conditions are adjusted so that the input to integrator 1 is kept above 100 mV for all rates measured. Therefore, the drift in the millivolt range, characteristic of the operational amplifier used, does not contribute significant error and this integrator need not be stabilized. On the other hand the input to integrator 2 is driven as near zero as possible. Consequently this integrator must be stabilized.

The operational amplifier used is that produced by Heath (Model EUW-19 A, Heath Co., Benton Harbor, Mich.). The control circuit is wired into a blank chassis (Heath Model EUW-19 A-1) which plugs onto the front of the operational amplifier system[1]. Details of the circuit are shown in Figs. 2, 3 and 4. Connections are shown for appropriate pins of 5-pin female sockets in the blank chassis which plug on to the 5-pin male sockets of the operational amplifier. All resistors have 10% tolerence and all

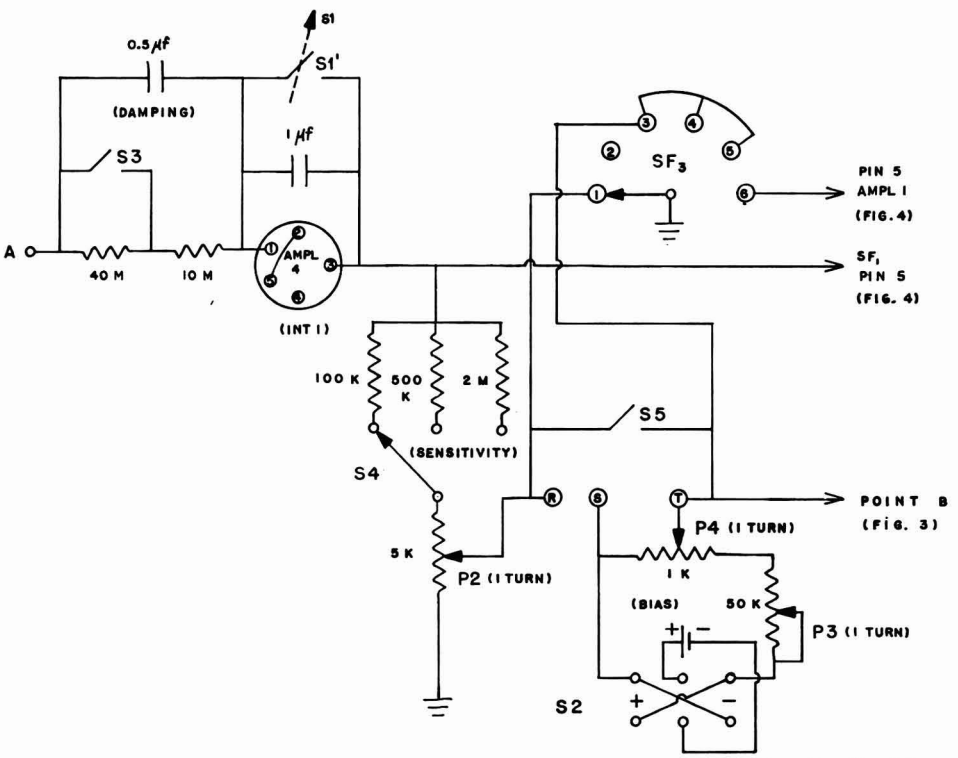

Fig. 2. Balancing integrator and bias source. P2, fine sensitivity; P3, coarse bias; P4, fine bias; S1 (open), measure; S1 (closed), reset; S3 (open), low const.; S3 (closed), high const.; S5 (open), measure; S5 (closed), stand-by; S2, bias polarity; S4, coarse sensitivity.

capacitors are paper mylar with 10% tolerance. S1 is a single-pole double-throw toggle and S2 is a double-pole double-throw center off toggle. Switches S3 and S5 are single-pole single-throw toggles. The general function of each control is given on the diagram on which it appears. The grounds shown represent connections to pin 4 of any amplifier.

Figure 2 represents the balancing integrator (Int. 1 in Fig. 1) with its divider circuit, jacks R and S for connection to the reference and sample electrodes and a bucking voltage (mercury cell) for nullifying any non-zero signal from the concentration cell at zero time. Wafer 3 (SF_3) of the function switch permits grounding of various points in the circuit for each function. The 0.5 μF condenser across the input resistance to integrator 1 provides sufficient damping for the application described here. S_3 permits the integrator constant to be changed from 20 (open) to 100 (closed) mV per sec per volt input. S1′ (reset) permits the integrator to be reset to zero between runs. S5 (stand-by) shorts out the cell and bias and prevents an open circuit at the input to integrator 2 when sample is removed from the sample compartment. S2 is a reversing switch for the bias. Jack T permits measurement of the bias required to buck out the cell voltage at zero time. This bias indicates deterioration of the reference electrode solution and should not exceed $\pm$25mV.

Figure 3 represents integrator 2 and the inverter. A Philbrick K2-P stabilizing

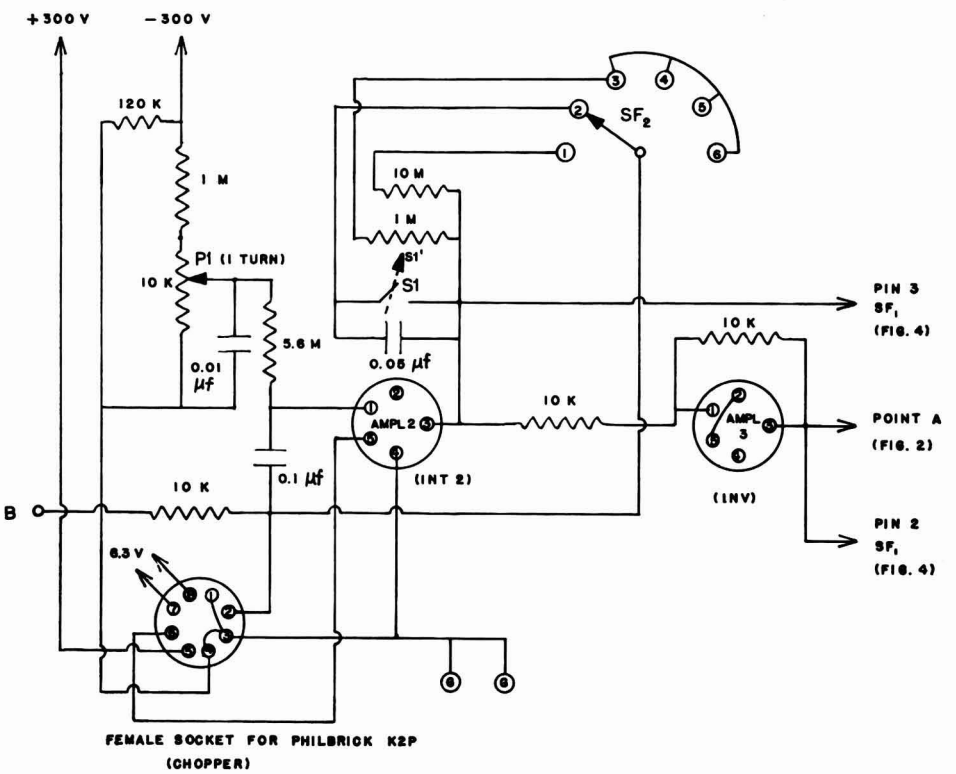

Fig. 3. Stabilized integrator and inverter. S1 (open), measure; S1 (closed), reset; P1, ampl. 2 balance; SF_2, shorting switch.

amplifier (Philbrick Researches, Boston Mass.), is used to stabilize this integrator. Input leads to the stabilized amplifier are shielded as recommended in the Philbrick literature. The 300 V supplies are taken from the jacks on the front panel of the operational amplifier. The 6.3 V supply for the K2-P is brought to the front panel of the amplifier by replacing one of the dummy 3-pin connectors with a pair of jacks connected to the 6.3 V supply of the amplifier. This required mounting a second pair of banana plugs in the plug-on chassis. P1 is the balance control for integrator 2. S1 permits resetting integrator 2 to zero between runs. SF_2 permits this amplifier to be changed rapidly from an integrator (position 2) to an amplifier with a closed loop gain of 1000 (position 1) and 100 (positions 3–6). SF_2 is a shorting switch so that the feedback loop is never opened. The two jacks marked G permit external access to ground.

Figure 4 represents connections to wafer 1 of the function switch, the follower and the digital voltmeter. Jack W permits connection of any desired voltage measuring device such as a recorder, panel meter, etc.

The purpose of each position of the function switch is indicated on Fig. 4. However, these functions are discussed briefly for clarity. In position 1 amplifier 2 acts as a high gain voltage amplifier and amplifies any difference between the cell and bias voltage. The bias voltage is adjusted until this difference is less than about 0.05 mV. Position 2 is the measure position and connections are as represented in Fig. 1.

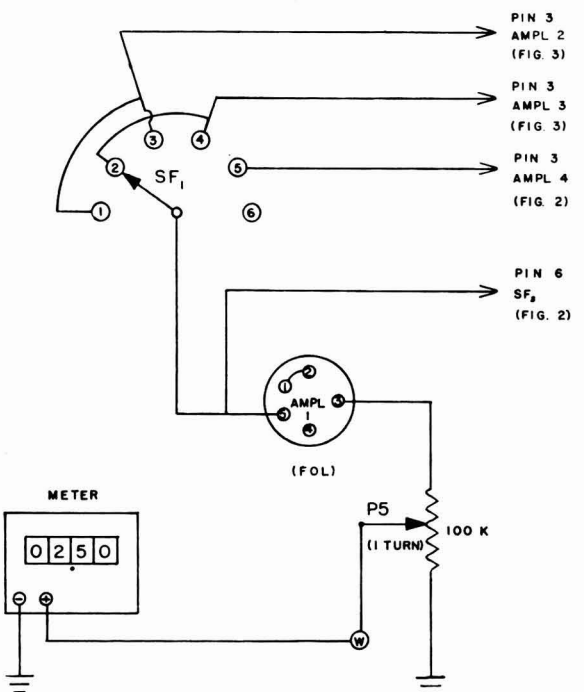

Fig. 4. Readout circuit. P5, calibration. SF (3 – wafer switch) functions: (1), initial null; (2), measure; (3), balance ampl. 2 (INT 2); (4), balance ampl. 3 (INV); (5), balance ampl. 4 (INT 1); (6), balance ampl. 1 (FOL).

Positions 3–6 permit balancing the amplifiers as indicated in Fig. 4. The balancing operations for amplifiers 2, 3 and 4 are performed with the input to amplifier 2 grounded (positions 3–5 of SF_3) and with this amplifier operating as a voltage amplifier with a closed loop gain of 100 (positions 3–6 of SF_1). SF_1 connects the output of appropriate amplifiers through the follower to the meter. Balancing amplifier 2 as a voltage amplifier with open loop gain of 100 may result in a small drift when it is operating as an integrator. This drift shows up as a noise level of about 1 mV in the output. This noise level does not contribute significant error. Amplifier 4 is balanced as an integrator by adjusting its balance control to give minimum drift. Any drift in this amplifier shows up as a constant offset in the output. This offset is compensated for in the zero adjust operation described below. Amplifiers 1 and 3 are balanced in the conventional manner.

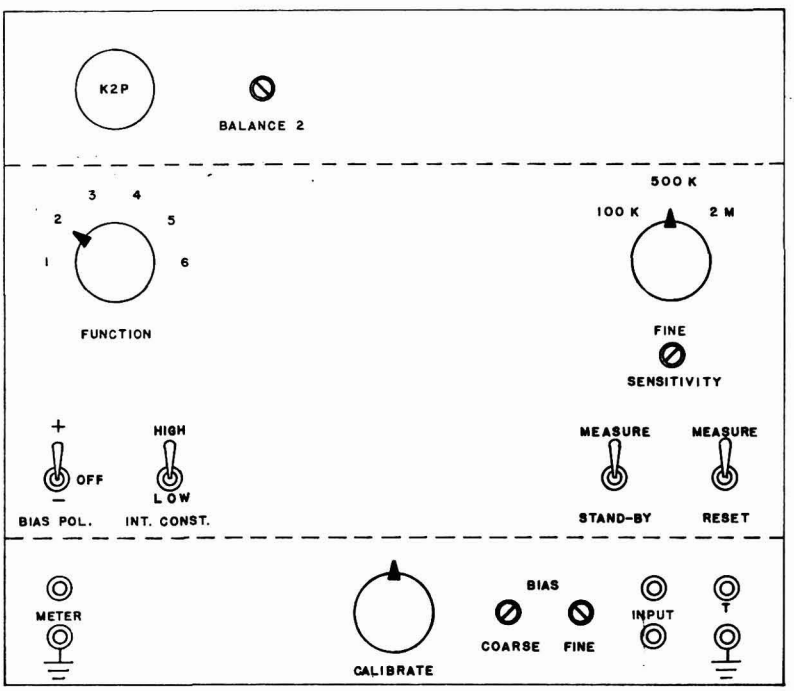

Fig. 5. Panel layout of slope-measuring instrument.

The front panel layout of the plug-on chassis is shown in Fig. 5. The function of each control is indicated and has been discussed above. The input jacks are R and S on Fig. 2. The K2-P chopper amplifier is mounted near the front of the top panel so that it does not interfere with plugging the chassis onto the operational amplifier system. After initial adjustments are made the only controls changed are the stand-by and reset switches. These are referred to below as the control switches.

Reagents

Reagents used in this work are those described in detail earlier[3] except as follows: For the 1–10 p.p.m. range the final pH is 5.8. For the 4–25 p.p.m. range the final pH is 5.2. Important working reagents are sodium azide, acidified iodine–iodide, standard cystine, and reference electrode solutions all prepared in deionized water. The reference electrode solutions contains iodine, iodide, and sodium chloride as an electrolyte. Cystine standards are prepared by dilution of a 50-p.p.m. solution.

Procedure

The procedure described is applicable to cystine over the range of 1–25 p.p.m.

Preparation of equipment. The reference electrode solution is added to the reference compartment through a hole in the compartment cover. The hole is then sealed with paraffin. The sodium azide, acidified iodine–iodide (in a glass-stoppered bottle) and sample solutions are adjusted to the working temperature (25.0°) by immersion in a water bath. Reagents and samples are handled with tuberculin-type hypodermic syringes fixed with teflon tips (Hamilton KF 18TF, Hamilton Company, Inc., Whittier, Calif.) Solutions are removed from the sample compartment by an aspirator tube.

The operational amplifier system is permitted to warm up for one-half hour before use. With the stand-by switch in stand-by the integrator constant switch in high and the reset switch in measure positions, the amplifiers are balanced starting with No. 1 and working up to No. 4. While balancing amplifier 4 it may be necessary to change the reset switch between reset and measure a few times.

Zero adjustment. After the amplifiers are balanced the function switch is set to position 1 and the coarse sensitivity control is set at 500 K. The fine sensitivity control is set at 1 K (measured between R and ground with power off and stand-by switch in measure position). Then 0.500 ml each of azide and iodine solutions and 1.00 ml of water are added to the sample compartment and the stirrer is started. The control switches are set to the measure positions and the bias control is adjusted until the digital voltmeter reads zero. The function switch is then set to position 2 and the balance control of amplifier 1 is adjusted until the digital voltmeter again reads zero. The instrument is now ready for calibration to read out directly in concentration units.

Calibration. After the above adjustments are completed, the solution in the sample compartment is replaced by the same amounts of reagents and 1.00 ml of a 20.0 p.p.m. cystine solution (final concentration of 10.0 p.p.m.). The control switches are set to measure and after the meter reading becomes constant the calibration adjustment is made so that the meter reads 1.00 V. The instrument is now calibrated.

Measurement step. The control switches are thrown to reset and stand-by. The sample compartment is rinsed with water. Then 0.500 ml each of azide and acidified iodine solutions are added to the compartment followed by 1.00 ml of sample solution containing between 2 and 50 μg of cystine. The control switches are thrown to measure and the cystine concentration is read from the meter after about 10–15 seconds when the reading becomes constant.

RESULTS AND DISCUSSION

Data presented in Tables 1 and 2 were taken on a digital voltmeter to evaluate the

reproducibility of the method. These tables show the raw data as read from the meter as well as computed values of relative standard deviations and errors.

Table 1 shows data obtained over a range of 1.00–10.0 p.p.m. cystine in a reaction solution with a pH of 5.8. Direct readout in concentration units is obtained with a relative standard deviation of less than 1%.

TABLE 1

AUTOMATIC RESULTS FOR AQUEOUS CYSTINE SOLUTIONS[a]

Cystine concn. (p.p.m.)	*Meter reading, R*			*Rel. error (%)*	*Rel. std. dev. (%)*
	R_1	R_2	R_3		
1	0.100	0.102	0.102	+ 1.3	0.94
2	0.199	0.200	0.201	0.0	0.41
4	0.403	0.404	0.401	+ 0.67	0.31
6	0.606	0.600	0.602	+ 0.45	0.42
8	0.804	0.802	0.796	+ 0.08	0.40
10	calibration (1.000)	1.000	1.000	—	—

[a]Solution pH is 5.8

TABLE 2

AUTOMATIC RESULTS FOR AQUEOUS CYSTINE SOLUTIONS[a]

Cystine concn. (p.p.m.)	*Meter reading, R*			*Rel. error (%)*	*Rel. std. dev. (%)*
	R_1	R_2	R_3		
4	0.395	0.396	0.396	1.08	0.12
12	1.190	1.206	1.192	0.33	0.59
20	2.015	2.005	2.010	0.50	0.20
25	calibration (2.500)	2.500	—	—	—

[a]Solution pH is 5.2

At a reaction pH of 5.8 it has not been possible to obtain a linear calibration plot for cystine up to 25 p.p.m. However, this linearity is approached at lower values of pH. Table 2 shows data taken at a pH of 5.2. These data are linear for concentrations of cystine over the range 4–25 p.p.m. and again represent direct readout. The disadvantage of operating at the lower pH is that the response curves become non-linear and readings must be taken as close as possible to zero reaction time.

This system enables accurate measurement of reaction rates near zero reaction time. As a method of analysis it offers rapid and precise determination using relatively compact and inexpensive apparatus which should be applicable to signal systems other than the potentiometric cell discussed here. Extensions of the method are being investigated.

ACKNOWLEDGEMENT

This investigation was supported in part by PHS Research Grant GM 10681 from the National Institutes of Health and in part by a David Ross XR Grant from the Purdue Research Foundation.

SUMMARY

A new method is described for the automatic measurement of reaction rates. Slopes of response curves are matched with output slopes from an electronic integrator. When the net output is zero, the input to the integrator is proportional to the slope of the response curve and is read directly on a meter near zero reaction time. All the necessary circuitry is wired into a blank plug-on chassis for commercially available equipment.

The method is evaluated for the determination of cystine in a reaction where the slope of the response curve is proportional to the cystine concentration. Cystine is determined over the range of 1.0–24 p.p.m. with a relative standard deviation of less than 1%. Automatic direct readout of p.p.m. cystine is obtained within 15 sec after mixing sample and reagents.

REFERENCES

1 C. G. ENKE AND R. A. BAXTER, *J. Chem. Educ.*, 41 (1964) 202.
2 H. L. PARDUE, *Anal. Chem.*, 36 (1964) 633.
3 H. L. PARDUE AND S. A. SHEPHERD, *Anal. Chem.*, 35 (1963) 21.

DIE MODELLIERUNG DER ELEKTROLYSE BEI KONSTANTEM STROM IM FALLE EBENER, ENDLICHER DIFFUSION MIT HILFE DES ANALOGRECHNERS

ROMULUS V. BUCUR, ION COVACI UND COSTIN MIRON

Institut für Atomphysik, Section Cluj (Rumänien)

(Eingegangen den 12. Mai, 1964)

EINLEITUNG

Vor kurzem zeigten CHRISTENSEN UND ANSON[1], dass die Elektrolyse bei konstantem Strom im Falle einer ebenen, endlichen Diffusion den Anwendungsbereich dieser Methode beim Studium der Kinetik der Elektrodenprozesse erweitert. Die analytische Lösung der Diffusionsgleichung für endliche Bedingungen hat aber eine viel kompliziertere Form[2] als im halbendlichen Fall. Deshalb ist sie zur Bestimmung des Einflusses der verschiedenen Parameter auf diese Erscheinung schwer anwendbar.

Aus diesem Grund ist das Studium der genannten Autoren durch die Wahl einer solchen Dicke der Diffusionsschichte beschränkt, die eine genügend genaue Annäherung der Lösung der Gleichung durch einen einfachen Ausdruck gestattet. Um diese Einschränkung zu beseitigen und die Anwendung des Studiums auf einen weiten Änderungsbereich der Versuchsparameter auszudehnen, wird in der vorliegenden Arbeit die Benützung eines Analogmodells der Erscheinung vorgeschlagen. Zur Verwirklichung dieses Modells diente ein universeller Analogrechner mit geringen Abmessungen[3].

VORBEREITUNG DER DIFFUSIONSGLEICHUNG ZUM ZWECKE DER MODELLIERUNG

Die Diffusionsgleichung

Die Elektrolyse bei konstantem Strom im Falle einer ebenen, endlichen Diffusion ist mathematisch durch die Differentialgleichung mit partiellen Ableitungen

$$\frac{\partial c(x,t)}{\partial t} = D \frac{\partial^2 c(x,t)}{\partial x^2} \tag{1}$$

gegeben, mit folgenden Anfangs- und Randbedingungen

$t = 0,\ 0 \leqslant x \leqslant l$: $$c(x,0) = c^0 \tag{2}$$

$t \geqslant 0$: $$\left.\frac{\partial c(x,t)}{\partial x}\right|_{x=0} = \frac{i}{nFD} \tag{3}$$

$t \geqslant 0$: $$\left.\frac{\partial c(x,t)}{\partial x}\right|_{x=l} = 0 \tag{4}$$

Der Sinn der benützten Bezeichnungen ist der übliche.

Zur Vereinfachung der Schreibweise wird im folgenden die normierte Form dieser Beziehungen angewendet

$$\frac{\partial \eta(\xi,t)}{\partial t} = v \frac{\partial^2 \eta(\xi,t)}{\partial \xi^2} \tag{1'}$$

$t = 0, 0 \leqslant \xi \leqslant 1$: $$\eta(\xi,0) = 1 \tag{2'}$$

$t \geqslant 0$: $$\left.\frac{\partial \eta(\xi,t)}{\partial \xi}\right|_{\xi=0} = u \tag{3'}$$

$t \geqslant 0$: $$\left.\frac{\partial \eta(\xi,t)}{\partial \xi}\right|_{\xi=1} = 0 \tag{4'}$$

dabei bezeichnet man

$$\xi = \frac{x}{l}, \quad \eta(\xi,t) = \frac{c(x,t)}{c^0} \tag{5}$$

und

$$v = \frac{D}{l^2}, \quad u = \frac{il}{nFDc^0} \tag{6}$$

Die Annäherung der Diffusionsgleichung

Die Lösung der partiellen Differentialgleichung der Diffusion mit Hilfe des elektronischen Analogrechners setzt die Reduzierung des Problems auf ein System von gewöhnlichen Differentialgleichungen und algebraischen Gleichungen, die der gegebenen Gleichung und den vorgeschriebenen Randbedingungen gleichwertig ist, voraus. Deshalb wird der Änderungsbereich [0,1] der Grösse ξ in N gleiche Bereiche geteilt. Man bezeichnet

$$\eta_k = \eta(\xi_k,t) \tag{7}$$

$$\xi_k = k \cdot h \quad (k = 0,1,2, \ldots N) \tag{8}$$

und

$$h = \frac{1}{N} \tag{9}$$

In Gl. (1') werden die Ableitung zweiten Grades in Verhältnis zu ξ in jedem Knotenpunkt ξ_k ($k = 1,2,3, \ldots N-1$) durch die Differenz zweiten Grades

$$\left.\frac{\partial^2 \eta(\xi,t)}{\partial \xi^2}\right|_{\xi=\xi_k} \simeq \frac{\eta_{k+1} - 2\eta_k + \eta_{k-1}}{h^2} \quad (k = 1,2,3 \ldots N-1) \tag{10}$$

angenähert und im Ausdruck (3') und (4') die Ableitungen ersten Grades durch die Formeln der numerischen Ableitung in drei Knotenpunkten

$$\left.\frac{\partial \eta}{\partial \xi}\right|_{\xi=0} \simeq \frac{-3\eta_0 + 4\eta_1 - \eta_2}{2h} \tag{11}$$

bzw.

$$\left.\frac{\partial \eta}{\partial \xi}\right|_{\xi=1} \simeq \frac{3\eta_N - 4\eta_{N-1} + \eta_{N-2}}{2h} \tag{12}$$

angenähert.

Die Annäherungsformeln wurden so gewählt, dass die durch Gl. (10) bzw. (11) und (12) eingeführten Fehler derselben Grössenordnung sein sollen.

Folglich erhält man das System,

$$\eta_0 = \tfrac{1}{3}(4\eta_1 - \eta_2 - 2hu)$$

$$\frac{d\eta_k}{dt} = \frac{v}{h^2}(\eta_{k+1} - 2\eta_k + \eta_{k-1}) \quad (k = 1,2,3 \ldots N-1) \tag{13}$$

$$\eta_N = \tfrac{1}{3}(4\eta_{N-1} - \eta_{N-2})$$

das die Gl. (1′) und die Bedingungen (3′) und (4′) annähert.

Das Analogmodell

Beim Analogrechner entsprechen den Funktionen η_k die elektrischen Spannungen Y_k, in Maschineneinheiten gemessen und der Zeit t die Maschinenzeit t' in Maschinensekunden gemessen, (M.E. bzw. M.S.).

Nach Änderung der Variabeln

$$Y_k = a_Y \cdot \eta_k \quad (k = 0,1,2, \ldots, N) \tag{14}$$

$$t' = a_t \cdot t$$

wobei a_Y und a_t Konstanten sind, und Einführung der Bezeichnungen

$$a = 2ha_Y u = 2ha_Y \frac{il}{nFDc^0} \tag{15}$$

$$b = \frac{1}{a_t h^2} v = \frac{1}{a_t h^2} \frac{D}{l^2}$$

erhält man aus dem System (13) die Maschinengleichungen in der Form

$$Y_0 = \tfrac{1}{3}(4Y_1 - Y_2 - a)$$

$$\frac{dY_k}{dt'} = b(Y_{k+1} - 2Y_k + Y_{k-1}) \quad (k = 1,2,3, \ldots N-1) \tag{16}$$

$$Y_N = \tfrac{1}{3}(4Y_{N-1} - Y_{N-2})$$

Zur Lösung dieses Gleichungssystems wird die in Abb. 1 a dargestellte Programmierskizze benützt. Sie enthält $(N + 1)$ Operationsverstärker, davon $(N - 1)$ Integrierer und zwei Summierer, und liefert alle Spannungen Y_k (t') $(k = 0,1,2, \ldots N)$.

Soll die Grösse Y_N nicht getrennt mit dem Analogrechner erhalten werden, so kann der letzte Operationsverstärker fortfallen und somit sinkt die Gesamtzahl der Ver-

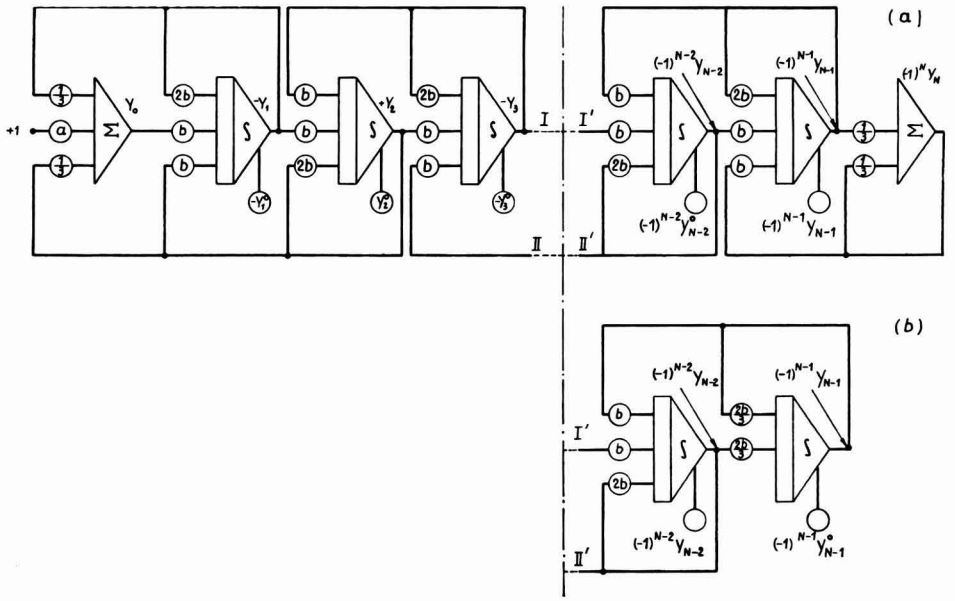

Abb. 1. Programmierskizze: (a), vollständige; (b), vereinfachte. $\int$ = Integrierer, Σ = Summierer.

stärker auf N. Dafür wird Y_N aus den zwei letzten Gleichungen des Systems (16) beseitigt und man erhält

$$Y_0 = \tfrac{1}{3}(4Y_1 - Y_2 - a)$$

$$\frac{dY_k}{dt'} = b(Y_{k+1} - 2Y_k + Y_{k-1}) \quad (k = 1,2,3 \ldots, N-2) \tag{17}$$

$$\frac{dY_{N-1}}{dt'} = \tfrac{2}{3}b(Y_{N-2} - Y_{N-1})$$

Die entsprechende Programmierskizze ist in Abb. 1b dargestellt.

In einem gegebenen numerischen Fall besteht die Arbeitsmethode zur Verwirklichung des Analogmodells aus folgenden Etappen:

(1) man wählt aus den Daten des Problems und den Arbeitsbereichen (Spannung und Zeit der Lösung) des vorhandenen Analogrechners die passenden Werte für die Koeffizienten a_Y und a_t, die in den Gl. (14) enthalten sind;

(2) man wählt einen Wert für N und achtet dabei darauf, dass der in den Gl. (10), (11) und (12) begangene Annäherungsfehler proportionell mit $1/N^2$ ist;

(3) mit Hilfe der Gl. (11) berechnet man die Grössen a und b, bzw. $2b$ und $2b/3$, die in den Maschinengleichungen (17) erscheinen und verwirklicht auf dem Analogrechner die der Abb. 1b entsprechende Rechenschaltung;

(4) man setzt die Rechenschaltung in Betrieb und misst die Zeit τ'(M.S.), in der die Spannung Y_0 annulliert wird. Die Übergangszeit ist

$$\tau = \frac{\tau'}{a_t} \tag{18}$$

DISKUSSION

Die Möglichkeiten des Analogmodells.

Mit Hilfe des Modells kann sehr leicht die Änderung der Übergangszeit in Abhängigkeit von der Stromdichte i, der Anfangskonzentration c^0 oder der Elektronenzahl n bestimmt werden. Aus den Gl. (15) ist ersichtlich, dass diese Parameter nur den Wert des Koeffizienten a beeinflussen und in Abb. 1b sieht man, dass dieser nur an einer einzigen Stelle in der Programmierskizze erscheint. Folglich bedeutet die Änderung von i, c^0 oder n das Regeln eines einzigen Potentiometers entsprechend dem neuen Werte a.

Das Studium der Änderung von τ in Abhängigkeit von l oder D scheint auf den ersten Blick komplizierter. Tatsächlich, da l und D in beiden Koeffizienten a und b vorkommen, fordert ihre Änderung das Regeln mehrerer Potentiometer. Man kann aber folgenden Kunstgriff machen: für jeden neuen l- oder D-Wert, ändert man a_t so, dass das Verhältnis $D/a_t l^2$ und demnach der Wert des Koeffizienten b, unverändert bleiben. Durch diese Methode benötigt jeder neue l- oder D-Wert die Regelung eines einzigen Potentiometers für den entsprechenden neuen a- Wert und ändert den Koeffizienten a_t, mit dessen Hilfe τ aus der Gl. (18) berechnet werden kann.

Das Studium an einem Modell bietet zusätzliche Möglichkeiten gegenüber der experimentellen Untersuchung. Tatsächlich ist die einzige, den Messungen zugängliche Grösse das Potential der Phasengrenze Elektrode/Elektrolyt ($\xi = 0$). Durch eine schwerfällige Rechnung kann daraus die Konzentration an der Phasengrenze bestimmt werden. Mit Hilfe des Modells dagegen erhält man diese Grösse direkt (bzw. die mit der normierten Konzentration proportionelle Spannung Y_0). Wird die Programmierskizze aus Abb. 1 a benützt, so erhält man sowohl die Konzentration für $\xi = 1$, als auch die Verteilung der Konzentration in der Tiefe der Diffusionsschicht in jedem Moment $t' \leqslant \tau'$ ($t \leqslant \tau$). Diese Grössen sind den experimentellen Bestimmungen unzugänglich, ihre Kenntnis jedoch trägt zur genaueren Beschreibung der Erscheinung bei und ist sehr nützlich.

Genauigkeit des Analogmodells

Die systematischen Fehler in den Resultaten sind durch die Annäherungen in den Gl. (10), (11) und (12) gegeben. Wie bereits gezeigt wurde, sind sie proportionell mit $1/N^2$ und können beliebig klein gemacht werden, durch die Wahl eines entsprechend grossen Wertes für N. Zwar ist dann eine grössere Zahl von Operationsverstärkern notwending, doch wenn die Programmierskizze einmal verwirklicht ist, ist die Behandlung des Modells unabhängig vom Wert N; wie oben gezeigt wurde, kann jede Änderung durch die Regelung eines einzigen Potentiometers wiedergegeben werden.

Die zufälligen Fehler sind durch die Nennfehler des benützten Analogrechners bestimmt. Hier muss erwähnt werden, dass, wenn nach der Regelung des Potentiometers nicht bestimmte Vorsichtsmassregeln getroffen werden, diese Fehler im Laufe der Modellierung vervielfacht werden und der Endfehler viel grösser ist als der eigentliche Fehler des Rechners. Diese Vervielfachung tritt praktisch nicht auf, wenn bei Abwesenheit des Stromes an der Phasengrenze ($i = 0$ bzw. $a = 0$) die Spannung Y_0 konstant ist. Um dieses zu erlangen, wurde durch Versuche der Wert des Potentiometers, der zwischen Eingang und Austritt des die Spannung Y_0 liefernden Verstärkers geschaltet ist, justiert, (für $N = 4$).

ZAHLENBEISPIEL

Zahlenangaben

Um die vorangehende Darlegung zu veranschaulichen, wurde ein durch folgende Zahlenwerte kennzeichneter Fall gewählt:

$$i = 10^{-2}\ \text{A cm}^{-2}$$
$$n = 2$$
$$F = 9.65 \times 10^{4}\ \text{C mol}^{-1}$$
$$D = 6.5 \times 10^{-6}\ \text{cm}^2\ \text{sec}^{-1}$$
$$c^0 = 1.6 \times 10^{-4}\ \text{mol cm}^{-3}$$
$$l = 12 \cdot 10^{-3}\ \text{cm}$$

Verwirklichung des Analogmodells

1. Der Arbeitsbereich des benützten Rechners ist für Spannungen $-1 \ldots +1$, und für die Maschinenzeit einige zehn Maschinensekunden.

Nach [5] wählt man für den Koeffizienten a_Y den Wert $a_Y = 1$ und für a_t den Wert $a_t = 1$, da wahrscheinlich für den vorliegenden Fall die Übergangszeit einige zehn Sekunden beträgt.

2. Man wählt $N = 4$; dadurch sind die systematischen Fehler $1/N^2 = 6\%$. Nachdem der Fehler des benützten Analogrechners $1 - 2\%$ ist, kann der Gesamtfehler etwa 8% betragen. Obwohl dieser Fehler gross ist, ist er doch annehmbar, da der behandelte Fall nur zur Veranschaulichung der Methode dienen soll.

3. Es folgt:

$$a = 0.299$$
$$b = 0.722$$
$$2b = 1.444$$
$$2b/3 = 0.481$$

Auf dem Rechner wird die der Abb. 1b entsprechende Rechenschaltung, die in diesem Fall vier Operationsverstärker enthält, verwirklicht. Da mit Hilfe der Potentiometer Koeffizienten, die die Einheit überschreiten, nicht verwirklicht werden können, wird überall wo der Koeffizient $2b$ erscheint, die in Abb. 2 dargestellte Änderung vorgenommen.

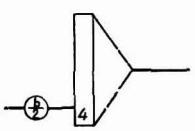

Abb. 2. Verwirklichung des Koeffizienten $2b > 1$.

4. Die Rechenschaltung wird in Betrieb gesetzt und man misst

$$\tau' = 28.3\ \text{M.S.}$$

wonach

$$\tau' = \tau = 28.3\ \text{sec}$$

Der entsprechende theoretische Wert ist $\tau = 30.8$ sec, der Fehler beträgt also -8.1% und entspricht den Erwartungen.

Bestimmung der Abhängigkeit $\tau = \tau\ (i)$

Mit dem dargestellten Modell kann man leicht jede gewünschte Abhängigkeit bestimmen. Zur Veranschaulichung wurde die Abhängigkeit $\tau = \tau\ (i)$ gewählt, da in den experimentellen Untersuchungen diese am meisten verfolgt wird.

Abb. 3 zeigt die Kurven $Y_0(t')$, die mit Hilfe des Schreibers des Analogrechners für

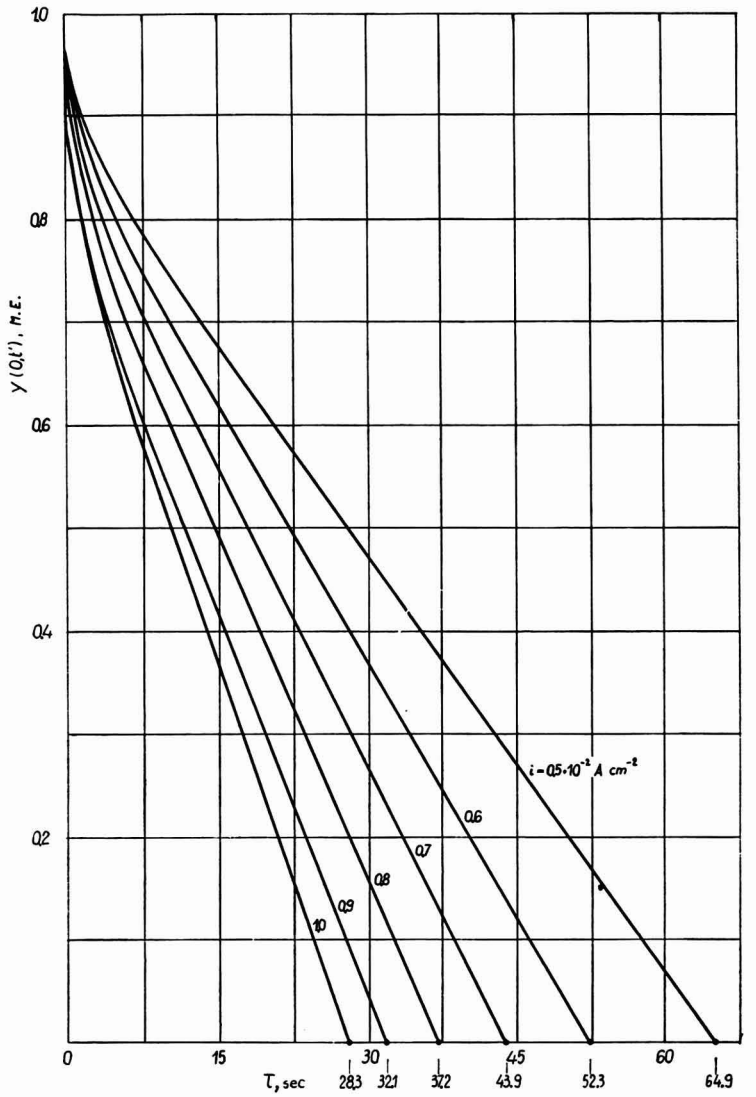

Abb. 3. Zeitliche Änderung der Konzentration an der Phasengrenze, in M.E. ausgedrückt.

i-Werte zwischen 0.5 — 1.0 · 10^{-2} A cm^{-2} erhalten werden. Die aus diesen Kurven entnommenen Werte $\tau = \tau'$ ($a_t = 1$) sind durch Punkte in Abb. 4 in Abhängigkeit von i dargestellt. Dieselbe Abbildung enthält auch die stetige Kurve, die den genauen, aus der analytischen Lösung berechneten Werten, entspricht. Die mit dem Analog-

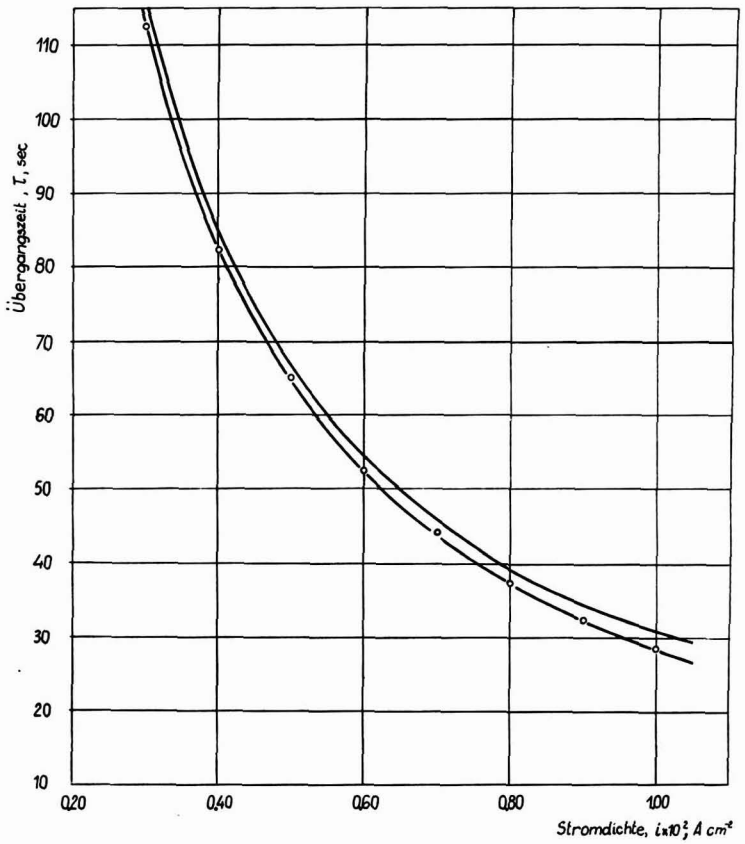

Abb. 4. Abhängigkeit Übergangszeit–Stromdichte, analytisch bestimmt (volle Kurve) und analogrechnerisch bestimmt (punktierte Kurve).

rechner erhaltenen Werte haben Fehler zwischen 3 — 8%, wobei die kleineren Werte kleineren Stromdichten entsprechen. Man sieht, dass das Modell den Charakter der Abhängigkeit $\tau = \tau\ (i)$ gut wiedergibt.

ZUSAMMENFASSUNG

Es wird ein elektronisches Analogmodell der Elektrolyse bei konstantem Strom im Falle einer ebenen, endlichen Diffusion dargestellt. Dieses ermöglicht die Komplikationen, die bei der praktischen Benützung der analytischen Lösung der Diffusionsgleichung auftreten, zu beseitigen.

Die Verwirklichung des Modells mit Hilfe eines universellen elektronischen Analogrechners und die Arbeitsmethode werden angegeben. Die Möglichkeiten des Modells werden besprochen und es wird gezeigt, dass man die Änderung der Konzentration nicht nur in der Grenzschichte, sondern auch im Innern der Diffusionsschichte verfolgen kann und dass somit die Verteilung der Konzentration in Abhängigkeit von der Tiefe in jedem Moment bekannt ist. Es wird gezeigt, dass der Mindestfehler des Modells durch die Nennfehler des benützten Analogrechners bedingt ist. Es wird ein Zahlenbeispiel angeführt aus dem hervorgeht, dass selbst bei Anwendung von nur vier Operationsverstärkern der Fehler nicht grösser als etwa 8% ist und dass dieser Wert, von den Zahlenwerten abhängig, bis zu 3% sinkt. Daraus geht hervor, dass mit Hilfe einer, auf ein Mindestmass reduzierten Schaltung, schnell eine nützliche Auskunft erhalten werden kann.

Das vorgeschlagene Analogmodell kann leicht verwirklicht und benützt werden. Es benötigt nur elementare Kenntniss der Analogrechnung und kann mit einem Analogrechner mit kleinen Abmessungen, der nur lineare Elemente enthält, ausgeführt werden.

SUMMARY

An electronic analogue of electrolysis at constant current in the case of plane finite diffusion is presented. This makes it possible to avoid the complications in the use of the analytical solution of the diffusion equation in practice.

The realization of the model with a universal electronic analogue computer and the procedure are indicated. The possibilities of the model are discussed and it is shown that the alteration of the concentration can be followed not only in the boundary layer, but also in the inside of the diffusion layer; the distribution of the concentration as a function of the distance is also known at every moment. It is shown that the minimum error of the model is conditioned by the nominal error of the analogue computer. A numerical example is given from which it is evident, that even when using only four operational amplifiers, the error does not exceed 8% and that this value, dependent upon the numerical values, drops to 3%. From this it is obvious, that with the aid of a minimal switching arrangement, useful information can be obtained quickly.

The suggested analogue can be constructed and employed easily. Only elementary knowledge of analogue calculation is needed and can be performed with a small analogue computer containing only linear elements.

LITERATUR

1 C. R. CHRISTENSEN UND F. C. ANSON, *Anal. Chem.*, 35 (1963) 205.
2 J. CRANK, *The Mathematics of Diffusion*, Clarendon Press, Oxford, 1956.
3 M. HANGANUT UND C. MIRON, *Probleme de Automatizare III*, Arbeitstagung, 13. Okt. 1960, S. 109.
4 G. A. KORN UND TH. M. KORN, *Electronic Analogue Computers*, McGraw-Hill, New York, 1956, S. 145.
5 G. A. KORN UND TH. M. KORN, *Electronic Analogue Computers*, McGraw-Hill, New York, 1956, S. 31.

POLAROGRAPHY OF BISMUTH(III)–GLUCONATE COMPLEXES

JAMES R. BRANNAN AND DONALD T. SAWYER

Department of Chemistry, University of California, Riverside, California (U.S.A.)

(Received May 29th, 1964)

Although the polarography of bismuth(III) ion has been extensively studied[1,2], the majority of the work has been concerned with acidic solutions. The limited research in basic media has indicated that, in general, poorly defined waves of little analytical use are obtained. Furthermore, the limited solubility of bismuth ion in alkaline solutions has precluded many polarographic studies[3]. Because gluconic acid is known to be an effective complexing agent and polarographic supporting electrolyte for many metal ions in strongly alkaline solutions[4], a study of the polarographic behavior of bismuth(III) in basic gluconate solutions has been undertaken. This investigation has led to development of a useful analytical procedure for the determination of bismuth ion in alkaline solutions. In addition, some understanding of the formula and stability of the bismuth(III)–gluconate complex has been gained from the polarographic data.

EXPERIMENTAL

Polarographic waves were recorded with a Sargent Model XV recording polarograph using a modified H-cell to prevent attack of the agar–salt bridge by the strongly alkaline sample solutions[5]. The polarographic cell was thermostatted to 25.0 $\pm$ 0.1° and the sample solutions were de-aerated with pre-purified nitrogen. The diffusion currents were corrected for residual current and were measured using the maxima of the oscillations; thus they represent the maximum rather than the average current. All potentials were measured *versus* the saturated calomel electrode (S.C.E.) with an error in measurement of less than $\pm$ 10 mV. For the dropping mercury electrode the rate of flow of mercury was 2.41 mg/sec and the drop time was 3.60 sec at −0.90 V applied potential. pH measurements were made with a Leeds and Northrup line-operated pH meter equipped with wide-range glass electrodes; the meter was standardized with N.B.S. buffers.

Bismuth(III) solutions were prepared from reagent-grade $Bi(NO_3)_3 \cdot 5H_2O$ and were standardized by titration with EDTA using a potentiometric end-point[6]. Sodium and potassium gluconate were prepared determinately from D-glucono-δ-lactone (Matheson, Coleman, and Bell), using sodium and potassium hydroxide to adjust the solution acidity. All other materials were reagent-grade.

RESULTS

Bismuth(III) ion in alkaline gluconate solutions has a well-defined, irreversible reduction wave as illustrated by curve A of Fig. 1. For a solution which is 0.1 *F* in sodium gluconate and approximately 1 *F* in hydroxide ion the half-wave potential for bismuth(III) is — 0.80 V. With these solution conditions the diffusion current is directly proportional to bismuth(III) concentration for metal ion concentrations

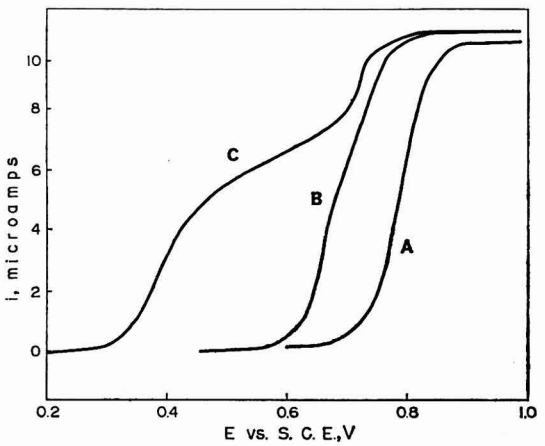

Fig. 1. Polarograms for the reduction of $10^{-3}F$ bismuth(III) in the presence of 0.1 *F* sodium gluconate. Curve A is for a solution which is 1 *F* NaOH. Curves B and C are for solutions which have been adjusted to pH 11.3 and pH 5.5, respectively.

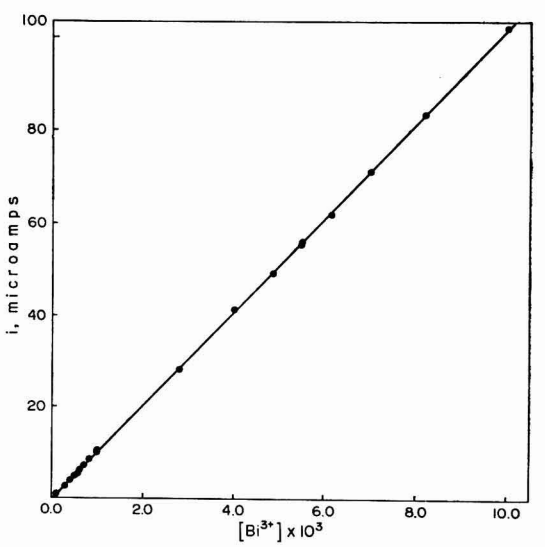

Fig. 2. Diffusion current as a function of bismuth ion concentration for a solution containing 0.1 *F* sodium gluconate and 1 *F* NaOH. The points represent the maximum rather than the average current and were adjusted for residual current.

from 10^{-5} to 10^{-2} F as illustrated by Fig. 2. From the data given in this figure the diffusion current constant, I_{max}, is calculated to be 4.26 $\pm$ 0.04. For bismuth ion concentrations greater than 10^{-4} F the mean deviation of the diffusion current is less than $\pm$ 1%. The average of a series of plots of E *vs.* log $(i_d - i)/i$ for bismuth ion in gluconate solutions gives a slope of 0.048 V per log unit. Thus, the reduction wave is highly irreversible and cannot be used for thermodynamic data. However, the gluconate concentration does have a significant effect upon the half-wave potential and this is illustrated by Fig. 3 for solutions containing 1 F KOH (the slope of the curve is 0.055 V per log unit).

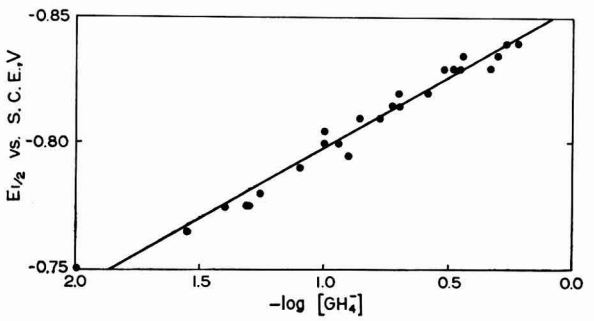

Fig. 3. Half-wave potentials for the reduction of $10^{-3}F$ bismuth(III) ion in 1 F NaOH as a function of the concentration of gluconate ion. The slope of the curve is — 0.055 V per log unit.

Above pH 13.5 the half-wave potential for bismuth ion in 0.1 F gluconate solutions shifts to more negative potentials in a linear fashion with increasing pH (slope equal to —0.077 V per pH unit). However, studies at pH values below pH 13.5 indicate that the reduction wave separates into two distinct waves. This is illustrated by curves B and C in Fig. 1. The relative heights of the two waves are independent of time of equilibration and their total height is essentially independent of pH. Thus, the two waves appear to be due to a slow hydrolysis equilibrium between two species of the bismuth(III)–gluconate complex. The double wave is observed until the pH is below 5.5.

A possible method of assessing the stability of the bismuth(III)–gluconate complex is to determine the increased solubility of the bismuth ion in alkaline solutions by the addition of gluconate ion. However, a knowledge of the solubility of bismuth ion in the absence of gluconate is first necessary, and specifically for the experimental conditions being used. This was accomplished by saturating 1–6 F NaOH solutions with $Bi(OH)_3$ and allowing them to equilibrate for two weeks prior to a polarographic analysis for dissolved bismuth ion. Because the polarograms for bismuth ion are reversible in nitric acid supporting electrolyte[2], this media has been used for determining the solubilities by neutralizing the equilibrated alkaline solutions with HNO_3 and adjusting the final solution to 1 F HNO_3 and 2 F $NaNO_3$. Table 1 summarizes the solubility data for bismuth ion at various concentrations of NaOH as well as the calculated equilibrium constant, K, for the reaction

$$Bi(OH)_3\,(s) + OH^- \rightarrow Bi(OH)_4^-,$$

TABLE 1

SOLUBILITY OF $Bi(OH)_3$ IN NaOH SOLUTIONS

[NaOH] (moles/l)	*[Bi (III)]·10⁵ (moles/l)*	*K·10⁵*
0.99	5.0	5.1
1.86	9.0	4.9
3.91	22.7	5.8
4.84	27.7	5.7
5.84	37.8	6.5

Thus, the value of K at 1 F NaOH is 5.1×10^{-5} which is significantly larger than the value reported from spectrophotometric measurements[7] (5×10^{-6}).

For a solution containing 1 F sodium gluconate and 1 F NaOH, bismuth(III) ion has a solubility of about 1.0 F. Thus, the formation of a gluconate complex enhances the solubility of the metal ion by a factor of approximately 10^5.

DISCUSSION

It can be seen from Fig. 2 that bismuth(III) ion can be determined polarographically in alkaline gluconate solutions over a wide concentration range. Because of the limited solubility of bismuth ion in basic solutions (see Table 1), the gluconate complex represents a real advantage for sample systems that are alkaline.

Unfortunately the irreversible nature of the reduction wave precludes reliable evaluation of the formula and stability constant of the bismuth(III)–gluconate complex. However, by considering the system as an irreversible process some tentative, approximate proposals can be made. Although this approach is only qualitative, some insight into the nature of the complex may be gained. Consideration of the slope for a plot of E *vs.* log $(i_d - i)/i$ for the reduction wave gives an average value of 1.08 for αn_a; *i.e.*, for the product of the transfer coefficient and the number of electrons in the rate-controlling reduction step[8]. If the species being reduced can be assumed to be the complex itself rather than the free ion, then an estimate of the number of ligands per metal ion might be gained by using the expression[8]

$$\frac{\Delta(E_{\frac{1}{4}})_c}{\Delta(-\log[GH_4^-])} = \frac{0.0591}{\alpha n_a} p$$

where GH_4^- represents the gluconate ion and p represents the number of ligands per bismuth ion. The slope from Fig. 3 is 0.055 V per log unit, which leads to a value of 1.0 for p and thus indicates that there is one gluconate ion per bismuth ion in the complex. This assumes that the electro-active species contains the same metal-to-ligand ratio as the stable complex species in the bulk of the solution. A similar evaluation of the pH dependence of the half-wave potential gives a value for p of 1.5 which indicates that 1.5 hydroxide ions per bismuth ion are apparently released in the reduction reaction for the complex.

Thus, if the assumptions are valid, the reduction reaction for the complex can be written

$$Bi_2(GH_4)_2(OH)_3^+ + 6\,e \rightarrow 2\,Bi + 2\,GH_4^- + 3\,OH^-$$

This then indicates that the formation reaction in alkaline solutions can be written

$$2\ Bi(OH)_4^- + 2\ GH_4^- \rightarrow Bi_2(GH_4)_2(OH)_3^+ + 5\ OH^-\ (K_f)$$

Finally, as an extremely crude approximation the stability of the bismuth(III)–gluconate complex can be estimated by using the expression

$$(E_{\frac{1}{2}})_c - (E_{\frac{1}{2}})_s = \frac{-0.059}{2\alpha\, n_a} \log K_f$$

for the conditions of 1 F $NaGH_4$ and 1 F KOH. While there is no direct justification for this expression, it should give some indication of the magnitude of the formation constant, K_f. Using the half-wave potential for bismuth(III) in 1 F KOH, $(E_{\frac{1}{2}})_s = -0.6$ V[2], and in 1.0 F $NaGH_4$ plus 1 F KOH, $(E_{\frac{1}{2}})_c = -0.9$ V (Fig. 3), the value of K_f is estimated to be 10^{10}. Considering that this constant is for the dimeric form of the complex, the value is in qualitative agreement with the observed enhancement of bismuth ion solubility.

Although the interpretation of the irreversible polarographic data for the bismuth complex is extremely tentative, the results are reasonable and should be indicative of the actual complex and its stability constant.

ACKNOWLEDGEMENT

This work was supported by the United States Atomic Energy Commission under Contract No. UCR-34P45.

SUMMARY

The polarographic behavior of the bismuth(III)–gluconate complex in alkaline solution has been studied. For a solution containing 0.1 F sodium gluconate and 1 F NaOH, a well-defined irreversible reduction wave is obtained with a half-wave potential of −0.80 V *vs.* S.C.E. and a diffusion current constant, I_{max}, of 4.26 ± 0.04. The diffusion current is proportional to bismuth(III) concentration for metal ion concentrations from 10^{-5} to 10^{-2} F. The data indicate that the complex contains one gluconate group and one and one-half hydroxide ions per metal ion. Polarographic determinations of the solubility of bismuth(III) in KOH solutions has permitted the formation constant for the reaction $Bi(OH)_3$ (s) + $OH^- \rightarrow Bi(OH)_4^-$ to be evaluated, $K = 5.1 \times 10^{-5}$.

REFERENCES

1 I. M. KOLTHOFF AND J. J. LINGANE, *Polarography*, Interscience Publishers Inc., New York, 2nd ed., 1952.
2 L. MEITES, *Polarographic Techniques*, Interscience Publishers Inc., New York, 1955.
3 J. BJERRUM, G. SCHWARZENBACH AND L. G. SILLÉN, *Stability Constants*, Part II: *Inorganic Ligands*, The Chemical Scciety, London, 1958.
4 D. T. SAWYER, *Chem. Rev.*, in press, 1964.
5 R. L. PECSOK AND R. S. JUVET, JR., *Anal. Chem.*, 27 (1955) 165.
6 H. A. FLASCHKA, *EDTA Titrations*, Pergamon Press, New York, 1959, p. 111.
7 W. C. SCHUMB AND E. S. RITTNER. *J. Am. Chem. Soc.*, 65 (1943) 1055.
8 L. MEITES, *Treatise on Analytical Chemistry*, Part I, Vol. 4, edited by I. M. KOLTHOFF AND P. J. ELVING, Interscience Publishers Inc., New York, 1964, chapter 46.

ZUM PROBLEM DER IDEALEN QUECKSILBERTROPFELEKTRODE

II*. DÜNNWANDIGE SPITZKAPILLAREN

J. FLEMMING UND H. BERG

Deutsche Akademie der Wissenschaften zu Berlin, Institut für Mikrobiologie und experimentelle Therapie, Jena (D.D.R.)

Herrn Prof. Dr. Dr. h. c. J. HEYROVSKÝ zum 74. Geburtstag gewidmet

(Eingegangen den 17. Juni 1964)

EINLEITUNG

Das zentrale Problem der exakten Polarographie liegt in der unvollständigen Übereinstimmung zwischen Experiment und Theorie beim Strom–Zeit-Verlauf des Einzeltropfens. Seit der Aufstellung der klassischen ILKOVIČ-Gleichung[1] ist viel Mühe und Scharfsinn darauf verwendet worden, die noch bestehende Diskrepanz zu eliminieren. Dabei sind seit der Entdeckung des Verarmungseffektes durch HANS *et al.*[2] zwei Wege beschritten worden.

Von seiten der Theorie wurden vereinfachte Tropfenmodelle berechnet. Eine hohe Genauigkeit erreichten darin KOUTECKÝ[3] und LOS[4]. Wenn auch ab und an neue Gleichungen in der Literatur auftauchen, so hat sich doch von der experimentellen Seite her ein bewährtes Kriterium für einwandfreie Strom–Zeit-Kurven herausgebildet. Danach lässt sich in recht guter Näherung[6] eine Strom–Zeit-Kurve ohne "Verarmung" aus einer der verbesserten ILKOVIČ-Gleichungen

$$i_d = Bt^{\frac{1}{6}}\,(1 + At^{\frac{1}{6}}) \tag{1}$$

ableiten.

Die in Gl. (2) definierte Grösse $\alpha(t)$ ergibt sich mit Hilfe von (1) zu

$$\alpha\,(t) \equiv \frac{\mathrm{d}\ln i_d}{\mathrm{d}t}\,\frac{1}{\mathrm{d}\ln t/\mathrm{d}t} = \frac{i_d'}{i_d}\,t = \frac{1 + 2At^{\frac{1}{6}}}{6(1 + At^{\frac{1}{6}})} \tag{2}$$

Die Auftragung von Gl. (2), unter der Annahme $A = 39\,\bar{D}^{\frac{1}{2}}/m^{\frac{1}{3}}$ mit $\bar{D} = 1.74 \times 10^{-5}$ cm^2 sec^{-1} und $m = 3.21$ mg sec^{-1}, ergibt einen Kurvenverlauf für $\alpha\,(t)$, der im Bereich 0.1 sec $< t <$ 3.4 sec vom Wert $\alpha = 0.183$ bei $t = 1$ sec nur um $\pm 3\%$ abweicht. Auf Grund der experimentellen Ungenauigkeiten ist man daher berechtigt, einen mittleren Exponenten $\bar{\alpha}$ aus dem Diagramm $\log i_d$–$\log t$ zu entnehmen, wodurch die Strom–Zeit-Kurve nach

$$i_d = x\,t^{\bar{\alpha}} \tag{3}$$

darzustellen ist[8] und erwartet wird, dass $\bar{\alpha}$ über die volle Tropfzeit τ konstant bleibt.

* Für I. Mitteilung siehe Ref. 12.

Nach unseren Erfahrungen ergibt jede Kapillare einen individuellen $\bar{\alpha}$-Wert im mittleren Streubereich von $0.17 < \bar{\alpha} < 0.21$. Es gelang SMOLER[9,10,11] mit nicht horizontalen Stirnflächen der Kapillaren (90° und 45° geneigt) dieses Ziel für alle Strom–Zeit-Kurven praktisch zu erreichen.

Diese Kapillaren bieten folgende Vorteile[10] gegenüber der klassischen Form mit waagerechter Stirnfläche:

(1) der Verarmungseffekt (d.h. die Übertragung der Konzentrationspolarisation von einem Tropfen auf den nächsten) wird vermieden;
(2) die Diffusionsstromgleichung mit sphärischer Korrektur wird erfüllt;
(3) Maxima 2. Art werden erniedrigt;
(4) unlösliche Produkte oder Gasblasen setzen sich nicht so leicht an der Kapillarenmündung fest;
(5) eine kurze Tropfzeit bei langsamem Quecksilberausfluss m wird erreicht.

Man darf wohl daraufhin mit einigem Recht sagen, dass die 45°–SMOLER-Kapillare den Anforderungen in praktisch idealer Weise gerecht wird. Eine nähere Betrachtung der Tropfenbildung jedoch lässt erkennen, dass hier ein unsymmetrisches System vorliegt:

(A) der Tropfen wächst in "Anlehnung" an die Stirnfläche mit teilweise verkleinertem Diffusionsraum;
(B) der Tropfen wird vom Quecksilber unsymmetrisch (einseitig) durchströmt (Fig. 3 in Ref. 9);
(C) der Tropfenabriss erfolgt unter Mitwirkung von Scherkräften und wahrscheinlich unter besonderen Schwingungen der Oberfläche[9];
(D) nach dem Tropfenabfall strömt die Umgebungsflüssigkeit unsymmetrisch zur Kapillarenmündung und scheint dadurch die Reste der an Depolarisator verarmten Lösung zu verteilen bzw. eine Strömung zu begünstigen.

Um diese theoretisch kaum zu erfassenden Besonderheiten zu vermeiden, haben wir in Jena einen anderen Weg eingeschlagen. Ihm liegt der Gedanke zugrunde, Verarmung und Abschirmung durch Spitzkapillaren gleichzeitig auszuschalten.

Die ersten Spitzkapillaren wurden geschliffen[11]. Ihre Stirnfläche verringert sich dabei auf etwa 1/150 der einer üblichen Tropfkapillare. Dennoch gelang es nicht, völlige Übereinstimmung zwischen 1. und 2. Tropfen zu erzielen[12], sowie Maxima 1. Art zu beseitigen, wie man es nach der Abschirmungstheorie der positiven Maxima[13] erwarten durfte. An dieser Stelle soll nun über Strom–Zeit-Kurven bei dünnwandigen gezogenen Spitzkapillaren (III) im Vergleich zur 45°–SMOLER-Kapillare (I) und zu einer weiteren 45°–Kapillare (II) mit vertikalem Quecksilberausfluss berichtet werden.

EXPERIMENTELLES

Kapillaren

Neben den neuen dünnwandigen Spitzkapillaren wurden die dickwandige 45°–SMOLER-Kapillare und eine unter 45° abgesprengte dickwandige Vertikalkapillare hergestellt.

(1) *Die dünnwandigen Spitzkapillaren.* In Tabelle 1 sind die Daten von drei gezogenen Spitzkapillaren (Abb. 1) enthalten. Sie wurden nach Erhitzen (Bunsenbrenner, Vorversuche dazu erfolgten mit glühendem Platinwiderstandsdraht) ausgezogen, und zwar die Kapillaren III-2 und III-3 aus Rasothermglas (d_a = 6 mm, d_i = 4 mm) die

Kapillare III-1 aus Geräteglas ($d_a = 7$ mm, $d_i = 1.8$ mm). Das Hauptproblem besteht darin, einen gleichmässig sich verjüngenden Innendurchmesser und eine glatte Stirnfläche zu erzeugen. Beides gelang besonders gut durch Auseinanderreissen bei Kapillare III-2 (Abb. 2) und Absprengen bei III-1, während die Mündung von

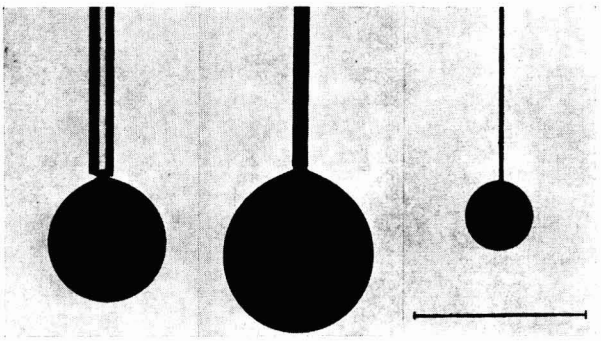

Abb. 1. Gezogene Spitzkapillaren mit Quecksilbertropfen am Ende der Tropfzeit. Von links nach rechts: Kapillare III-1 und die dünnwandigen Kapillaren III-2 und III-3 (Strichmarke ≙ 1 mm). Aufnahmedaten: (1), Praktina FX, Belichtungszeit 1/1000 sec; (2), Exakta Varex, Belichtungszeit 1/500 sec; (3), Praktina FX, Belichtungszeit 1/500 sec.

TABELLE 1

DATEN DER KAPILLAREN

Kapillare	d_i *(mm)*	d_a *(mm)*	$(d_a - d_i)/2$ *(mm)*	$\frac{2d_i}{(d_a - d_i)}$	A_K *(mm²)*	A_T *(mm²)*	$\frac{A_K}{A_T}$
Zylinderkap.	0.05	5	2.47	0.02	19.6	3.8	5.16
Geschliff. Spitzkap.	0.05	0.4	0.175	0.28	0.1235	3.8	0.0325
Spitzkap. III-1	0.03	0.15	0.06	0.5	0.0170	2.0	0.0085
Spitzkap. III-2	0.06	0.08	0.01	6	0.0022	2.45	0.0009
Spitzkap. III-3	0.018	0.024	0.003	6	0.0002	0.55	0.0004

d_a, Aussendurchmesser; d_i, Innendurchmesser; $(d_a - d_i)/2$, Wandstärke; $2d_i/(d_a - d_i)$, Dünnwandigkeitskriterium; A_K, Stirnfläche der Kapillarenwandung; A_T, Tropfenoberfläche; A_K/A_T, Abschirmungskriterium.

Kapillare III-3 unter dem Mikroskop Einbuchtungen erkennen liess. Trotz dieses Fehlers und ihrer extrem dünnen Wand (entspricht einer sehr niederohmigen Glaselektrode!) konnten normale Strom–Zeit-Kurven (Abb. 7) erhalten werden. Gegenüber den üblichen Kapillaren konnte die Wandstärke $(d_a - d_i)/2$ entscheidend verringert werden, so dass jetzt ein Kapillarentyp vorliegt, dessen Innendurchmesser d_i grösser als die Wandstärke ist. Wir möchten solche Kapillaren als dünnwandig bezeichnen, wenn für sie gilt: $2d_i/(d_a - d_i) > 1$, was für III-1 zwar nicht ganz, jedoch bei III-2 und III-3 zutrifft. Es war zu erwarten, dass die empfindlichsten Kapillaren mit den höchsten Werten für $2d_i/(d_a - d_i)$ die günstigsten Resultate ergeben würden. Abbildung 2 gibt eine Vorstellung der Wandung und Mündung von Spitzkapillare III-2 nach Zurücksteigen des Quecksilbers.

(2) *Die 45°–*SMOLER*-Kapillare (I).* Die Herstellung erfolgte in der üblichen Weise durch Biegen einer gewöhnlichen Zylinderkapillare (Stumpfkapillare, $d_a = 5$ mm, $d_i = 0.05$ mm; Abb. 3). Nicht mit jedem Exemplar erhielten wir übereinstimmende Strom–Zeit-Kurven, ohne dass die Ursache aufgefunden werden konnte.

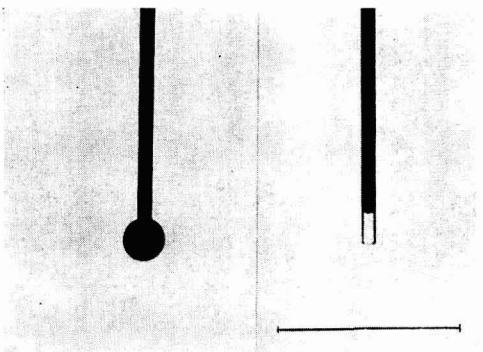

Abb. 2. Dünnwandige Spitzkapillare III-2 mit jungen Tropfen und zurückgestiegenem Quecksilber, um die Wandung sichtbar zu machen (Strichmarke ≙ 1 mm). Aufnahmedaten: Exakta Varex, Belichtungszeit 1/500 sec.

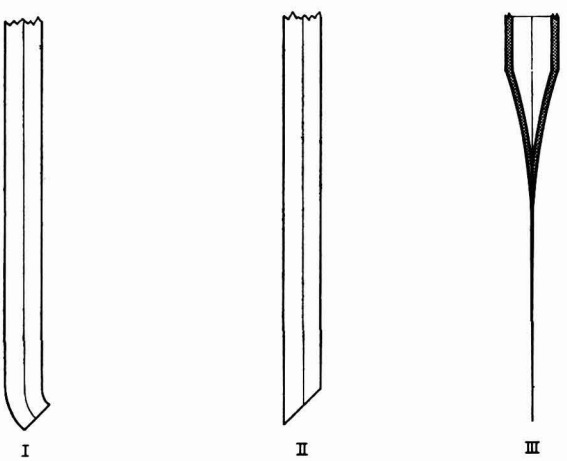

Abb. 3. Verwendete Kapillarentypen: (I), 45°–SMOLER-Kapillare; (II), 45°–abgesprengte Kapillare; (III), gezogene Spitzkapillare.

(3) *Die 45°-abgeschrägte Vertikalkapillare (II).* Sie wurde ebenfalls aus einer normalen Zylinderkapillare hergestellt, und zwar durch schräges Absprengen, so dass eine unter 45° geneigte Stirnfläche entstand (Abb. 3).

Registrierung

Zur Aufzeichnung der i–t-Kurven von Tl^+ wurde ein schnellschwingendes Stylo-Galvanometer Typ A80 der Firma Kipp und Zonen mit den Daten $f_r = 64$ Hz,

$G_i = 2.1 \times 10^{-8}$ A/mm/m in Verbindung mit einer automatischen Schaltapparatur (für den 1. Tropfen) und einer Photoregistrierkassette verwendet. Die 50 Hz Überlagerung wurde zur Zeiteichung herangezogen.

Messlösung

Die wässrige Messlösung enthielt 10^{-3} *M* Tl^+, 10^{-1} *M* KCl, 10^{-2} % Gelatine. Die Messtemperatur betrug 21°.

ERGEBNISSE

Die 45°-SMOLER-Kapillare (I)

Zunächst wurde mit unserem Registriersystem die 45°-SMOLER-Kapillare geprüft. Wie Abb. 4 deutlich erkennen lässt, besteht bei einem ausgesuchten Exemplar bis

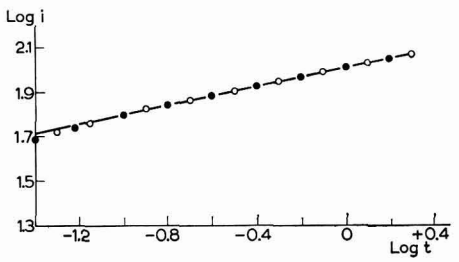

Abb. 4. log i–log t-Kurve der 45°-SMOLER-Kapillare (I) mit Tl^+-Lösung bei einem Potential von −1 V gegen die NCE. Die Stromstärke i wurde aus den experimentellen i–t-Kurven in willkürlichen Einheiten (Millimetern) entnommen. ●, 1. Tropfen; ○, 2. Tropfen.

zu den kürzesten Zeiten eine ausgezeichnete Übereinstimmung zwischen 1. und 2. Tropfen, wobei der Wert für $\bar{\alpha} = 0.205$ beträgt. Allerdings weichen im vorliegenden Beispiel bei Zeiten < 0.06 sec nach Tropfenbeginn die Messpunkte etwas von der Geraden ab.

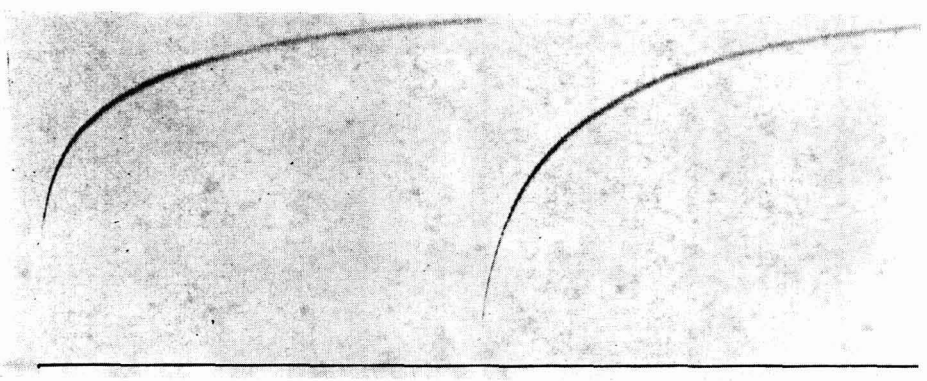

Abb. 5. i–t-Kurven der 45°-abgesprengten Kapillare (II) mit Tl^+-Lösung bei einem Potential von −1 V gegen die NCE. 1. und 2. Tropfen, $\tau = 2.65$ sec.

Die 45°-abgeschrägte Vertikalkapillare (II)

Mit der Kapillare II sind ausser der 45°-Neigung der Stirnfläche nur die zwei Besonderheiten von I, nämlich (A) und (D) verwirklicht.

Tropfzeit und Abriss entsprechen denen der senkrechten Zylinder- oder Stumpfkapillare, obwohl die Mündung einen mehr ovalen Querschnitt aufweist.

Abbildung 5 zeigt den bedeutenden Unterschied zwischen 1. und 2. Tropfen mit einer Einlaufzeit t' von 2 sec, etwa wie im Falle der gewöhnlichen Stumpfkapillare. Die 45°-Abschrägung an sich hat zu keiner Verbesserung geführt. Der einzige äusserliche Unterschied zur 45°–SMOLER-Kapillare besteht darin, dass der Quecksilberzufluss nicht unter 90°, sondern unter 45° durch die Stirnfläche erfolgt.

Die dünnwandigen Spitzkapillaren

In genau senkrechter Position können die dünnwandigen Spitzkapillaren ebenso verwendet werden wie die üblichen Stumpfkapillaren. Nach Schrägstellung traten Besonderheiten im Tropfenbild auf, die zunächst bei Lupenvergrösserung studiert wurden.

(1) *Das Tropfenbild.* Bei den Kapillaren III-2 und III-3 ist die Glaswandung nur dann sichtbar zu machen, wenn das Quecksilber in der Kapillare zurücksteigt (Abb. 2). Der Hals des Tropfens erscheint während des Tropfenwachstums als Verlängerung der Gesamtkapillare, so dass eine Abschirmung nicht mehr wirksam werden kann. Gegenüber der dickwandigen Stumpfkapillare lassen sich nunmehr auch der Abreissvorgang und das Zurücksteigen (Rückdruckeffekt) optisch einwandfrei filmen.

Nach 45°-Schrägstellung dieser Kapillaren, um den SMOLER-Effekt nachzuweisen, beobachteten wir bei der dünneren Kapillare III-2 folgende Besonderheiten (Abb. 6):

(a) mit Zunahme des Tropfengewichtes wird das Kapillarenende langsam nach unten gebogen und schnellt nach Tropfenabriss in seine Ausgangslage zurück (Kippschwingung);

(b) der Tropfen wächst nahezu symmetrisch, da die Stirnfläche nicht mehr wie bei der SMOLER-Kapillare im Wege ist;

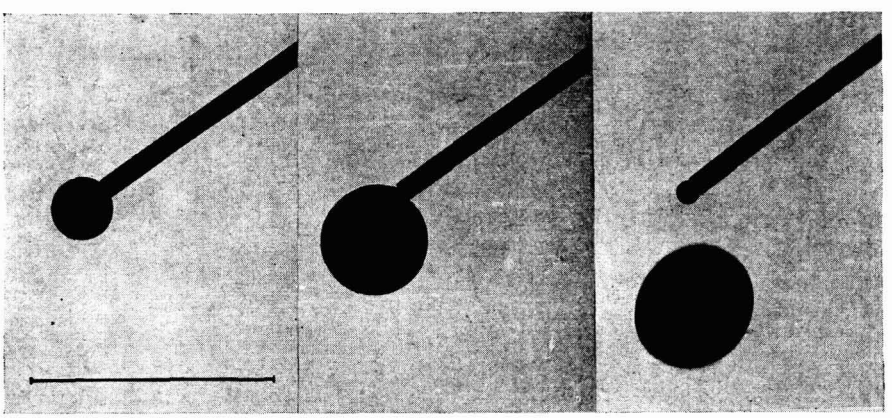

Abb. 6. 45°–Schräggestellte dünnwandige Kapillare (III-2) mit verschiedenen Phasen der Tropfenbildung. Junger, älterer und abgerissener Tropfen bei einem Potential von − 1 V gegen die NCE (Strichmarke ≙ 1 mm). Aufnahmedaten: Exakta Varex, Belichtungszeit 1/1000 sec.

(c) nach dem Abriss erleidet die Quecksilberkugel Deformationsschwingungen (Abb. 6);

(d) gegenüber der noch verhältnismässig starren Kapillare III-1 nehmen diese i–t-Kurven eine Form an, die denen in strömendem Medium bei senkrechter Kapillare ähneln (Abb. 9a).

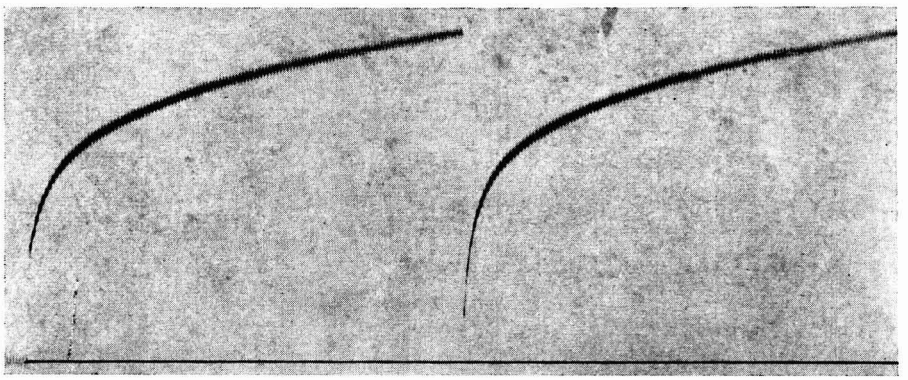

Abb. 7. i–t-Kurven der Kapillare III-3 mit Tl^+-Lösung bei einem Potential von -1 V gegen die NCE. 1. und 2. Tropfen, $\tau = 2.65$ sec.

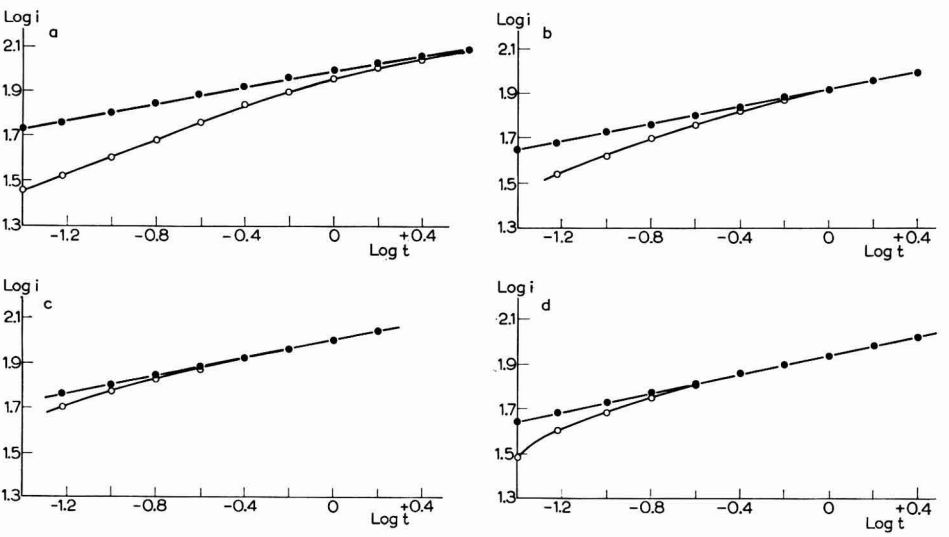

Abb. 8. log i–log t-Kurven der Kapillaren II (a), III-1 (b), III-2 (c) und III-3 (d) bei dem Potential -1 V (i in willkürlichen Einheiten (Millimetern) gemessen). ●, 1. Tropfen; ○, 2. Tropfen.

Auf Grund von Biegung und Abtropfen vollführt die Mündung dieser Kapillare regelmässige Kippschwingungen (Abb. 9b).

(2) *Die Strom–Zeit-Kurven.* In Abb. 7 sind die Strom–Zeit-Kurven für den 1. und 2. Tropfen der senkrechten Kapillare III-3 dargestellt. Sie sind von Ansehen kaum zu unterscheiden. Erst die log i–log t-Darstellung (Abb. 8) lässt eine anfängliche

Differenz erkennen. Nach einer Einlaufzeit t' (vgl. Tabelle 2), die für vertikale Stellung bisher nicht unter 0.2 sec vermindert werden konnte, wird der erstrebte Verlauf des 1. Tropfens erreicht.

(3) *Die Maxima 1. Art.* Entgegen den theoretischen Erwartungen[13] führt die Be-

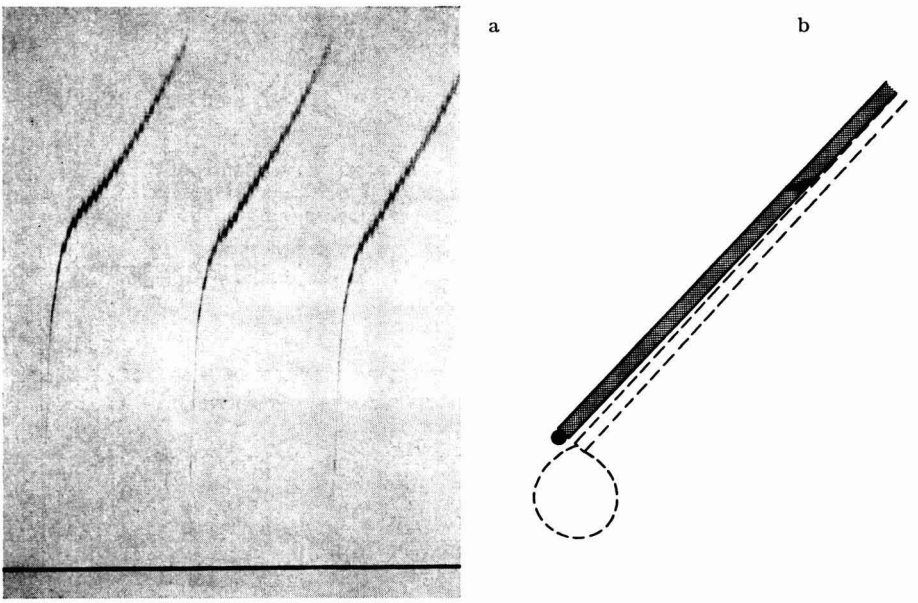

Abb. 9. (a) i–t-Kurven des 1., 2. und 3. Tropfens der Kapillare III-2 bei einer Neigung von 45°. Tl^+-Lösung. Potential gleich -1 V gegen die NCE. $\tau = 0.58$ sec.
(b) Schematische Darstellung der Amplitude von Kippschwingungen und der Tropfenform einer dünnwandigen Kapillare vom Typ III-2.

seitigung der Abschirmung unter Verwendung von Kapillare III-2 nicht zum Verschwinden des Sauerstoff-Maximums 1. Art in Übereinstimmung mit früheren Ergebnissen an der geschliffenen Spitzkapillare[12]. Form und Abbruchpotential des Maximums bleiben weitgehend erhalten.

DISKUSSION

Man muss sich zunächst die Frage vorlegen, ob die dünnwandige Spitzkapillare noch weiter zu vervollkommen ist. Wir sind der Ansicht, dass eine Kapillarenwandung aus Glas (oder einem anderen Nichtleiter) kaum dünner als 0.002 mm herzustellen ist, wobei die Mündung als glatter Rand erhalten bleiben muss. In Tabelle 1 sind entsprechende Daten unserer bisherigen Kapillaren zusammengestellt. Während für polarographische Untersuchungen bislang ausschliesslich dickwandige Tropfkapillaren mit $d_i \ll (d_a - d_i)/2$ benutzt wurden, trifft für unsere dünnwandigen Spitzkapillaren erstmals die Umkehrung $d_i > (d_a - d_i)/2$ zu. Mit dieser dünnen Wandung resultiert eine sehr geringe Stirnfläche der Kapillare A_K, die zur maximalen Tropfenoberfläche A_T, in einem sehr kleinen Verhältnis A_K/A_T steht. Damit können die

Abschirmung am Tropfenhals und ein zusätzlicher Strömungswiderstand durch A_K vernachlässigt werden. Dennoch wird ein Rest der verarmten Schicht des vorhergehenden Tropfens sich nach oben auf die Mündung zu bewegen, in die Wachstumssphäre des neuen Tropfens geraten und damit die Einlaufszeit t' bestimmen.

Wenn wir als "Übereinstimmung" zwischen 1. und 2. Tropfen bis zu 3% Abweichung in der Stromstärke vorgeben, so zeigen die mittleren Einlaufszeiten t' (Tabelle 2), dass gegenüber der geschliffenen Spitzkapillare[12] eine beträchtliche Verminderung des Verarmungseffektes erzielt wurde, jedoch nun ein von der Tropfzeit kaum abhängiger Grenzwert erreicht zu sein scheint. Dieser hängt weniger von d_a als vielmehr von der Wandstärke bzw. von dem Verhältnis: $2d_i/(d_a - d_i)$ ab. Unsere Ergebnisse lassen erkennen, dass in günstigen Fällen eine minimale Einlaufszeit von $t' \approx 0.1$ sec zu erreichen ist. Das bedeutet eine lineare log i– log t-Abhängigkeit (konstantes $\bar{\alpha}$) für *ca.* 97% der Standardtropfzeit von 3 sec.

TABELLE 2

MITTLERE EINLAUFSZEIT t' UND ÜBEREINSTIMMUNGSKRITERIUM ZWISCHEN 1. UND 2. TROPFEN, BEZOGEN AUF $\tau = 3$ sec

Kapillaren	τ *(sec)*	t' *(sec)*	$\frac{3\ sec - t'}{3\ sec}$
Kapillare II	2.65	2.0	0.33
Geschliff. Spitzkap.	3.0	0.80	0.73
Kapillare III-1	2.9	0.70	0.77
Kapillare III-2	1.6	0.30	0.90
Kapillare III-3	2.65	0.25	0.92

Trotz anfänglicher Zuversicht (vgl. Tabelle 1), auf dem Wege einer Verringerung der Wandstärke zu einer idealen Tropfkapillare in ruhendem Medium zu gelangen, steht man vor einem prinzipiellen Hindernis durch Verarmungsreste. Diese verbleiben an der Kapillarenmündung oder werden nach dem Abreissvorgang je nach Rückdruck sogar in die Kapillare hineingezogen.

Es erhebt sich nun die Frage, weshalb die umgebogenen dickwandigen SMOLER-Kapillaren $[d_i < (d_a - d_i)/2]$ demgegenüber praktisch keine Auswirkungen von Verarmungsresten erkennen lassen.

Einleitend war festgestellt worden, dass im Vergleich zur senkrechten dickwandigen Tropfkapillare für den Erfolg der SMOLER-Kapillare 4 Besonderheiten: (A) bis (D) von Bedeutung sind. Die 45°-abgeschrägte Vertikalkapillare (II) weist davon (A) und (D) auf. Die gezogene Spitzkapillare (III-1) in 45°-Stellung besitzt davon (B) und (C). Leider kennen wir noch keinen Kapillarentypus, der drei von den vier Besonderheiten aufweist, weshalb folgender Rückschluss mit Vorbehalt getroffen wird. Obwohl die Kombination (B) + (C) weitaus wirksamer als (A) + (D) ist, andererseits mit (B) + (C) die vertikale dünnwandige Spitzkapillare nicht übertroffen und die SMOLER-Kapillare bei weitem nicht erreicht wird, kann keine der vier Besonderheiten für sich allein in Anspruch nehmen, die entscheidende zu sein. Vielmehr is das theoretisch wohl kaum zu analysierende Zusammenwirken von (A), (B), (C) und (D) für den SMOLER-Effekt erforderlich. Unsere Bestrebungen gehen nun dahin, passende Bedingungen zu

schaffen, um die Restverarmung an dünnwandigen Spitzkapillaren vollends zu beseitigen.

DANK

Frau L. BERG ist es zu verdanken, dass die dünnwandigen Spitzkapillaren III-2 und III-3 entstanden sind.

ANMERKUNG

Erst nach Abschluss unserer Untersuchungen wurde uns bekannt, dass KIMLA UND STRAFELDA[16] zur Verifizierung einer neuen Diffusionsstromgleichung senkrechte gezogene Spitzkapillaren mit $d_a = 0.11$ mm und $d_i \approx 0.01$ mm verwendet haben. Nach unserem Kriterium $2d_i/(d_a - d_i) \approx 0.2$ zählen sie jedoch nicht zu den neuartigen dünnwandigen Spitzkapillaren. Da die Auswertungen nicht auf den 1. Tropfen bezogen wurden, ist ein direkter Vergleich der Ergebnisse vorerst unmöglich.

ZUSAMMENFASSUNG

Mit extrem dünnwandigen Quecksilbertropfkapillaren werden Strom–Zeit-Kurven des 1. und 2. Tropfens in einer 10^{-3} N Tl^+ Lösung mittels schnellschwingender Stylo-Schleifen registriert. Eine vollständige Beseitigung des Verarmungseffektes wie mit der 45°–SMOLER-Kapillare gelingt selbst bei Schrägstellung nicht, obwohl die Abschirmung und der Strömungswiderstand durch die Kapillarenwandung (Stärke 0.003 bis 0.01 mm) zu vernachlässigen sind. Da die Einlaufszeit t' des Stromes vom 2. Tropfen in den des 1. Tropfens bei den dünnwandigsten Kapillaren immer noch 0.2 Sekunden beträgt, erscheint es prinzipiell unmöglich, eine ideale vertikale Quecksilbertropfkapillare in "ruhendem" Medium unter normalen Bedingungen zu realisieren. Entgegen den theoretischen Erwartungen bleibt das Sauerstoffmaximum erhalten.

Die Ursachen der Effekte und Unterschiede werden diskutiert.

SUMMARY

Current–time curves were recorded with a ~~short period pen recorder~~ quick oscillating "Sty/o" galvanometer using extremely thin-walled dropping mercury capillaries in a 10^{-3} N Tl^+-solution. Even by inclining the capillary it was not possible to eliminate completely the depletion effect as with the 45°–SMOLER capillary, although the shielding and resistance to streaming of the capillary wall (thickness 0.003 to 0.01 mm) are negligible. Since the time t' which elapses before the current on the second drop coincides with that on the first still amounts to 0.2 sec for the thinnest-walled capillaries, it seems impossible in principle to realise an ideal vertical dropping mercury capillary in "unstirred" medium under normal conditions. Contrary to theoretical expectations the oxygen maximum continues to be observed.

The causes of these effects and discrepancies are discussed.

LITERATUR

1 D. ILKOVIČ, *Collection Czech. Chem. Commun.*, 6 (1934) 498.
2 W. HANS, W. HENNE UND E. MEURER, *Z. Elektrochem.*, 58 (1954) 836.
3 J. KOUTECKÝ, *Czech. J. Phys.*, 2 (1953) 50.

4 J. Los und W. Murray, *Advances in Polarography*, Vol. 2, Pergamon Press, Oxford, 1960, pp. 408, 425, 437.
5 M. von Stackelberg und V. Toome, *Collection Czech. Chem. Commun.*, 25 (1960) 2958.
6 H. Berg und H. Kapulla, *Naturwissenschaften*, 44 (1957) 395.
7 H. Kapulla, Diplomarbeit, Jena, 1957.
8 J. Smoler, Thesis, Polarogr. Inst., Prag, 1958.
9 J. Smoler, *Collection Czech. Chem. Commun.*, 19 (1954) 238.
10 J. Smoler, *J. Electroanal. Chem.*, 6 (1963) 465.
11 H. Zeidler, unveröffentlichte Versuche, Jena, 1957.
12 H. Triebel und H. Berg, *J. Electroanal. Chem.*, 2 (1961) 467.
13 M. von Stackelberg und R. Doppelfeld, *Advances in Polarography*, Vol. 1, Pergamon Press, Oxford, 1960, p. 68.
14 R. Newcombe und R. Woods, *Trans. Faraday Soc.*, 57 (1961) 130.
15 H. Matsuda, *Bull. Chem. Soc. Japan*, 26 (1953) 342.
16 A. Kimla und F. Strafelda, *Collection Czech. Chem. Commun.*, 28 (1963) 3206.

INVESTIGATION OF THE ANODIC OXIDATION OF AZIDE ION ON PLATINUM ELECTRODES

G. A. WARD AND C. M. WRIGHT

Research Center, Hercules Powder Company, Wilmington, Delaware (U.S.A.)

(Received June 18th, 1964)

INTRODUCTION

Numerous methods for the determination of azide ion have been reported. Various adaptations of ceric oxidimetry have been employed by several workers[1,2,3,4,5], and titration methods based on reaction with iodine[6], potassium permanganate[7,8], nitrous acid[9], silver chromate[10], and silver nitrate[11] have been reported. The red color formed by the ferric azide complex has been extensively used in spectrophotometric methods[12,13,14]. Polarographic methods based on the reduction of hydrazoic acid in 8–18 *N* sulfuric acid solution[15] and on the anodic current from mercury dissolution in the presence of azide[16] have been published.

Although several studies of the anodic discharge of the azide ion according to the reaction

$$N_3^- \rightarrow e + \tfrac{3}{2} N_2 \qquad (1)$$

have been published[17,18,19], no one has reported the use of this reaction as the basis of an analytical method for the determination of the azide ion.

The subject of the present work has been a detailed investigation of the mechanism of this reaction, using the techniques of cyclic voltammetry, coulometry, and chronopotentiometry, and the development of an electrochemical method of analysis for azide, based on cyclic voltammetry.

EXPERIMENTAL

The basic instrument used in all work involving cyclic voltammetry, coulometry, and chronopotentiometry was a modular instrument based on operational amplifier circuitry as described by DEFORD[20]. For the recording of cyclic voltammetri ccurves, a Moseley Autograf x-y recorder was used at voltage scan rates of less than 0.2 V/sec. At faster scan rates, a Tektronix Model 502 oscilloscope was used. In coulometric and chronopotentiometric work, in which a time-base recorder was required, a Sargent Multi-Range Recorder, Cat. No. S-72150, was used.

All voltammetric work was carried out in a water-jacketed electrolysis cell maintained at 25 $\pm$ 0.1°. A three-electrode system was used to minimize voltage drop effects between the indicator and reference electrodes. The reference electrode was a Beckman No. 1170 fiber-type saturated calomel electrode. Auxiliary electrodes consisted of a 1.0 cm^2 platinum foil welded to a platinum contact wire sealed in glass. In

chronopotentiometric experiments, two such auxiliary electrodes were used, mounted on each side of the indicator electrode, parallel to it, and 1.0 cm distant from it. Several indicator electrodes were used in cyclic voltammetry, ranging in area from 0.049 to 2.07 cm^2. The smallest electrode was a cylindrical platinum wire sealed in glass and coated with Apiezon wax everywhere except on the end, which was ground flat and polished. Other electrodes used in this work were platinum foils of various sizes.

All chemicals were reagent-grade and were used without further purification.

The electrolysis cell used in microcoulometric experiments consisted of a polarographic H-cell in which the anode and cathode compartments were separated by a porous glass frit. The anode was a platinum foil, 1 cm by 8 cm, which was placed in one compartment of the cell, while the reference and auxiliary electrodes were placed in the other compartment. The anode solution was stirred with a glass-coated magnetic stirring bar in the anode compartment. The procedure used in a determination of n was as follows.

The cell, stirrer, and electrodes were assembled with the cell mounted in a constant temperature water bath maintained at 25.0°. Five milliliters of aqueous 0.2 M $NaClO_4$ was placed in each compartment of the cell, the anode potential was set at 1.20 V *vs.* S.C.E., and the cell current was recorded as a function of time until it decayed to a constant value (less than 1.0 μA). Then an aliquot of aqueous 0.049 M NaN_3 was added to the anode compartment and the anode current recorded as a function of time (Sargent recorder, chart speed 0.5 in. per min). The amount of the previously standardized NaN_3 solution used was determined by withdrawing the aliquot from the storage bottle in a hypodermic syringe, weighing the syringe and the solution to the nearest 0.2 mg, adding the sample to the cell, and reweighing the syringe.

When the cell current had decreased to approximately half its initial value, the experiment was stopped. The amount of N_3^- consumed was calculated from the amount originally added to the cell multiplied by the ratio of the final cell current to the original cell current. The quantity of electricity used was determined by measuring the area under the recorded current–time curve, and n was calculated from these values using the expression:

$$n = \frac{\text{(coulombs of electricity used)}}{\text{(moles } NaN_3 \text{ consumed)} \times F}$$

where F is the Faraday (96, 484 coulombs).

RESULTS AND DISCUSSION

Cyclic voltammetry

In preliminary experiments, aqueous solutions of sodium azide were found to undergo oxidation over the entire pH range from pH 0.7 to 10.5. At pH values at which azide ion is the predominant species in solution (pH > 6), the observed peak potential (E_p), using a 50 mV/sec voltage scan rate, is approximately 1.08 V *vs.* S.C.E. At pH values at which HN_3 is the predominant species, the oxidation takes place at a slightly more anodic potential, with an estimated E_p of $+1.25$ V *vs.* S.C.E. Except for the intermediate pH range (pH 3–6) in which appreciable amounts of both N_3^- and HN_3 are present, E_p is not pH dependent.

Typical current–voltage curves for the azide oxidation at various pH values are

shown in Fig. 1. From these we see that the more cathodic wave observed in neutral and basic systems is well-separated from the base current rise, while in acidic systems the base current overlaps the azide oxidation peak, and measurement of the peak current (i_p) would be more difficult. In addition, these waves show no cathodic peak due to reduction of the products of the azide oxidation. Therefore, the overall reaction is irreversible.

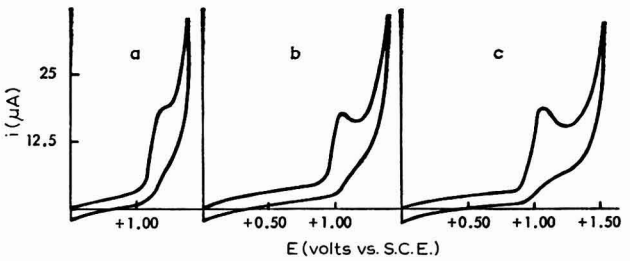

Fig. 1. Cyclic voltammetry of azide ion in various electrolytes. Voltage scan rate, 50 mV/sec; $C_{N_3^-}$ = 0.009 *M*. (a), pH = 2.01, 0.3 *M* $NaClO_4$, 0.01 *M* $HClO_4$; (b), pH = 6.04, 0.3 *M* $NaClO_4$, 0.0057 *M* NaOH, 0.0050 *M* KH_2PO_4; (c), pH = 10.10, 0.3 *M* $NaClO_4$, 0.003 *M* NH_4OH.

The variation of i_p with the concentration of azide in the solution ($C_{N_3^-}$) and the voltage scan rate (v) was studied in a neutral supporting electrolyte system containing sodium perchlorate. The data obtained, which are shown in Figs. 2 and 3, respectively, show that i_p is proportional to both $C_{N_3^-}$ and $v^{\frac{1}{2}}$, so that the wave may be assumed to be diffusion-controlled.

The effect of varying the electrode area and configuration, as well as the voltage scan rate, was studied to determine the practical limit of detection for the cyclic voltammetric determination of azide ion. With a 1.0-cm^2 platinum foil indicating electrode, a voltage sweep rate of 100 mV/sec, and the Moseley x-y recorder for recording the current–voltage curves, the limit of detection is approximately $2 \cdot 10^{-4}$ *M*. This could be improved somewhat by using a faster voltage scan rate, but an oscilloscopic recording system would be necessary, since it was found that the Moseley recorder will not accurately record the current–voltage curve at scan rates faster than 200 mV/sec.

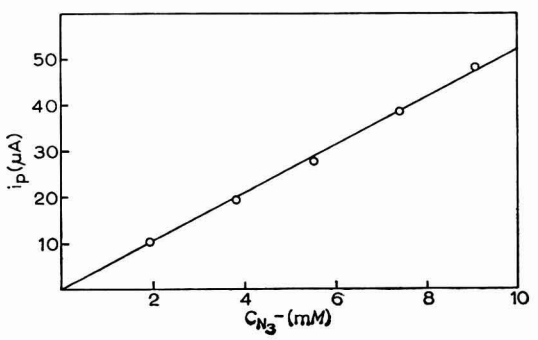

Fig. 2. Variation of peak current (i_p) with azide ion concn. ($C_{N_3^-}$). Supporting electrolyte, 0.2 *M* $NaClO_4$. Voltage scan rate, 50 mV/sec.

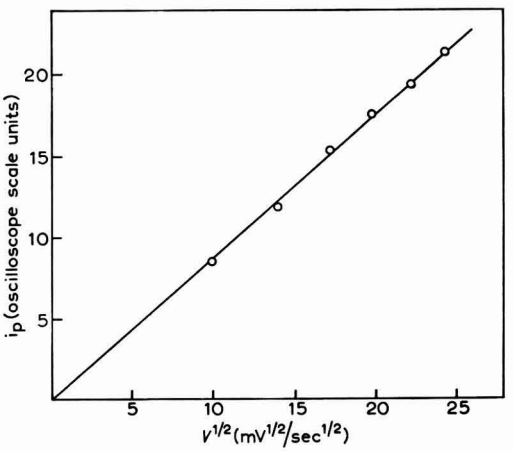

Fig. 3. Variation of peak current (i_p) with voltage scan rate (V). Supporting electrolyte, 0.3 M $NaClO_4$; $C_{N_3^-} = 0.009$ M.

Coulometric and macro-scale electrolytic studies

The microcoulometric procedure described in the Experimental Section was used to determine the number of equivalents of electricity consumed per mole of azide ions oxidized, and in two trials the values 1.07 and 1.03 were obtained. From these data we may conclude that one electron per azide ion is involved in the electrode reaction, and the initial step of the electrode reaction may be written

$$N_3^- \rightarrow \cdot N_3 + e \qquad (2)$$

Macro-scale electrolyses of azide solutions have confirmed the conclusion of earlier workers[17,18,19] that the final product of the electrode reaction is nitrogen gas, so that it appears that the azide radicals formed in the initial step of the electrode reaction react further as in the equation

$$\cdot N_3 \rightarrow \tfrac{3}{2} N_2 \qquad (3)$$

Additional evidence which supports the existence of the azide radical as the inital product of the oxidation of azide ion according to eqn. (2) is the fact that the electrolytically-generated azide radical may be made to react with radical acceptors at the electrode surface in anodic substitution reactions. For example[21], methyl azide and pentyl azide may be prepared by the reaction of electrolytically-generated azide radical with methyl and pentyl radicals simultaneously generated at the electrode surface by a Kolbe-type oxidation of an aliphatic acid.

Chronopotentiometry

To obtain further information on the mechanism of the oxidation of azide, the chronopotentiometry of the azide ion was studied in a supporting electrolyte of 0.1 N $NaClO_4$. Preliminary experiments showed that the wave was not affected by either anodic or cathodic pre-treatment of the electrode, except in cases in which enough hydrogen ion was reduced on the electrode that on reoxidation the hydrogen oxidation wave interfered with that of azide ion.

A typical chronopotentiogram for azide ion in 0.1 N $NaClO_4$ is shown in Fig. 4. A study of the variation of the chronopotentiometric constant, $i\tau^{\frac{1}{2}}/C_{N_3^-}$ (in which i is the applied current and τ is the transition time) with i, showed that $i\tau^{\frac{1}{2}}/C_{N_3^-}$ remained constant over a wide range of values of i. This result shows that the oxidation of azide

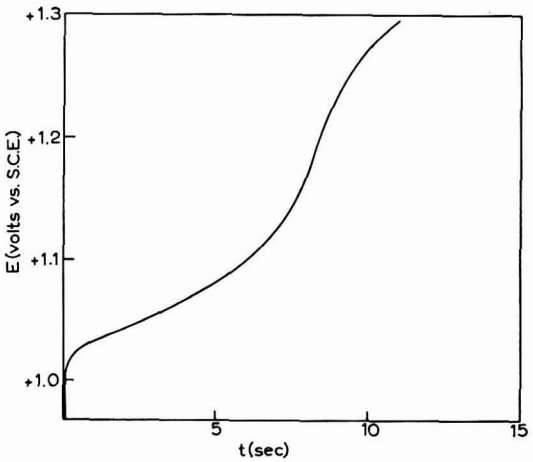

Fig. 4. Chronopotentiometric wave of N_3^-. 0.10 M $NaClO_4$ + 0.0040 M NaN_3; Pt electrode 0.164 cm^2 area.

under these conditions is diffusion-controlled and obeys the well-known SAND equation[22]

$$\frac{i\tau^{\frac{1}{2}}}{C} = \frac{nFAD^{\frac{1}{2}}\pi^{\frac{1}{2}}}{2} \tag{4}$$

In this equation, F is the Faraday constant, A is the electrode area, and D is the diffusion coefficient of the azide ion. Typical data showing the constancy of $i\tau^{\frac{1}{2}}/C_{N_3^-}$ are given in Table 1.

Using the average value of $i\tau^{\frac{1}{2}}/C_{N_3^-}$ obtained in this manner, one can calculate the value of n from eqn. (4), if A, C, and D are known. In our work A and C are measurable quantities. D was estimated from conductometric data reported by BRINER AND WINKLER[18] using the equation[23]

$$D = \frac{RT\lambda^\circ}{ZF^2} \tag{5}$$

in which R is the gas constant, 8.317 joules/degree mole, T is the absolute temperature, Z is the ionic charge of the azide ion, and λ° is the limiting specific conductance of the azide ion at infinite dilution. The value of D obtained in this manner is referred to infinite dilution, and will be only slightly different from the value expected in the electrolysis solution used in the present work. The value of D obtained from the data of BRINER AND WINKLER using eqn. (5) is 1.43×10^{-5} cm^2/sec. With this value and the average value of $i\tau^{\frac{1}{2}}/C_{N_3^-}$ from Table 2, the value of n was calculated to be 1.034, in excellent agreement with the value obtained by microcoulometry earlier.

TABLE 1

Variation of $i\tau^{\frac{1}{2}}/C_{N_3^-}$ with i and $C_{N_3^-}$. Supporting electrolyte, 0.1 N $NaClO_4$; area of the Pt electrode, 1.64 cm^2; temp., 25.0°. Each value given is the average of three runs under the same conditions.

i (mA)	$C_{N_3^-}$ (mM)	τ (sec)	$i\tau^{\frac{1}{2}}/C_{N_3^-}$ ($C\ cm^3/mole\ sec^{\frac{1}{2}}$)
0.60	2.02	3.13	527
0.50	2.02	4.95	552
0.40	2.02	7.56	546
0.30	2.02	13.83	553
1.30	4.00	2.87	551
1.00	4.00	5.03	561
0.80	4.00	7.50	548
0.60	4.00	13.85	559
0.50	4.00	21.0	572

Additional information on the mechanism of the oxidation of N_3^- can be obtained from a quantitative study of the potential–time curve obtained in chronopotentiometry. REINMUTH[24] has presented a summary of various criteria which may be used to determine the mechanism of an electrochemical reaction from chronopotentiometric data, once the reaction has been shown to be diffusion-controlled.

For the azide ion, the following values of the various criteria were obtained.

(1) No cathodic transition time was obtained in reversed-current chronopotentiometric experiments, thus τ_r/τ_f, the ratio of the reverse and forward transition times, is equal to zero.

(2) A plot of $\log_{10}(\tau^{\frac{1}{2}} - t^{\frac{1}{2}})$ *vs.* E was found to be linear.

(3) The slope of the $\log_{10}(\tau^{\frac{1}{2}} - t^{\frac{1}{2}})$ *vs.* E plots was 62 mV (± 5%), which is within experimental error of the theoretical slope of 59.1 mV calculated by assuming the slope to be equal to RT/nF.

(4) Both $\partial E_{\frac{1}{4}}/\partial \ln i$ and $\partial E_{\frac{1}{4}}/\partial \ln C$ are positive for the azide ion oxidation.

Applying these results to the various mechanisms given by REINMUTH, the only mechanisms which have the characteristics found for the azide reaction are those of the types

(3a) $A \rightarrow B$ (irreversible one-step reaction),

(3b) $A \rightarrow B$ (as (3a) except product insoluble),

(3c) $A \overset{\text{rapid}}{\rightleftharpoons} B \overset{\text{rapid}}{\longrightarrow} C$ (reversible electron-transfer step followed by rapid, irreversible chemical step),

in which A is the electroactive species, B is the initial product of the electrode reaction, and C is a non-electroactive product of a chemical reaction involving B. For the azide, schemes (3a) and (3b) may be discounted since we know from previous experience with azide anodic substitution reactions that the primary product of the electrode reaction is $\cdot N_3$, which is rapidly converted to N_2. Thus, the azide oxidation fits scheme (3c), and may be written:

$$N_3^- \overset{\text{rapid}}{\rightleftharpoons} \cdot N_3 + e$$

$$\cdot N_3 \xrightarrow{\text{rapid}} \tfrac{3}{2}N_2$$

Effect of interfering anions

Since other anions which are oxidized at potentials close to the E_p for the azide ion would constitute an interference, the anodic behavior of a number of other anions was studied under the conditons used for the azide ion. In this work it was found that ClO_4^-, NO_3^-, SO_2^{2-}, Cl^-, PO_4^{3-}, and OCN^- do not interfere in concentrations 100 times the azide concentration. Several other anions, such as NO_2^-, Br^-, I^-, S^{2-}, CN^-, ClO^-, and SCN^- are oxidized at potentials near that for the azide ion and would interfere if present in a concentration which was not negligible with respect to the azide concentration. Both ClO_2^- and SO_3^{2-} give oxidation waves at potentials sufficiently more cathodic than that of the azide ion that the i_p for the azide may be measured if the concentration of the interfering ion is equal to or less than the azide ion.

Some typical current–voltage curves for these ions are shown in Fig. 5. The excellent waves observed for several of them suggest that they may provide the basis for useful analytical procedures which will be investigated.

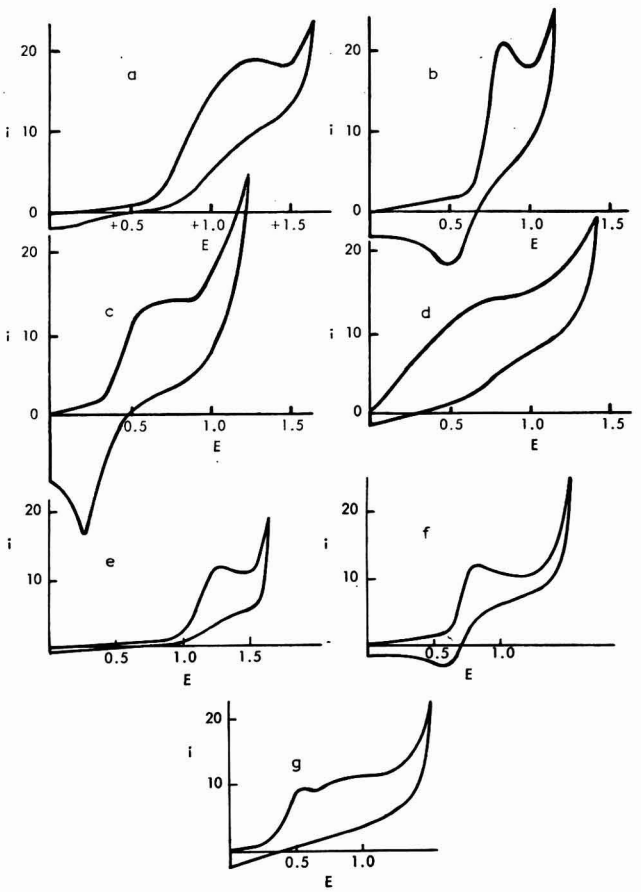

Fig. 5. Cyclic voltammetry of anions in 0.1 *M* $NaClO_4$. (a), 0.01 *M* NO_2^-; (b), 0.01 *M* Br^-; (c), 0.01 *M* I^-; (d), 0.01 *M* S^{2-}; (e), 0.01 *M* ClO^-; (f) 0.1 *M* ClO_2^-; (g), 0.01 *M* SO_3^{2-}.

ACKNOWLEDGEMENT

Research reported in this publication was supported ty the Bureau of Naval Weapons Contract NOrd 16640. The authors wish to express their thanks to Professor H. A. LAITINEN for his many valuable suggestions and discussions concerning the work.

SUMMARY

A detailed study of the mechanism of the anodic oxidation by the azide ion was carried out using cyclic voltammetry, chronopotentiometry, coulometry, and macro-scale electrolysis. The results of this work show that the oxidation of the azide ion on platinum electrodes in neutral and basic aqueous media proceeds according to the mechanism:

$$N_3^- \overset{\text{rapid}}{\rightleftharpoons} \cdot N_3 + e$$
$$\cdot N_3 \xrightarrow{\text{rapid}} N_2$$

In acidic solutions, HN_3 is also oxidized, but at a slightly more anodic potential.

This reaction has been shown to be diffusion-controlled, and may be used as the basis of a cyclic voltammetric method for the determination of azide, with a limit of detection of $2 \cdot 10^{-4}$ M under typical conditions.

Other anions which are also oxidized at the platinum electrode, and thus interfere in the method are: NO_2^-, Br^-, I^-, S^{2-}, CN^-, ClO^-, ClO_2^-, SO_3^{2-} and SCN^-.

REFERENCES

1 F. SOMMER AND H. PINCAS, *Ber.*, 48 (1915) 1963.
2 J. MARTIN, *J. Am. Chem. Soc.*, 49 (1927) 2133.
3 J. W. ARNOLD, *Ind. Eng. Chem., Anal. Ed.*, 17 (1945) 215.
4 E. L. GROVE, R. S. BRAMAN, H. F. COMBS AND S. B. NICHOLSON, *Anal. Chem.*, 34 (1962) 682.
5 Y. MIZUSHIMA AND S. NAGAYAMA, *J. Ind. Explosives Soc., Japan*, 17 (1956) 113.
6 F. FEIGL AND E. CHARGAV, *Z. Anal. Chem.*, 74 (1928) 376.
7 M. MARQUEYROL AND P. LORIETTE, *Bull. Soc. Chim. France*, 23 (1918) 401.
8 J. H. VAN DER MEULEN, *Rec. Trav. Chim.*, 67 (1948) 600.
9 J. F. REITH AND J. H. A. BOUWMAN, *Pharm. Weekblad*, 67 (1930) 475.
10 E. KREJZOVÁ, V. SIMON AND J. ZÝKA, *Chem. Listy*, 51 (1957) 1764.
11 R. A. W. HAUL AND G. UHLEN, *Z. Anal. Chem.*, 129 (1949) 21.
12 G. LABRUTO AND D. RANDISI, *Ann. Chim. Appl.*, 22 (1932) 319.
13 C. E. ROBERSON AND C. M. AUSTIN, *Anal. Chem.*, 29 (1957) 854.
14 A. ANTON, J. G. DODD and A. E. HARVEY, *Anal. Chem.*, 32 (1950) 1209.
15 J. MASEK, *Collection Czech. Chem. Commun.*, 25 (1960) 3137.
16 J. I. BRYANT AND M. D. KEMP, *Anal. Chem.*, 32 (1960) 758.
17 H. P. STOUT, *Trans. Faraday Soc.*, 41 (1945) 64.
18 E. BRINER AND P. WINKLER, *J. Chim. Phys.*, 20 (1923) 201.
19 J. G. N. THOMAS, *Trans. Faraday Soc.*, 58 (1962) 1412.
20 D. D. DEFORD, private communication, presented at *The 133rd American Chemical Society Meeting*, San Francisco, California, April, 1958.
21 C. M. WRIGHT, publication in preparation.
22 H. J. S. SAND, *Phil. Mag.*, 1 (1901) 45.
23 H. S. HARNED AND B. B. OWEN, *The Physical Chemistry of Electrolytic Solutions*, Reinhold Publishing Co., New York, 3rd ed., p. 245, 1958.
24 W. H. REINMUTH, *Anal. Chem.*, 32 (1960) 1514.

VERIFICATION OF THE COULOMETRIC METHOD OF ANALYSIS OF HYDROGEN IN IRON

THOMAS C. FRANKLIN AND NELLIE F. FRANKLIN

Chemistry Department, Baylor University, Waco, Texas (U.S.A.)

(Received June 18th, 1964)

A recent paper[1] showed a proportionality between the amount of hydrogen in palladium measured by a coulometric technique and that measured by a "bakeout" technique. Two of the questions that remain concerning the use of the coulometric method are the questions of whether it measures the absolute amount of hydrogen and whether it is applicable to metals such as iron. To study these questions a comparison was made of the volume of hydrogen diffusing out of iron[2] and the amount of hydrogen determined coulometrically.

EXPERIMENTAL

The samples used were reagent-grade iron wires, 0.235 mm in diameter, 18–36 in. long. The wire was coiled so that it could be placed in the neck of a Warburg reaction vessel. After degreasing with acetone, the iron wire was dipped in 6 *N* nitric acid and then rinsed with distilled water. The wire was then placed in a 2 *N* sodium hydroxide solution as one electrode and a large platinum gauze electrode was used as the other electrode. The iron wire was cathodically charged with hydrogen using constant currents that ranged from 5.1–12.4 mA. The hydrogen on the electrode was then oxidized with a polarograph by sweeping the voltage over the range for oxidation of hydrogen. The generation of hydrogen and its oxidation was repeated until the polarographic curves were approximately the same. As previously described[3] the area under the polarographic curve is a coulometric measure of the hydrogen adsorbed on and absorbed in iron.

One of the limitations of the coulometric method is the fact that all of the hydrogen must migrate to the surface of the metal in the time it takes to run a polarogram. This limits the size of the sample. In a study of the electrodeposition of nickel it was observed that the amount of hydrogen was linearly proportional to the length of time of depositing of nickel up to 11 min plating at a current density of 6.96 mA/cm^2. (This corresponds to a thickness of 1.6×10^{-3} mm.) Deposits of nickel thicker than this did not evolve all of their hydrogen on one voltage sweep. In all of these experiments the voltage was swept twice. In the two largest samples of hydrogen the second sweep showed a small amount of hydrogen. The amounts of hydrogen from the two voltage sweeps were added.

The electrode was again charged with hydrogen with the same current for the same length of time. This sample was transferred immediately to a nitrogen-filled Warburg apparatus containing anhydrous calcium sulfate. The sample was allowed to stand over night. Tests indicated that in these samples all of the hydrogen was evolved in this period of time. The Warburg manometer was calibrated in terms of volume and used to measure the volume of evolved hydrogen. In order to remove the effect of pressure on the residual nitrogen, a blank was run with an equal length wire, wet in the sodium hydroxide and placed in another Warburg apparatus at the same time. The two Warburg vessels and manometers were checked against each other on several occasions and on each occasion they were found to respond identically to changes in external conditions. The volume measured with this blank was subtracted from the volume obtained with the sample.

RESULTS

The results are summarized in Table 1. The average per-cent difference between the results is 27.3%. This is probably as good agreement as could be expected with

TABLE 1

A COMPARISON OF THE MOLES OF HYDROGEN OBTAINED BY VOLUMETRIC AND COULOMETRIC METHODS

Run no.	*Moles of hydrogen* $\cdot 10^6$	
	Volumetric	*Coulometric*
1	4.04	3.74
2	4.13	3.54
3	2.18	2.47
4	1.36	2.44
5	2.61	2.17
6	1.01	1.39
7	2.68	1.64
8	0.96	0.72

such small samples. Because of the many variables involved in the volumetric method and because of the fact that the coulometric method can be reproduced to within 2% it is felt that most of the variation lies in experimental difficulties involved with the volumetric method.

ACKNOWLEDGEMENT

The research reported in this paper has been sponsored by the Geophysics Research Directorate of the Air Force Cambridge Research Laboratories, Office of Aerospace under contract AF 19(604)- 8414.

SUMMARY

The coulometric method of analysis for hydrogen sorbed in iron was checked against the volume of hydrogen evolved from the iron on standing. The two methods were in agreement.

REFERENCES

1 T. C. FRANKLIN AND N. F. FRANKLIN, *J. Electroanal. Chem.*, 6 (1963) 242.
2 F. R. COE, *Iron Steel Inst. (London), Spec. Rept.*, 73 (1961) 111.
3 T. C. FRANKLIN AND F. MATSUDA, *U.S. Dept. Comm., Office Tech. Serv., P. B. Rept.*, AD 284, 582 (1962).

POTENTIOMETRIC ACID–BASE TITRATIONS IN MOLTEN SALTS

THE ACID CHARACTER OF GROUP V OXIDES AS INFERRED FROM THEIR REACTION WITH MOLTEN KNO_3

A. M. SHAMS EL DIN, A. A. EL HOSARY AND A. A. A. GERGES

Laboratory of Electrochemistry and Corrosion, National Research Centre, Dokki, Cairo (U.A.R.)

(Received June 12th, 1964)

INTRODUCTION

In a recent publication[1] we reported on the reaction between V_2O_5 and fused KNO_3. The results obtained were explained on the basis that the pentoxide acts as a Lux-acid[2], which takes its primary oxide ion from the nitrate base electrolyte to yield metavanadate:

$$V_2O_5 + 2NO_3^- \rightarrow 2VO_3^- + N_2O_5 \quad (1)$$

Metavanadate is also a strong Lux-acid. It reacts further with the nitrate to give pyrovanadate and a vanadium–nitrate complex of the probable formula $[VO_3\text{–}O\text{–}NO_2]^{2-}$

$$2VO_3^- + 2NO_3^- \rightarrow V_2O_7^{4-} + N_2O_5 \quad (2)$$

$$VO_3^- + NO_3^- \rightarrow [VO_3\text{–}O\text{–}NO_2]^{2-} \quad (3)$$

The presence of both pyrovanadate and the nitrate complex in the melt was ascertained by potentiometrically titrating the reaction products with Na_2O_2[1].

It was of interest to establish whether the pentoxides of phosphorus and arsenic behave in a similar fashion. The two pentoxides were made to react with fused KNO_3 under well-defined experimental conditions and the variation of the potential of an oxygen (Pt) electrode as a function of time was followed. When the reactions came to an end, the reaction products were determined by running potentiometric acid–base titrations *in situ* using Na_2O_2 as titrant. No similar work on P_2O_5 and As_2O_5 from this standpoint has been published.

The two pentoxides give rise to another series of acid salts derived from the ortho-acids H_3PO_4 and H_3AsO_4, respectively. The neutralization of NaH_2PO_4 and Na_2HPO_4 in molten KNO_3 at 350° has recently been studied[3]. In the present paper the behaviour of the arsenic analogues is examined. Acid–base equilibrium constants have been calculated and the acids of Group V oxides are arranged in order of their decreasing strengths.

EXPERIMENTAL

Weighed quantities of P_2O_5 and As_2O_5 were added to 50.000 g KNO_3 at 350° and

the variation in the potential of an oxygen electrode was followed as a function of time, relative to a Ag/Ag(I)/glass reference electrode[4]. When constant potentials were established, potentiometric acid–base titrations were conducted *in situ*. The technique for titrating in fused salts was described previously in detail[5,6]. Na_2O_2 was used as oxide donor[4]. Potentials were measured on a type 4C Radiometer pH meter to the nearest mV. All chemicals were of A.R. quality. KNO_3 was dried as described in a previous paper[6].

RESULTS

The addition of P_2O_5 to fused KNO_3 at 350° resulted in the evolution of brown nitrogen oxide fumes. Similarly, the potential of the oxygen electrode registered a rapid change to positive values and then dropped slowly to attain constant potentials (Fig. 1). When these steady-state potentials were established, the potentiometric

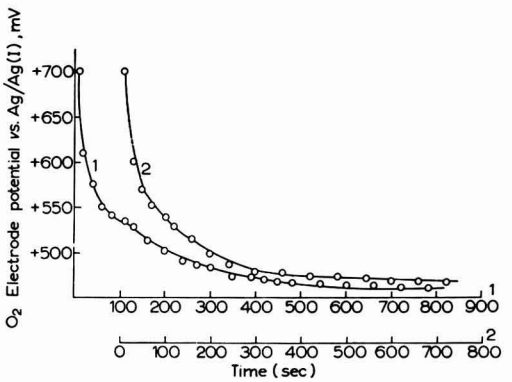

Fig. 1. Variation of the oxygen electrode potential during the reaction of P_2O_5 and KNO_3 at 350°. (1), 0.870 g; (2), 1.500 g P_2O_5/50.000 g KNO_3.

titration of the reaction products with Na_2O_2 gave rise to curves similar to those depicted in Fig. 2. These curves are characterized by two well-defined potential drops of 400 mV each. The quantities of Na_2O_2 consumed up to the inflexion point of each of the two steps are equal and each corresponds to exactly one-third of the theoretical quantity necessary to transfer P_2O_5 into the most basic salt, Na_3PO_4 (insert of Fig. 2).

In another series of experiments, charges of P_2O_5 were added to nitrate melts containing one equivalent of Na_2O_2. Under these conditions, the further neutralization of the reaction products gave rise to a single step at potentials characteristic for the second step of Fig. 2. The quantities of Na_2O_2 consumed along this step corresponded to one equivalent of O^{2-}.

The addition of extra $NaPO_3$ and $Na_4P_2O_7$ to the reaction products of P_2O_5–KNO_3 mixtures was also examined. Thus, when $NaPO_3$ was added to the reaction medium and the whole mixture was titrated with Na_2O_2, the consumption of Na_2O_2 along the two neutralization steps increased in proportions equivalent to the amounts of the salt added. On the other hand, when $Na_4P_2O_7$ was added to the reaction

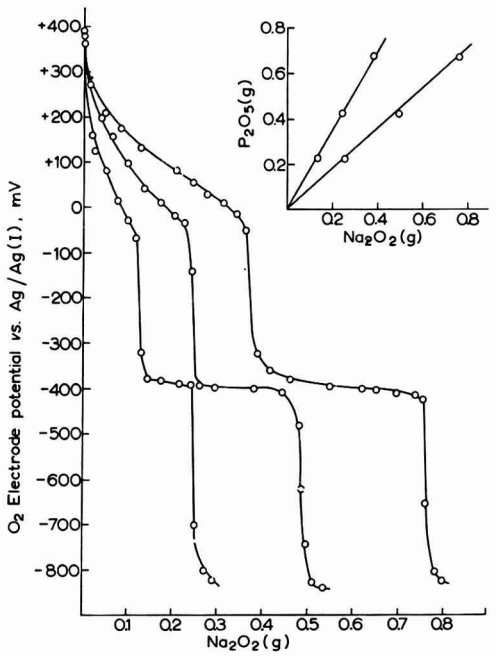

Fig. 2. Titration of the reaction products of P_2O_5–KNO_3 mixtures with Na_2O_2 at 350°. (1), 0.225 g; (2), 0.423 g; (3), 0.680 g P_2O_5/50.000 g KNO_3. Insert: relation between P_2O_5 and Na_2O_2, lines theoretically calculated.

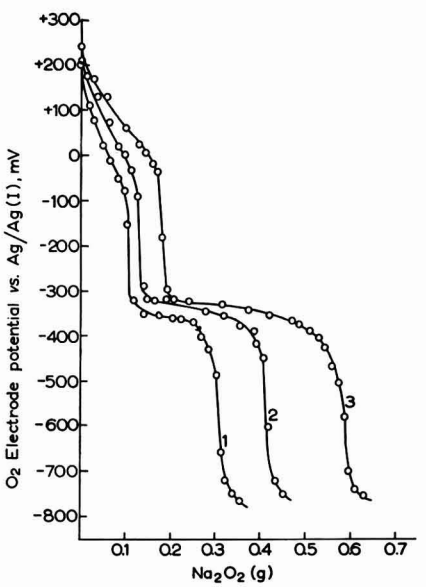

Fig. 3. Titration of P_2O_5–$Na_4P_2O_7$ mixtures with Na_2O_2 at 350°. (1), 0.200 g P_2O_5 + 0.500 g $Na_4P_2O_7$; (2), 0.250 g P_2O_5 + 0.750 g $Na_4P_2O_7$; (3), 0.330 g P_2O_5 + 1.250 g $Na_4P_2O_7$/50.000 g KNO_3.

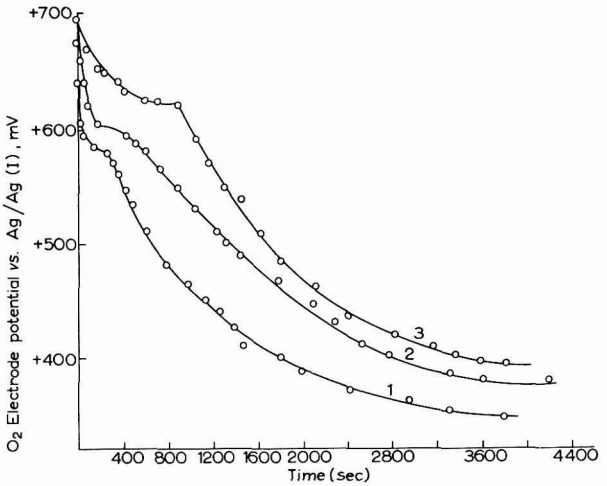

Fig. 4. Variation of the oxygen electrode potential during the reaction of As_2O_5 and KNO_3 at 350°. (1), 0.460 g; (2), 0.812 g; (3), 2.048 g As_2O_5/50.000 g KNO_3.

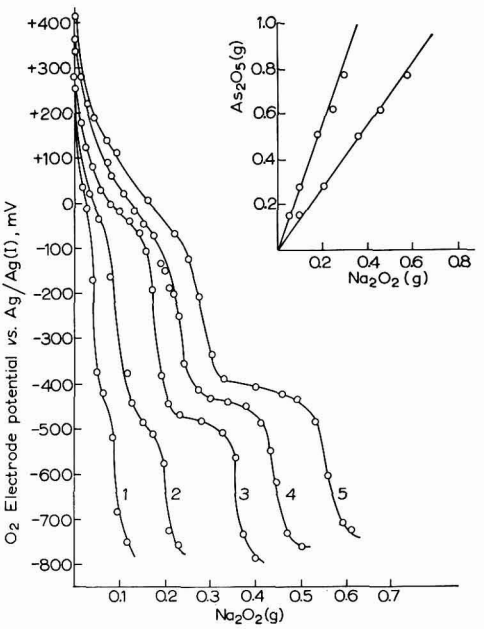

Fig. 5. Titration of the reaction products of As_2O_5–KNO_3 mixtures with Na_2O_2 at 350°. (1), 0.149 g; (2), 0.274 g; (3), 0.510; (4) 0.617 g; (5), 0.773 g As_2O_5/50.000 g KNO_3. Insert: relation between As_2O_5 and Na_2O_2, lines theoretically calculated.

medium, the consumption of Na_2O_2 increased only along the second neutralization step; the increase was equivalent to the extra pyrophosphate (Fig. 3).

The reaction between As_2O_5 and fused KNO_3 differs in few respects from that of P_2O_5. Thus, upon the addition of As_2O_5 to the nitrate melt, N_2O_5 gas was evolved and the potential of the oxygen electrode registered positive values. During the gradual fall of potential, a definite arrest in potential was recorded (Fig. 4). The length of this arrest increased with the increase of the quantity of As_2O_5 added to the nitrate melt.

As with P_2O_5–KNO_3 mixtures, the controlled addition of Na_2O_2 to the reaction product of As_2O_5–KNO_3 melts gave rise to two distinct neutralization steps similar to those of Fig. 5.

Each step is characterized by a potential drop of *ca.* 350 mV. The quantities of Na_2O_2 consumed up to the inflexion point of either step correspond to one-third of the theoretical amount necessary to transfer As_2O_5 into Na_3AsO_4 (insert of Fig. 5). Experiments in which As_2O_5 charges were added to molten KNO_3 containing one-third of the amount of Na_2O_2 necessary to form orthoarsenate were also performed. The titration curves of these mixtures had two steps similar to those of Fig. 5. The consumption of Na_2O_2 during these neutralizations was independent of the previous peroxide addition.

$NaAsO_3$ and $Na_4As_2O_7$ were prepared by fusing the mono- and disodium orthoarsenate to constant weight. The loss in weight upon fusion corresponded to that theoretically calculated for these transformations. When the meta- and pyro-salts

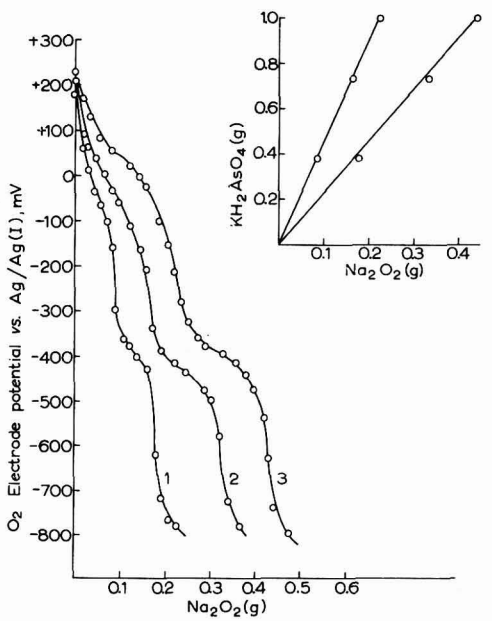

Fig. 6. Titration of KH_2AsO_4 with Na_2O_2 in molten KNO_3 at 350°. (1), 0.384 g; (2), 0.727 g; (3), 0.995 g KH_2AsO_4/50.000 g KNO_3. Insert: relation between KH_2AsO_4 and Na_2O_2, lines theoretically calculated.

were added in different quantities to the reaction products of As_2O_5–KNO_3 melts, the controlled neutralization of the mixtures showed that the consumption of Na_2O_2 increased equivalently along both steps in case of the meta-salt and along the second neutralization step in case of the pyro-salt.

We have recently titrated NaH_2PO_4 and Na_2HPO_4 with Na_2O_2 in molten KNO_3 at 350°[3]. The titration curves gave two inflexions corresponding to the transformation into the di- and tri-sodium salts respectively:

$$2H_2PO_4^- + O^{2-} \rightarrow 2HPO_4^{2-} + H_2O \quad (4)$$

$$2HPO_4^{2-} + O^{2-} \rightarrow 2PO_4^{3-} + H_2O \quad (5)$$

In the present study the titration of the acid KH_2AsO_4 has been investigated. The neutralization of Na_2HAsO_4 has already been reported[7].

The curves of Fig. 6 show two equal inflexions at the molar ratios acid: base of 2:1 and 1:1 respectively. Both steps are associated with potential drops of *ca.* 350 mV. The results of titrating mixtures of two acids KH_2AsO_4 and Na_2HAsO_4 with Na_2O_2 are shown in Fig. 7.

In all these titrations the average error in the determination of known quatities of the acids, whether alone or in mixture, was within the limits of ± 2–3%.

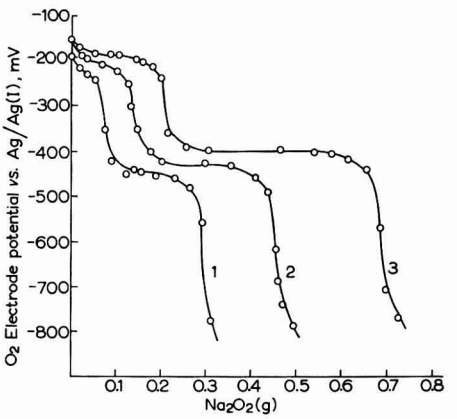

Fig. 7. Titration of $KH_2AsO_4 + Na_2HAsO_4$ mixtures in molten KNO_3 at 350°. (1), 0.324 g KH_2AsO_4 + 1.174 g Na_2HAsO_4; (2), 0.604 g KH_2AsO_4 + 1.433 g Na_2HAsO_4; (3), 0.957 g KH_2AsO_4 + 1.994 g Na_2HAsO_4/50.000 g KNO_3.

DISCUSSION

The transformation of P_2O_5 and As_2O_5 into the most basic ortho-salts requires three equivalents of O^{2-}:

$$X_2O_5 + O^{2-} \rightarrow 2XO_3^- \quad (6)$$

$$2XO_3^- + O_2^- \rightarrow X_2O_7^{4-} \quad (7)$$

$$X_2O_7^{4-} + O^{2-} \rightarrow 2XO_4^{3-} \quad (8)$$

In the experiments described above (Figs. 2 and 5), only two equivalents of O^{2-}

were supplied in the form of Na_2O_2. One is bound to conclude, therefore, that the third equivalent was taken from the nitrate base electrolyte. The results obtained when the meta- and pyro-salts were added to the reaction products (*e.g.*, Fig. 3 in the case of P_2O_5) leaves little doubt that the two neutralization steps of Figs. 2 and 5 correspond to reactions 7 and 8 respectively. The formation of the meta-salts from the two pentoxides (reaction 6) accounts, therefore, for the third equivalent of O^{2-} taken from the nitrate base electrolyte:

$$P_2O_5 + 2NO_3^- \rightarrow 2PO_3^- + N_2O_5 \quad (9)$$

$$As_2O_5 + 2NO_3^- \rightarrow 2AsO_3^- + N_2O_5 \quad (10)$$

Evidence for this conclusion was gained from the fall of the potential of the oxygen electrode with time (Figs. 1 and 4), from the evolution of brown nitrogen oxide fumes, and from the fact that the addition of As_2O_5 to nitrate melts containing one equivalent of Na_2O_2 had no effect on the subsequent neutralization of the meta-arsenate. Similar experiments with P_2O_5 showed that the first step of the titration curves of Fig. 2 was completely eliminated when the pentoxide was added to KNO_3–Na_2O_2 melts. Since nitrate melts containing meta-phosphate are stable, such behaviour can only be accounted for by assuming that the pentoxide reacted preferentially with the nitrate and not with the free oxide ion. The metaphosphate formed would then react with the free O^{2-} to yield pyro-phosphate.

A consideration of the results of the present investigation, as well as those obtained with V_2O_5 in the same melt[1], allows, thus far, the following qualitative conclusions to be drawn.

(i) The three pentoxides attack molten KNO_3 to yield the meta-salts. The reaction between P_2O_5 and the fused nitrate comes to an end in a matter of few minutes (Fig. 1). As_2O_5, although it vanishes in comparable times, does show a definite potential arrest along which the transformation into meta-arsenate takes place (Fig. 4). Equimolecular charges of V_2O_5 require a few hours to react completely with the nitrate[1]. The neutralization curves of this latter oxide exhibit, therefore, a definite step along which the formation of meta-vanadate takes place. The disappearence of V_2O_5 was found to be a zero-order reaction with respect to the pentoxide[1]. Taking the attack on molten nitrate as a measure for the acidity of the three pentoxides, it is immediately obvious that the acid strength decreases with the increase of the molecular weight of the pentoxide.

(ii) Of the three meta-salts, meta-vanadate is the strongest acid. It possesses an acidity number[8] higher (numerically) than -11.5. It does not exist in nitrate melts, but attacks the melt to yield pyrovanadate[1,4]. A quantitative estimation of the strength of the other meta- and pyro-salts will be given later.

(iii) The formation and existence of meta- and pyro-arsenate has always been a matter of dispute[9]. The results of the present investigation show clearly that these salts do exist; at least in fused media.

The titration of the acid KH_2AsO_4 is characterized by two distinct potential drops. By analogy with the phosphate compound, the reactions occurring during the two-stage neutralization can be represented as:

$$2H_2AsO_4^- + O^{2-} \rightarrow 2HAsO_4^{2-} + H_2O \quad (11)$$

and

$$2HAsO_4^{2-} + O^{2-} \rightarrow 2AsO_4^{3-} + H_2O \qquad (12)$$

The titration of $KH_2AsO_4 + Na_2HAsO_4$ mixtures, (Fig. 7), has also been carried out. The first potential drop corresponded to half the quantity of the mono-sodium salt, while the difference between the first and the second steps gave the disodium salt. It is worth noting that the addition of extra Na_2HAsO_4 to KH_2AsO_4–KNO_3 mixtures brings about a marked drop in the potential of the oxygen electrode along the first neutralization step. The drop in potential is more than can be accounted for by an increase in the amount of the base (Na_2HAsO_4). Most probably, the decrease in potential is related to the presence of traces of water dissolved in the melt.

Two quantitative procedures were developed in this laboratory to define the strength of a certain acid oxyanion. The first involved the measurement of the potential of the oxygen electrode in a nitrate melt 10^{-2} M with respect to the oxyanion. Assuming a reversible behaviour for the oxygen electrode, the difference between this potential and that measured in pure KNO_3, *i.e.*, $E_{\text{nitrate}} - E_{\text{oxyanion}}$, was divided by the value of the term 2.3 $RT/2F$ at the working temperature (61.6 mV at 350°). The resultant figure was termed the 'acidity (basicity) number' of the particular oxyanion[4,8]. On this basis, the acid oxyanions of phosphorous, arsenic and vanadium were found to possess the acidity (basicity) numbers grouped in column 2 of Table 1.

TABLE 1

ACIDITY NUMBERS AND EQUILIBRIUM CONSTANTS IN MOLTEN KNO_3 OF THE DIFFERENT OXYANIONS OF PHOSPHORUS, ARSENIC AND VANADIUM

Anion	*Acidity (basicity) number*	*Equilibrium constant*
PO_3^-	−11.20	3.1×10^{15}
AsO_3^-	−10.63	4.7×10^{13}
VO_3^-	< −11.50	—
$P_2O_7^{4-}$	− 0.85	6.6×10^{5}
$As_2O_7^{4-}$	− 1.78	4.3×10^{4}
$V_2O_7^{4-}$	− 2.63	4.5×10^{6}
$H_2PO_4^-$	−11.00	3.9×10^{13}
$H_2AsO_4^-$	− 9.49	7.4×10^{10}
HPO_4^{2-}	− 1.65	2.8×10^{5}
$HAsO_4^{2-}$	+ 1.25	2.6×10^{2}

The second procedure was based upon the calculation of the equilibrium constant of the general acid–base reactions: Acid + $O^{2-} \rightarrow$ Base. The normal O_2/O^{2-} potential in molten KNO_3 was indirectly calculated and the value was used in conjunction with the potentiometric titration curves to compute the first known acid–base equilibrium constants in fused salts[7]. The equilibrium constants of the reactions:

$$2PO_3^- + O^{2-} \rightarrow P_2O_7^{4-} \qquad K = 3.1 \times 10^{15}$$

$$2H_2PO_4^- + O^{2-} \rightarrow 2HPO_4^{2-} + H_2O \qquad K = 3.9 \times 10^{13}$$

$$2HPO_4^{2-} + O^{2-} \rightarrow 2PO_4^{3-} + H_2O \qquad K = 2.8 \times 10^5$$

$$V_2O_7^{4-} + O^{2-} \rightarrow 2VO_4^{3-} \qquad K = 4.5 \times 10^6$$

$$P_2O_7^{4-} + O^{2-} \rightarrow 2PO_4^{3-} \qquad K = 6.6 \times 10^5$$

$$2HAsO_4^{2-} + O^{2-} \rightarrow 2AsO_4^{3-} + H_2O \qquad K = 2.6 \times 10^2$$

were reported in a previous communication[7]. In the present study similar computations were made for the neutralization reactions:

$$2AsO_3^{-} + O^{2-} \rightarrow As_2O_7^{4-} \tag{13}$$

$$As_2O_7^{4-} + O^{2-} \rightarrow 2AsO_4^{3-} \tag{14}$$

$$2H_2AsO_4^{-} + O^{2-} \rightarrow 2HAsO_4^{2-} + H_2O \tag{15}$$

For these calculations, the potential of the oxygen electrode was considered at 25, 50 and 75% neutralization. The normal O_2/O^{2-} potential in the nitrate melt was taken as -796.6 mV relative to our reference electrode[7]. Further, in the calculation of the equilibrium constant of reaction 15, we assumed that the water formed remained dissolved in the melt. Its molarity was set equal, therefore, to that of the added peroxide. The data necessary for the calculation of the equilibrium constants of reactions 13–15 are given in Tables 2–4. The potentials given in columns 3 of the tables were obtained by interpolation of the curves of Figs. 5 and 6. The concentrations of the O^{2-} ion appearing in columns 4 of the tables were calculated on the basis that the oxygen electrode changes its potential by the value of $2.3\,RT/2F$ V for every 10-fold change in the concentration of O^{2-}.

TABLE 2

CALCULATION OF THE EQUILIBRIUM CONSTANT OF THE REACTION

$2AsO_3^{-} + O^{2-} \rightarrow As_2O_7^{4-}$

$[AsO_3^-]$ *original molarity*	*Neutralization*	*O_2 electrode potential (mV)*	$[O^{2-}]$ *(mole/l)*	$K = \frac{[As_2O_7^{4-}]}{[AsO_3^-]^2[O^{2-}]}$
0.07279	25%	+ 40	2.612×10^{-14}	11.7×10^{13}
	50%	− 25	2.965×10^{-13}	4.6×10^{13}
	75%	−110	7.112×10^{-12}	1.2×10^{13}
0.13008	25%	+ 40	2.612×10^{-14}	6.5×10^{13}
	50%	− 25	2.965×10^{-13}	2.6×10^{13}
	75%	−100	4.886×10^{-12}	0.9×10^{13}
0.17864	25%	+ 55	1.503×10^{-14}	8.7×10^{13}
	50%	+ 5	9.661×10^{-14}	5.8×10^{13}
	75%	− 80	2.317×10^{-12}	1.5×10^{13}
			mean	4.7×10^{13}

The different acid–base equilibrium constants are grouped in column 3 of Table 1.

Consideration of the data grouped in Table 1 enables the following conclusions to be drawn regarding the acid strength of the different oxyanions.

TABLE 3

CALCULATION OF THE EQUILIBRIUM CONSTANT OF THE REACTION

$$As_2O_7^{4-} + O_2^- \rightarrow 2AsO_4^{3-}$$

$[As_2O_7^{4-}]$ original molarity	Neutralization	O_2 electrode potential (mV)	$[O^{2-}]$ (mole/l)	$K = \frac{[AsO_4^{3-}]^2}{[As_2O_7^{4-}][O^{2-}]}$
0.05455	25%	−425	9.247×10^{-7}	1.9×10^4
	50%	−460	3.420×10^{-6}	3.2×10^4
	75%	−485	8.709×10^{-6}	5.6×10^4
0.10230	25%	−430	1.115×10^{-6}	3.1×10^4
	50%	−455	2.838×10^{-6}	7.2×10^4
	75%	−470	4.969×10^{-6}	(18.5×10^4)
0.15530	25%	−430	1.115×10^{-6}	4.6×10^4
	50%	−455	1.953×10^{-6}	(15.9×10^4)
	75%	−485	8.709×10^{-6}	(16.0×10^4)
			mean	4.3×10^4

TABLE 4

CALCULATION OF THE EQUILIBRIUM CONSTANT OF THE REACTION

$$2H_2AsO_4^- + O^{2-} \rightarrow 2HAsO_4^{2-} + H_2O$$

$[H_2AsO_4^-]$ original molarity	Neutralization	O_2 electrode potential (mV)	$[O^{2-}]$ (mole/l)	$[H_2O]$ (mole/l)	$K = \frac{[HAsO_4^-]^2[H_2O]}{[H_2AsO_4^-]^2[O^{2-}]}$
0.07818	25%	+ 30	3.802×10^{-14}	9.995×10^{-3}	2.29×10^{10}
	50%	− 35	4.315×10^{-13}	1.999×10^{-2}	4.58×10^{10}
	75%	− 85	2.818×10^{-12}	2.998×10^{-2}	9.56×10^{10}
0.14960	25%	+ 40	2.612×10^{-14}	1.881×10^{-2}	8.00×10^{10}
	50%	− 25	2.965×10^{-13}	3.763×10^{-2}	12.69×10^{10}
	75%	−110	7.112×10^{-12}	5.644×10^{-2}	7.14×10^{10}
				mean	7.4×10^{10}

(1) Because of the strong acid character of metavanadate in fused KNO_3, the determination of either an acidity number or an acid–base equilibrium constant for this ion is not possible. Meta-phosphate, on the other hand, is stronger than meta-arsenate. This is apparent from the high acid number and the large equilibrium constant. In a LiCl–KCl eutectic at 450°, sodium meta-vanadate is also a stronger acid than meta-phosphate. Upon neutralization, the former changes to the ortho-salt, while the latter yields only the pyro-salt[4].

(2) From the acid numbers of the three pyro-salts it is also evident that acidity decreases in the series $V_2O_7^{4-} > As_2O_7^{4-} > P_2O_7^{4-}$. Consideration of the equilibrium constants of the three species confirms that pyro-vanadate is the strongest in the three pyro-acids. The equilibrium constant of pyro-phosphate is, however, *ca.* ten times larger than that for pyro-arsenate.

(3) Acid ortho-phosphates, *viz.*, $H_2PO_4^-$ and HPO_4^{2-} possess higher acid numbers as well as larger equilibrium constants than the corresponding arsenic analogues. The phosphate derivatives are, therefore, stronger acids. It is of interest to note that the same conclusion applies also to aqueous solutions. The second and third ionization constants of ortho-phosphoric and ortho-arsenic acids in water media are 6.2×10^{-8}, 1×10^{-12}, 5.6×10^{-8} and 3×10^{-13} respectively[10]. K_2/K_3 for both acids amount to 6.2×10^4 and 1.9×10^5. In fused KNO_3, the corresponding figures are 1.4×10^8 and 2.3×10^8 respectively.

(4) The fact that $H_2AsO_4^-$ and $HAsO_4^{2-}$ possess acidity numbers different from those for AsO_3^- and $As_2O_7^{4-}$ shows that the former ions retain their chemical entity at these low dilutions and do not change—by the action of heat—into the latter. The apparent similarity of the titration curves of $NaAsO_3$ and NaH_2AsO_4 (Figs. 5 and 6) seems to be only accidental.

(5) $HAsO_4^{2-}$ is the only anion basic with respect to fused KNO_3[7]. It possesses a basicity number of $+1.25$ and its 10^{-2} *M* solution in the nitrate melt furnishes *ca.* 18 times as much O^{2-} ion as that originally present in the base electrolyte. All the other oxy-anions, on the other hand, are acid towards the fused nitrate. The stability of these acids in the nitrate base electrolyte has been discussed in a previous publication[7].

Trials to study the reaction between Sb_2O_5 and fused KNO_3 were unsuccessful due to the slowness of the reaction. With the smallest addition of Na_2O_2 to the melt, the potential of the oxygen electrode dropped to very negative values and then changed very slowly (some hours) towards positive ones. True equilibrium potentials were, therefore, difficult to measure. The study was not pursued any further.

SUMMARY

The acid characters of P_2O_5, As_2O_5 and V_2O_5 were compared on the basis of their reaction with fused KNO_3 at 350°. The attack on the nitrate was found to decrease in the series $P_2O_5 > As_2O_5 > V_2O_5$. The products of these reactions were determined by conducting *in situ* potentiometric acid–base titrations using an oxygen electrode as indicator electrode and Na_2O_2 as titrant. In principle, the three pentoxide reacted with the nitrate melt in a similar fashion to yield the corresponding meta-salts. Meta-vanadate is, however, a strong Lux acid which directly attacks the base electrolyte to yield pyro-vanadate. Similarly, the controlled neutralization of meta-phosphate and meta-arsenate with Na_2O_2 gives rise to the corresponding pyro-salts. All pyro-compounds react with Na_2O_2 to yield the ortho-salts.

The neutralization of KH_2AsO_4 in molten potassium nitrate occurs in two successive steps due to the formation of the di- and tri-sodium salts.

Acidity (basicity) numbers and equilibrium constants of the different oxy-anions have been determined. On the basis of these figures, the different oxy-anions are arranged in the descending order of their strength as:

$$VO_3^- > PO_3^- > AsO_3^-$$

$$V_2O_7^{4-} > P_2O_7^{4-} > As_2O_7^{4-}$$

$$H_2PO_4^- > H_2AsO_4^-$$

$$HPO_4^{2-} > HAsO_4^{2-}$$

REFERENCES

1 A. M. SHAMS EL DIN AND A. A. EL HOSARY, *J. Electroanal. Chem.*, 7 (1964) 464.
2 H. LUX. *Z. Elektrochem.*, 45 (1939) 303.
3 A. M. SHAMS EL DIN AND A. A. A. GERGES, *Electrochim. Acta*, 9 (1964) 123.
4 A. M. SHAMS EL DIN, A. A. EL HOSARY AND A. A. A. GERGES, *J. Electroanal. Chem.*, 6 (1963) 131.
5 A. M. SHAMS EL DIN, *Electrochim. Acta*, 7 (1962) 285.
6 A. M. SHAMS EL DIN AND A. A. A. GERGES, *J. Electroanal. Chem.*, 4 (1962) 309.
7 A. M. SHAMS EL DIN AND A. A. A. GERGES, *Electrochim. Acta*, 9 (1964) 613.
8 A. M. SHAMS EL DIN AND A. A. A. GERGES, *Proceedings First Australian Conference on Electrochemistry*, Pergamon Press, in press.
9 J. W. MELLOR, *A Comprehensive Treatise on Inorganic and Theoretical Chemistry*, Vol. IX, Longmans and Green, London, p. 137.
10 W. M. LATIMER, *Oxidation Potentials*, Prentice Hall, New York, 1953, pp. 105, 112.

Book Review

Advances in Electrochemistry and Electrochemical Engineering, Vol. 3, *Electrochemistry*, edited by PAUL DELAHAY, Interscience Publishers Inc., New York and London, 1963, xi + 397 pages, 113 s.

This volume brings the number of edited articles in the series to 15, averaging just less than one pound apiece in cost. Academician A. N. FRUMKIN continues in Vol. 3 the review he began in Vol. 1, and will complete in Vol. 4.

The first chapter in the present volume is concerned with the interface between electrolytic solutions and the gas phase (J.E.B. RANDLES; 29 pp., 49 refs.). It begins with a brief and formal treatment, following GUGGENHEIM, of the thermodynamics of liquid surfaces, offering to the reader no easement of the difficult concept that γA depletes the Gibbs free energy of the interphase. The observed dependence of surface tension on concentration is compared with the theoretical treatments of ONSAGER, SAMARAS and SCHMUTZER, of which the last appears to be the most profitable. Conclusions are limited to the existence of an ion-free layer at the surfaces of electrolytic solutions, and the probable importance of structural factors in dealing with unexplained specific effects. The temporal distribution of references shows a peak in the 1935 to 1939 period, with only one since 1959; this tends to confirm the view that the subject might have awaited a little further progress. The article is marred by numerous printing errors, not all of them trivial.

The second chapter (J. N. AGAR; 99 pp., 104 refs.) is an account of thermogalvanic cells, with the associated topics of SORET effect and thermoelectric power. These subjects have received impetus from applications of the principles of irreversible thermodynamics (which are clearly presented), from improvements in technique and from the interest of the ionic properties (transported entropy, heats of transport) to which they are related. The chapter demands undivided attention from the reader, but is rewarding. It is wide in scope, dealing with a variety of systems (normal electrolytes, semi-conductors, fused salts) with due attention to experimental aspects and the recording of useful data. It is well written, clear in definition and authoritative.

Chapter 3 (M. FLEISCHMANN AND H. R. THIRSK; 87 pp., 193 refs.), on metal deposition and electrocrystallisation begins with an apologia that the subject is treated from a background of the authors' own work. It becomes clear that this is fully justified by the major contributions they have made. The epitaxy and morphology of electrodeposits is discussed with particular reference to the STRANSKI-KAISHEV approach and a brief summary of the present position concludes a section on the non-steady state in crystal growth. The final and most original section is concerned with the growth of discrete centres on electrodes. It includes a survey of the recent very remarkable work that has been carried out by the Newcastle school. This chapter is exacting. The reader requires quite an extensive knowledge of the field and of many of the numerous references cited, to make effective use of it. There is no doubt of the value of this exhaustive review.

The fourth chapter (D. A. VERMILYEA; 75 pp., 186 refs.) is a highly readable and interesting account of anodic films of all kinds, treated from the points of view of thermodynamics, growth kinetics, structure, composition, morphology and electrical properties.

The final chapter (A. N. FRUMKIN; 104 pp., 212 refs.) is Part II of a review on hydrogen overvoltage and adsorption phenomena which covers a wide field of old and new investigation. It compels attention from those interested in the field, but it presents the critical reviewer with an impossible task. The distinguished author has an uncanny insight into electrode processes, but there are probably very few electrochemists who find themselves able to agree with him all the time. Perhaps the most valuable quality of this chapter is the stimulation it provides in the reader's mind to thought and argument.

The book is well produced. The glossary of symbols to each chapter is an asset. A volume of this nature requires an author index.

D. J. G. IVES, Birkbeck College, London

J. Electroanal. Chem., 8 (1964) 323–324

CONTENTS

Original papers

ELSEVIER PUBLISHING COMPANY, AMSTERDAM

Printed in The Netherlands by

NEDERLANDSE BOEKDRUK INRICHTING N.V., 'S-HERTOGENBOSCH

RODD'S CHEMISTRY OF CARBON COMPOUNDS

Second Edition

edited by S. COFFEY, M.Sc. (London), D.Sc. (Leyden). Formerly of I.C.I. Dyestuffs Division, Blackley, Manchester. Assisted by an Advisory Board of prominent scientists.

More than 12 years have passed since the appearance of the first volume of CHEMISTRY OF CARBON COMPOUNDS. During this period great advances have been made in both theoretical and experimental organic chemistry, and these are being recorded in a completely new and revised edition.

In all important respects the second edition will be the same as the first, although some minor changes will be made. The large volume of new material will certainly cause an increase in total size and thus make it necessary to produce a greater number of sub-volumes. However, to reduce the delay between the appearance of these sub-volumes, each will be of smaller size than was the case for the first edition.

VOLUME IA - GENERAL INTRODUCTION, HYDROCARBONS, HALOGEN DERIVATIVES

General Introduction

1. The saturated or paraffin hydrocarbons. Alkanes. 2. Unsaturated acyclic hydrocarbons. 3. Halogen derivatives of the aliphatic hydrocarbons.

6 × 9″ xx + 569 pages subscription price £7.0.0.
non-subscription price £8.0.0.

VOLUME IB - MONOHYDRIC ALCOHOLS, THEIR ETHERS AND ESTERS, SULPHUR ANALOGUES; NITROGEN DERIVATIVES; ORGANOMETALLIC COMPOUNDS

4. Monohydric alcohols, their ethers and esters. 5. Sulphur analogues of the alcohols and their derivatives. 6. Nitrogen derivatives of the aliphatic hydrocarbons. 7. Aliphatic organometallic and organometalloidal compounds.

6 × 9″ xx + 277 pages + index, 16 tables; to appear late in 1964

VOLUME IC - ACYCLIC ALDEHYDES, KETONES AND MONOCARBOXYLIC ACIDS; CARBON MONOXIDE, ISOCYANIDES AND FULMINIC ACID; CARBONIC ACID AND ITS DERIVATIVES

VOLUME ID - DIHYDRIC ALCOHOLS, THEIR OXIDATION PRODUCTS AND DERIVATIVES

VOLUME IE - TRIHYDRIC ALCOHOLS, THEIR OXIDATION PRODUCTS AND DERIVATIVES

VOLUME IF - TETRA-, PENTA- AND HIGHER POLYHYDRIC ALCOHOLS, THEIR OXIDATION PRODUCTS AND DERIVATIVES; SACCHARIDES

VOLUME IG - ENZYMES; MACROMOLECULES; CUMULATIVE INDEX TO VOLUME I

To follow

Volume II Alicyclic Compounds
Volume III Aromatic Compounds
Volume IV Heterocyclic Compounds
Volume V Miscellaneous; General Index

Multi-volume works such as Rodd's Chemistry of Carbon Compounds represent a considerable outlay for the purchaser. In order to alleviate this to a certain extent, the publishers offer a discount of 15% on the publication price. Subscribers to the complete series will thus be able to acquire the work for only 26s. (approx.) per 100 pages.

ELSEVIER PUBLISHING COMPANY
AMSTERDAM LONDON NEW YORK